2006

BIOKINETIC STUDY OF BIOFUEL CELLS

Jamal Taysir Daoud
Western University

BIOKINETIC STUDY OF BIOFUEL CELLS

Thesis format: Integrated Article

by

Jamal Taysir Daoud

Graduate Program in Engineering Science

Department of Chemical and Biochemical Engineering

Submitted in partial fulfillment
of the requirements for the degree of
Master of Engineering Science

Faculty of Graduate Studies
The University of Western Ontario
London, Ontario
August, 2006

THE UNIVERSITY OF WESTERN ONTARIO
FACULTY OF GRADUATE STUDIES

CERTIFICATE OF EXAMINATION

Supervisor	Examiners
Dr. Dimitre Karamanev	Dr. Anand Prakash
Supervisory Committee	Dr. Maurice Bergougnou
Dr. Kibret Mequanint	Dr. Xueliang (Andy) Sun

The thesis by

Jamal Taysir Daoud

entitled:

Biokinetic Study of Biofuel Cells

is accepted in partial fulfillment of the
requirements for the degree of
Master of Engineering Science

Date_____

_____
Chair of the Thesis Examination Board

ABSTRACT

The main of goal of this study is to improve the operation of a biofuel cell system through addressing various factors that negatively impact fuel cell operation. Firstly, jarosite precipitation creates mechanical as well as electrical resistances by depositing in the flow channels for iron and the cathode in the fuel cell.

Investigation of the jarosite precipitation parameter was conducted with the classic chemolithotrophic iron oxidizing organism, *Acidithiobacillus ferrooxidans*. We arrived at favorable conditions of pH 1.6-1.7 and temperature of 35 °C, that limit jarosite precipitation to 0.0125-0.0209 g per gram of iron while not compromising the oxidation rate, maintained at 0.181-0.194 g/L·h. However, considering the low iron concentration in our experiment, this jarosite precipitation still poses a problem to our fuel cell operation, and thus a lower pH is required. This lower pH requirement is appropriate for the newly researched iron oxidizing chemolithotroph *Leptospirillum* sp., operating optimally at pH of 1.0.

The second factor of organic metabolite accumulation was addressed by kinetically characterizing a mixotroph, *Ferroplasma acidiphilum*, in light that it potentially utilizes the organic by-products of chemolithotrophic growth and thus limits the organic accumulation and maintains it below the threshold lethal level of 250 ppm total organic carbon. *F. acidiphilum* cultured with the chemolithotroph *Leptospirillum* sp. at intermediate conditions was able to utilize the organic accumulation and limit the total organic concentration to 20 ppm, after initial domination by *Leptospirillum*. However, *F. acidiphilum*, like *A. ferrooxidans*, operates optimally at relatively high pHs in comparison

to *Leptospirillum* sp. thus rendering its use unacceptable in a biofuel cell setting due to the promotion of jarosite precipitation.

Using the earlier analysis, an open biofuel cell system was operated at pH of 1.0 and temperature of 40 ^{o}C using solely *Leptospirillum* in order to investigate the stability of such a system and to identify further restraints. The experiment yielded steady operation at of 1.3 A, 0.65 V (0.845 W) with an oxidation rate of 1.08 g/L·h while maintaining high biomass concentrations of 3.3 x 10^{9} cells/mL. Also, the total organic carbon of the system was approaching critical levels. Furthermore, the resistance of the fuel cell was increasing throughout the course of the operation due to significant jarosite deposits in the iron flow channels and cathode material, thus indicating the need for alternative operating conditions.

Keywords: biofuel cell, oxidation rate, jarosite, organic metabolites, chemolithotrophic, mixotrophic, *Ferroplasma acidiphilum*, *Leptospirillum* sp., *A. ferrooxidans*

CO-AUTHORSHIP

Chapter 3: Formation of Jarosite during Fe^{2+} Oxidation by *Acidithiobacillus ferrooxidans*

J. D. Daoud was the principal author. Revisions and recommendations were made by the Supervisor Dr. D. Karamanev. A version of Chapter 3 has been published by the Minerals Engineering Journal. Daoud, J. & Karamanev, D. (2006). Formation of Jarosite during Fe^{2+} Oxidation by *Acidithiobacillus ferrooxidans*. *Minerals Engineering*, 19(9), 960-967.

Chapter 4: Biokinetic Characterization of *Ferroplasma acidiphilum*

J. D. Daoud was the principal author. Revisions and recommendations were made by the Supervisor Dr. D. Karamanev. A version of Chapter 4 has been written in journal article format. The article will be submitted for publication to the Biotechnology and Bioengineering Journal.

Chapter 5: Biokinetic Study of Biofuel Cells

J. D. Daoud was the principal author. Revisions and recommendations were made by the Supervisor Dr. D. Karamanev. A version of this chapter is ready for submission.

ACKNOWLEDGEMENTS

First and foremost I want to thank Allah for giving me the strength, knowledge and endurance to undertake this study. Furthermore, there are many individuals that supported me both academically and emotionally. I would like to thank my supervisor Dr. Karamanev for providing me with the opportunity to pursue this research study and guiding me throughout the course of the project, never hesitant to share his vast knowledge. Also, much thanks goes to Dr. Glibin for guiding me through many laboratory techniques crucial to the success of my project. I want to express my gratitude to my family; my father, mother and brothers, Jamil and Abdulla, as well as all my colleagues. Last but not least, I'd also like to thank Joanna Blom, Kathy Lesko and Jean Wortley for all of their invaluable administrative assistance regarding numerous items.

TABLE OF CONTENTS

LIST OF TABLES

LIST OF FIGURES

CHAPTER 1

INTRODUCTION

1.1. Background

Present day energy consumption is increasing dramatically while non-renewable resources are diminishing, particularly among developing nations. Recently, there has been public awareness towards the irreversible environmental damage. Fuel cells can potentially provide the solution to this dilemma.

Fuel cells operate by using readily available substrates from renewable sources and converting them into environmentally friendly by-products with the generation of electricity.

The main goal of this study is to investigate parameters that affect the operation of a microbial biofuel cell. Some of these parameters include proper microbial selection, appropriate electrode materials, jarosite formation and metabolite accumulation by the biocatalyst selected. Further analysis of these parameters will lead to an increased efficiency in biofuel cell operation.

1.2. Fuel Cells

Fuel cell types are generally characterized by the electrolyte material. The electrolyte is the substance between the positive and negative terminals, serving as the bridge for the ion exchange that generates electrical current (Vielstich et al., 2003). There are six main types of fuel cells, each distinguished by the electrolyte material used.

1.2.1. Alkaline Fuel Cell (AFC)

Alkaline fuel cells (AFCs) normally use a moving or immobilized aqueous solution of potassium hydroxide (KOH) as an electrolyte. AFCs operate at temperatures between 100 °C and 250 °C. The fuel supplied to an AFC must be pure hydrogen. The electrochemical reactions inside an AFC are

$$2H_2 + 4OH^- \rightarrow 4H_2O + 4e^- \quad \text{(anode reaction)} \quad (1.1)$$
$$O_2 + 4e^- + 2H_2O \rightarrow 4OH^- \quad \text{(cathode reaction)} \quad (1.2)$$
$$2H_2 + O_2 \rightarrow 2H_2O \quad \text{(overall reaction)} \quad (1.3)$$

The hydroxyl anions diffuse from the cathode to the anode. The water produced leaves on the anode side (Cifrain & Kordesh, 2003).

A major disadvantage of an AFC is the CO_2 sensitivity of the alkaline electrolytes as carbonates are formed.

$$CO_2 + 2OH^- \rightarrow CO_3^{2-} + H_2O \quad (1.4)$$

This is referred to as CO_2 poisoning. The poor solubility of carbonates leads to the formation of carbonate crystals which block electrolyte pathways and pores (Cifrain & Kordesh, 2003).

1.2.2. Molten Carbonate Fuel Cell (MCFC)

The electrolyte in an MCFC is an alkali carbonate such as sodium, potassium, or lithium salts (eg. Na_2CO_3, K_2CO_2, or Li_2CO_3). These alkali carbonates are retained in a ceramic matrix of lithium aluminum oxide ($LiAlO_2$) (Vielstich et al., 2003). An MCFC operates at 600 to 700 °C where the alkali carbonates form a highly conductive molten salt with carbonate ions (CO_3^{2-}) providing ionic conduction through the electrolyte matrix

(Vielstich et al., 2003). Nickel and nickel oxide, which are relatively inexpensive, promote the reaction on the anode and cathode respectively at the required high operating temperature of an MCFC.

1.2.3. Phosphoric Acid Fuel Cell (PAFC)

PAFCs are the most technologically mature type of fuel cell in modern day use. They use a concentrated 100% phosphoric acid electrolyte retained on a silicon carbide matrix operating at temperatures between 150 and 220 °C. At lower temperatures, the fuel cell encounters problems with CO_2 poisoning of the anode electro-catalyst, usually platinum, and poor ionic conduction in the electrolyte. The electrodes are typically composed of Teflon™-bonded platinum and carbon (Vielstich et al., 2003).

1.2.4. Proton Exchange Membrane Fuel Cell (PEMFC)

The proton exchange membrane fuel cell is also known as the solid polymer or polymer electrolyte fuel cell. It contains an electrolyte that is a layer of solid polymer, usually a sulfonic acid polymer (Nafion™), that allows protons to diffuse from anode to cathode (Vielstich et al., 2003). This is a typical hydrogen fuel cell which uses hydrogen as a fuel and gives off water as a byproduct in the electrochemical process. The hydrogen fuel however has to be humidified prior to entering the fuel cell. Due to the thermal limitations of the membrane, PEMs operate at a much lower temperature than its counterparts. They are however vulnerable to contamination by CO_2, thus reducing the performance and damaging catalytic materials within the cell.

1.2.5. Solid Oxide Fuel Cell (SOFC)

Solid oxide fuel cells contain an oxygen-ion conducting, solid electrolyte and operate at temperatures between 650 and 1000 °C. At these temperatures the electrode reactions are usually fast which allows for the use of non-noble electro-catalysts as electrodes. Both the electrodes and the electrolyte form an all-solid-state-system, while the reacting species are in the gas phase (Holtappels & Stimming, 2003).

The high operating temperatures pose specific problems to the SOFC. For example, the materials must be compatible and physical properties such as the thermal expansion and dimensional stability in reducing and oxidizing environments are crucial (Holtappels & Stimming, 2003).

1.2.6. Direct Methanol Fuel Cell (DMFC)

The DMFC is similar to the PEMFC in that it uses a polymer membrane as an electrolyte, however, a catalyst on the DMFC anode draws hydrogen from methanol (Vielstich et al., 2003).

As of 2005, Toshiba produced the smalled commercially available fuel cell (DMFC) at 22 x 56 x 4.5 millimeters. This device outputs 100 milliwatts at 10 hours per milliliter of fuel, and takes advantage of new technology allowing the use of undiluted (99.5%) methanol.

1.3. Biofuel Cell

Microbial fuel cells, or biofuel cells, are most similar to the PEMFC in that a solid polymer electrolyte is utilized. In this research, a new type of microbial fuel cell was studied. Hydrogen is oxidized at the anode with the aid of platinum catalysts, while ferric

iron is reduced at the cathode. This eliminates the need for platinum catalysts at the cathode. Once the ferric iron is reduced, it is pumped back to a bioreactor, where an iron-oxidizing microorganism oxidizes Fe^{2+} to Fe^{3+}. The regenerated ferric iron is pumped back to the cathodic compartment of the fuel cell. A representation of the fuel system used is shown in Figure 1.1.

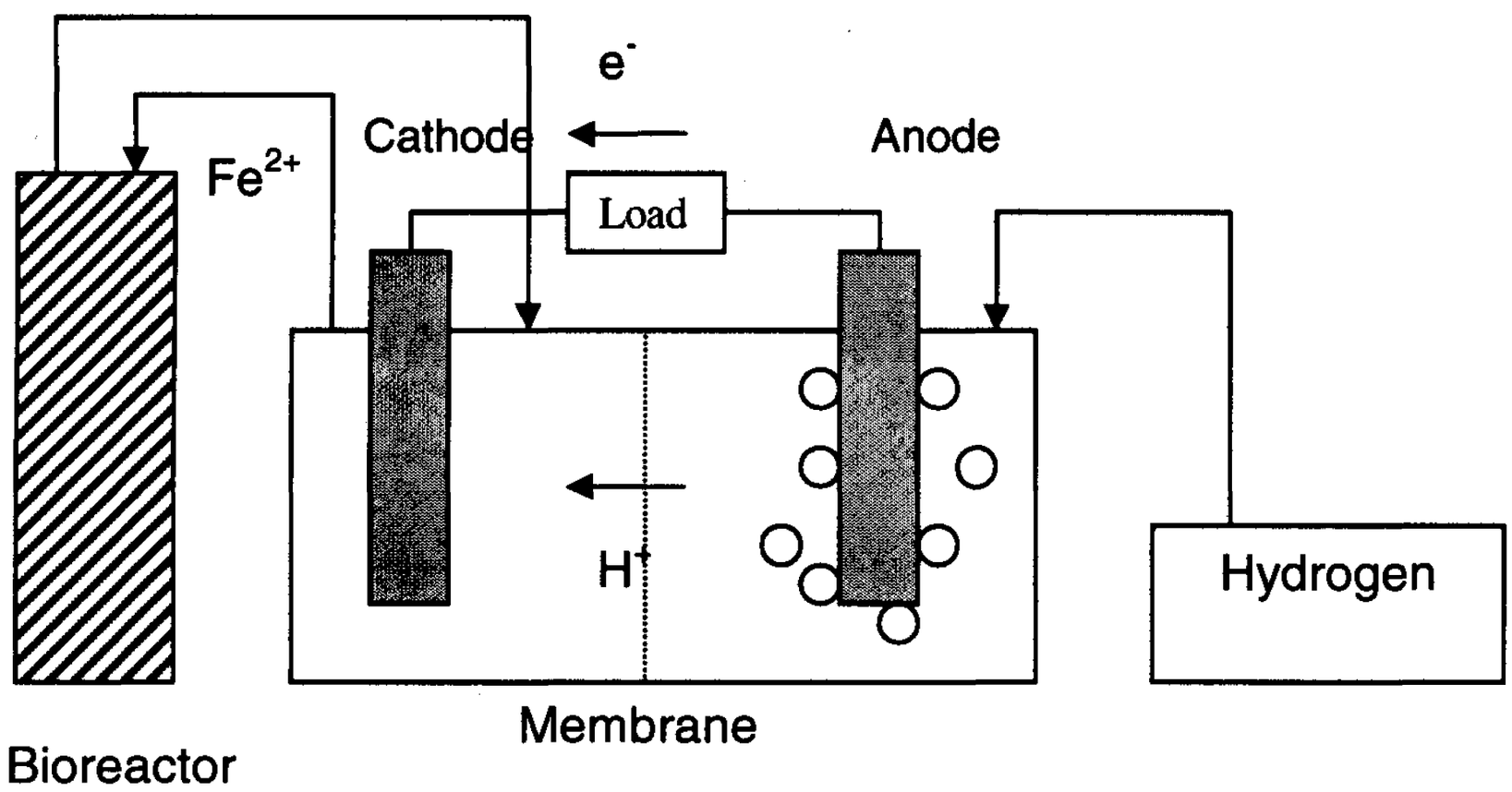

Figure 1.1 - Biofuel cell configuration

The electrochemical reactions occurring in our fuel cell are shown below:

Cathode: $Fe^{3+} + e^- \rightarrow Fe^{2+}$ (1.5)

Anode: $2H_2 \rightarrow 4H^+ + 4e^-$ (1.6)

Bioreactor: $4Fe^{2+} + 4H^+ + O_2 \rightarrow 4Fe^{3+} + 2H_2O$ (1.7)

This biofuel cell offers many advantages over its conventional counterparts. Most importantly, it eliminates the need for precious-metal catalysts, making it much cheaper.

1.3.1. Operation and Efficiency of Biofuel Cell Operation

The power of a fuel cell, P_{cell}, is the product of the cell voltage (V_{cell}) and the cell current (I_{cell}) as shown in equation 1.8.

$$P_{cell} = V_{cell} \times I_{cell} \tag{1.8}$$

There are many factors that lead to decreased values of the cell voltage such as irreversible losses in voltage (λ) as a result of kinetic limitations of the electron transfer processes at the electrode interfaces, ohmic resistances and concentration gradients (Katz et al., 2002). Equation 1.9 demonstrates the effect of these factors.

$$V_{cell} = (E_{ox} - E_{red}) - \lambda \tag{1.9}$$

Similarly, cell current is affected by the ion permeability and transport rates across the membrane separating the cathode and anode compartments.

As mentioned above, biofuel cell efficiency is the key to harnessing the maximum power that can be yielded from the electrochemical reaction. In this study, that reaction is the reduction of ferric iron at the cathode coupled with the oxidation of hydrogen gas at the anode. Biofuel cell efficiency is defined as the cell voltage obtained divided by the theoretical voltage that can potentially be derived from the electrochemical reaction. This is shown in equation 1.10.

$$\eta = \frac{V_{cell}}{E_{sol}} \tag{1.10}$$

The first step to optimizing the efficiency of the biofuel cell is to yield the maximum possible redox potential from the ferric iron solution, yielded by the bacterial oxidation of ferrous iron in the bioreactor.

The potential of the solution follows the Nernst relationship, shown in equation 1.11.

$$ORP = E_{sol} = E^o - \frac{RT}{nF}\ln\left[\frac{\mathrm{Re}d}{Ox}\right] = E^o - \frac{RT}{nF}\ln\left[\frac{Fe^{2+}}{Fe^{3+}}\right] \qquad (1.11)$$

The standard redox potential pertains to the reduction of ferric iron:

$$Fe^{3+} + e^- \rightarrow Fe^{2+}, \quad E^o = 0.77 \ mV$$

The redox potential of the solution is then increased as the ratio of Fe^{3+}/Fe^{2+} is increased. The greater redox potential leads to a greater cell voltage and thus greater efficiency. Furthermore, there are several factors that must be addressed in order to yield greater biofuel cell efficiency.

1.3.2. Factors Affecting Biofuel Cell Operation

There are a few factors that affect biofuel cell operation. Firstly, bacterial oxidation of Fe^{2+} precipitates solid ferric hydroxides known as jarosite. These solids have been known to interfere with electron transfer at the cathodic fuel cell compartment as well as clog the ferric iron flow channels. Secondly, as bacterial growth is prolonged, organics from the metabolic bacterial pathway are produced, which inhibits bacterial oxidation of ferrous iron.

1.3.3. Purpose of Research

The main goal of this research is to study the biological factors affecting biofuel cell operation. **Chapter 2** is a literature survey that covers the different types of iron-oxidizing bacteria that can be employed in the microbial fuel cell system. Also, it outlines and describes the different factors that affect biofuel cell operation, as well as the different reactor types that can be used in the system. **Chapter 3** describes the study of jarosite formation during Fe^{2+} oxidation by iron oxidizing bacterium, *Acidithiobacillus ferrooxidans*. **Chapter 4** describes the experimental work that deals with the kinetics of another iron oxidizing bacterium, *Ferroplasma acidiphilum*, which is a chemomixotrophic organism, potentially capable of controlling the organic metabolite concentration. Finally, **Chapter 5** reports a study of the continuous microbial biofuel system.

Nomenclature

E^o	Standard reduction potential, V
E_{ox}	Reduction potential of oxidized species, V
E_{red}	Reduction potential of reduced species, V
E_{sol}	Reduction potential of ferric iron solution, V
F	Faraday's constant, 6.6485309×10^4 C mol^{-1}
I_{cell}	Fuel cell current, A
n	Number of electrons transferred in the half-reaction
P_{cell}	Fuel cell power, W
R	Universal gas constant, 8.314510 J K^{-1} mol^{-1}
T	Temperature, K
V_{cell}	Fuel cell voltage, V

Greek Letters

λ	Irreversible losses in voltage
η	Fuel cell efficiency

References

Cifrain, M., & Kordesh, K. (2003). Hydrogen/Oxygen (Air) Fuel Cells with Alkaline Electrolytes. In W. Vielstich, A. Lamm & H. A. Gasteiger (Eds.), *Handbook of Fuel Cells* (Vol. 1): Wiley.

Holtappels, P., & Stimming, U. (2003). Solid Oxide Fuel Cells (SOFC). In W. Vielstich, A. Lamm & H. A. Gasteiger (Eds.), *Handbook of Fuel Cells* (Vol. 1): Wiley.

Katz, E., Shipway, A., & Willner, I. (2002). Biochemical fuel cells. In W. Vielstich, A. Lamm & H. Gasteiger (Eds.), *Hankbook of Fuel cells: Fundamentals, Technology and Applications*. Jerusalem: The Hebrew University of Jerusalem.

Vielstich, W., Lamm, A., & Gasteiger, H. A. (2003). *Handbook of fuel cells: fundamentals, technology, and applications*. Chichester, England; Hoboken, NJ: Wiley.

CHAPTER 2

LITERATURE REVIEW

In the proposed microbial biofuel cell system, the oxidant used at the cathode is ferric iron. It is in turn reduced to ferrous ions, which are regenerated by microbes in a bioreactor. There are many factors that affect the efficiency of this system such as the:

- type of microorganism(s) used in the bioreactor of the biofuel cell system,
- jarosite formation during ferric iron biooxidation,
- organic metabolite accumulation that hinders bacterial activity,
- bioreactor configuration which must ensure stable iron-oxidizing rate,
- fuel cell system and electrode material which must provide efficient iron-reduction in the fuel cell.

All these factors must be carefully analyzed and studied in order to arrive at an efficient configuration for the biofuel cell system. The aim of this chapter is to provide a thorough analysis of these factors based on past studies; this gives the foundation behind the experimental analysis described in the coming chapters.

2.1. Iron-Oxidizing Bacteria

There are several types of iron oxidizing bacteria that can be used in the biofuel cell. *Acidithiobacillus ferrooxidans* is the most well-known iron oxidizing bacterium that is found in acid mine drainage. This study utilizes *Acidithiobacillus ferrooxidans*, *Leptospirillum* sp. and *Ferroplasma acidiphilum*. *Leptospirillum* sp. is a promising bacterium, since it can operate at low pHs, thus limiting interference caused by jarosite precipitation. Further, *F. acidiphilum*, unlike the two other iron-oxidizing bacteria, is a

mixotrophic organism which utilizes organic substrates as growth factors and possible energy source. The goal is to utilize these bacteria in conjunction in order to arrive at a kinetically favorable system for the biofuel cell.

All microorganisms mentioned obtain energy from the oxidation of inorganic substances, the most common of which is ferrous sulfate. The overall biochemical reaction of the oxidation of ferrous ions is:

$$4Fe^{2+} + O_2 + 4H^+ \xrightarrow{microorganism.} 4Fe^{3+} + 2H_2O \qquad (2.1)$$

It is important to correlate factors including pH, temperature, and jarosite formation with iron oxidation. Another important factor is organic concentration, which is a result of metabolic organic compounds released by the microorganisms. This has adverse effects on cell growth and in turn iron-oxidizing capabilities. However, recent studies have confirmed the organic dependence of *F. acidiphilum*, which shares the same ecological niche as *A. ferrooxidans* and *Leptospirillum* sp. It is suggested that *F. acidiphilum*, along with the other strains, possess a symbiotic relationship in which *F. acidiphilum* controls the organic concentration while allowing maximal iron oxidation by the other strains.

Iron oxidation kinetics by *A. ferrooxidans* and *Leptospirillum* sp. has been widely studied. However, little work has been published with respect to the iron oxidation capabilities of *F. acidiphilum*. A recent study has examined the effects of temperature on the rates of iron oxidation by the mentioned microorganisms by employing the Ratkowsky equation at pH 1.6 (Franzmann et al., 2005). Equation 2.2 describes the relationship of microbial activity to temperature:

$$\sqrt{\frac{1}{Time}} = b(T - T_{MIN})(1 - e^{(c(T-T_{MAX})})} \quad (2.2)$$

Here T is the temperature, "time" is generally the generation time or the time taken to reach a specific condition, T_{MIN} is the theoretical extrapolated minimum temperature for growth, T_{MAX} is the theoretical extrapolated maximal temperature for growth, and "b" and "c" are fitting parameters (Franzmann et al., 2005).

2.1.1. *Acidithiobacillus ferrooxidans*

Acidithiobacillus ferrooxidans, recently renamed from *Thiobacillus ferrooxidans*, is a gram-negative bacterium that naturally thrives in acid mine drainage waters and is the most widely known organism in biohydrometallurgy. They are described as non-sporulating rods that are 0.5-0.6 μm wide and 1.0-2.0 μm long (Jensen & Webb, 1995). This species belong to a group of gram negative chemoautotrophic bacteria known as Thiobacilli. *A. ferrooxidans* is characterized by five properties listed in table 2.1.

Table 2.1 - Characteristics of *A. ferrooxidans*

Characteristic	*Description*
Chemolithotrophic	Oxidation of ferrous iron or reduced sulfur compounds provides energy for growth
Autotrophic	Cellular carbon source comes from carbon dioxide with nutrients for cellular growth mainly from nitrogen and phosphorous
Aerobic	Needs oxygen in order to grow
Mesophilic	An ideal temperature for growth is between 20-40 °C, with an optimum of approximately 33 °C. The oxidation and growth rates decrease dramatically above the optimum (Nemati et al., 1998)
Acidophilic	An acidic pH of 1.0-4.5 is required for bacterial growth, with an optimum between 2.0 and 2.3. Bacterial survival is ceased at pHs above 6.5 and below 1.0 (Nemati et al., 1998)

A. ferrooxidans is found naturally in acid mine drainage waters of iron and bituminous coal mines and is a dominant organism in biohydrometallurgy in the process of ore bioleaching (Jensen & Webb, 1995). Furthermore, it has been utilized in the processes of desulphurization of sour gases, treatment of acid mine drainage, and the desulphurization of coal.

Several factors including ferrous/ferric iron concentrations, cell and oxygen concentrations, pH, temperature, and reactor type have been shown to affect iron oxidation by *A. ferrooxidans*. Furthermore, studies have shown that ferric ions competitively inhibit ferrous ion oxidation by *A. ferrooxidans*; this however can be reduced by increasing cell concentration (Nyavor et al., 1996).

More importantly, pH and temperature have significant effects on the oxidation kinetics of iron by *A. ferrooxidans*. Several studies have investigated the optimum pH and temperature ranges for *A. ferrooxidans* operation.

Some findings are shown in table 2.2.

Table 2.2 - Optimum pH and Temperatures for A. ferrooxidans as reported by different sources

Source	*Optimum pH*
(D. G. Karamanev & Nikolov, 1988)	2.0
(Torma, 1977)	2.3
(Smith et al., 1988)	2.0-2.3
(Drobner et al., 1990)	2.0

Source	*Optimum Temperature (°C)*
(Ahonen & Tuovinen, 1989)	28
(Okereke & Stevens, 1991)	30
(Smith et al., 1988)	25-30
(Nemati et al., 1998)	35

Therefore, the pH and temperature at which the bacterial operation and oxidation rate are at a maximum are approximately 2.0 and 30 °C, respectively.

2.1.1. *Leptospirillum* sp.

Leptospirillum is a genus of iron-oxidizing bacteria which play an important role in industrial bioleaching and biooxidation. They comprise of two main species; *Leptospirillum ferrooxidans*, and *Leptospirillum ferriphilum.*, which share the same environmental niche. *Leptospirilla* have been found to be the primary iron-oxidizers in industrial continuous-flow biooxidation tanks. The reason for this bacterium's domination in biooxidation is most likely the fact that the high ferric-ferrous iron ratio inhibits all but species of *Leptospirillum*. *Leptospirilla* are also important contributors to the acid mine drainage process; these combine to make *Leptospirilla* more important players in the acid mine processes than previously thought.

Leptospirillum cells are Gram-negative and spiral-shaped, 0.3-0.5 microns wide and 0.9-3.0 microns in length. They share the same ecological environment as *A. ferrooxidans* and *Ferroplasma*, most popularly in Iron Mountain, California. They are some of the most metabolically-restricted organisms known. Generally *Leptospirillum sp.* have few distinct physiological characteristics which are listed in table 2.3.

Table 2.3 - Characteristics of *Leptospirillum* sp.

Characteristic	*Description*
Chemolithotrophic	Oxidation of ferrous iron or reduced sulfur compounds provide energy for growth
Autotrophic	Cellular carbon source comes from carbon dioxide with nutrients for cellular growth mainly from nitrogen and phosphorous
Aerobic	Needs oxygen in order to grow
Mesophilic	Temperature for growth is between 20-45 °C, with an optimum of approximately 40 °C. The oxidation and growth rates decrease dramatically above the optimum (Rawlings et al., 1999)
Acidophilic	More acid resistant than *A. ferrooxidans* and will grow at pH of 0.6 (Rawlings et al., 1999)

Oxidation kinetics by *Leptospirillum sp.* has been extensively studied and several important conclusions have been drawn. *Leptospirillum sp.* has been shown to tolerate higher ferric iron concentrations than its *A. ferrooxidans* counterpart. As a result *Leptospirillum* is dominant in environments that possess high ferric to ferrous iron ratio. Ferric iron concentration affects the redox potential (Rawlings et al., 1999), calculated using the Nernst equation (equation 1.11). Figure 2.1 shows the relationship between ferrous iron consumption rate and redox potential of the solution. It is quite clear that *Leptospirillum sp.* enjoys a much higher redox potential than *A. ferrooxidans*.

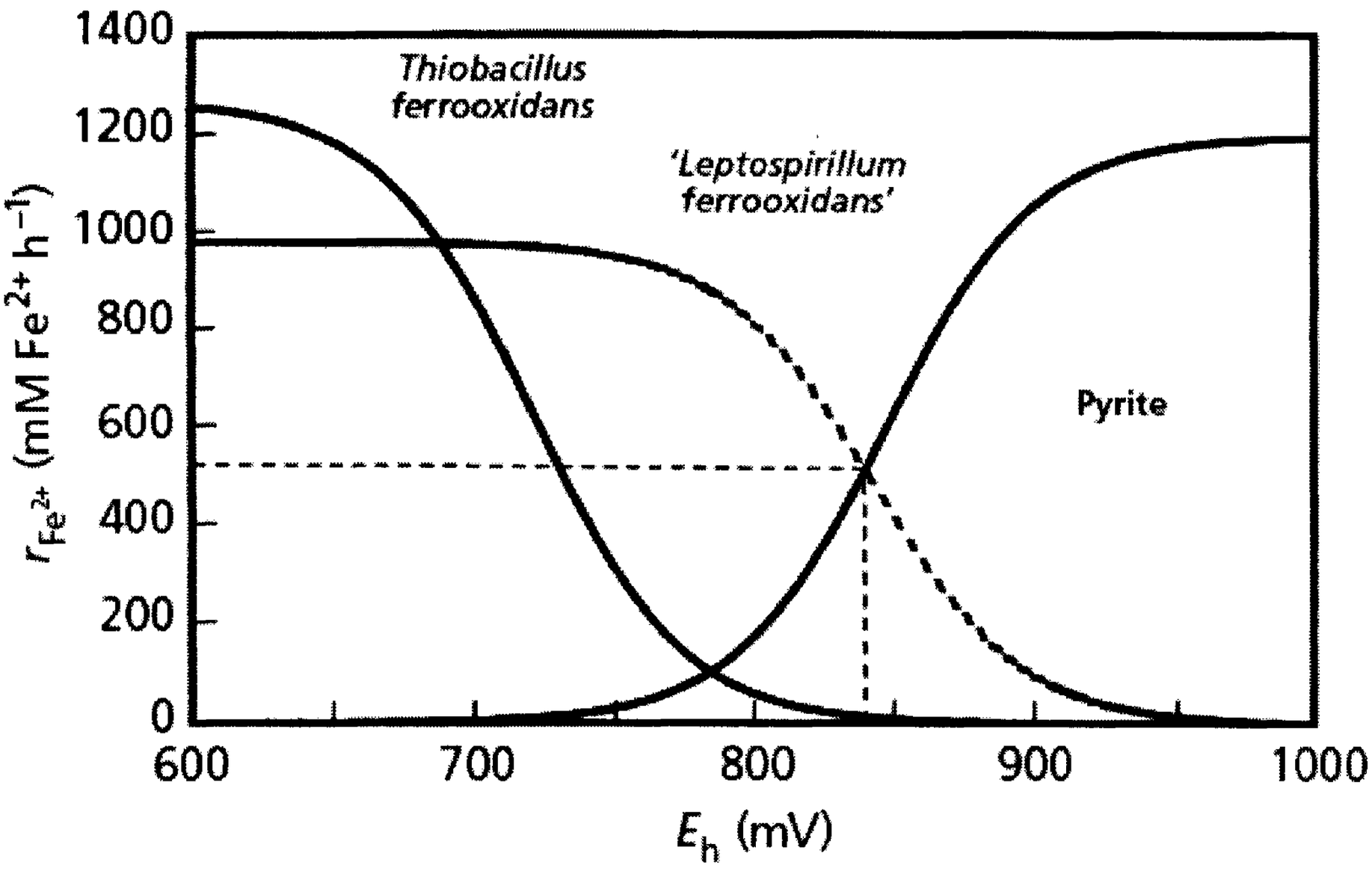

Figure 2.1 - Iron oxidation rate of pyrite vs. redox potential for *A. ferrooxidans* and *Leptospirillum sp.* *(Rawlings et al., 1999)*

As discussed earlier, it is crucial for the biofuel cell solution entering the cathode to possess a high redox potential in order maximize the cell voltage and thus generate

more power. Therefore, *Leptospirillum* sp. is a promising microorganism to be employed in the biofuel cell system.

2.1.2. Ferroplasma acidiphilum

F. acidiphilum is generally found in acidic mine tailings, primarily those containing pyrite (FeS_2). It is especially abundant in cases of severe acid mine drainage, where other organisms such as *Acidithiobacillus* and *Leptospirillum* have lowered the pH of the environment such that the obligate acidophilic *F. acidiphilum* is allowed to flourish.

This microorganism is an Achaea of the genus *Ferroplasma*. There are four known strains of *Ferroplasma* isolated from various environments:

- *Ferroplasma acidarmanus*, strain Fer1, found in Iron Mountain, California (Edwards et al., 2000).
- *Ferroplasma acidiphilum*, strain Y^T, is isolated from a pilot plant bioreactor for biooxidation of a gold-bearing aresenopyrite-pyrite concentrate (Golyshina et al., 2000).
- *Ferroplasma* strain MT17, isolated from a South African pilot scale bioleaching reactor oxidizing a polymetallic sulfide concentrate at 45 ^oC (Okibe et al., 2003).
- *Ferroplasma* strain DR1, cultured from a separate pilot scale biooxidation plant in South Africa (Dopson et al., 2004).

There have been many studies conducted using strains MT17, DR1 and Fer1. However, apart from the studies of (Golyshina et al., 2000)., little work has been done in analyzing strain Y^T, specifically the iron oxidation nature of the strain. In this study, we will further evaluate the kinetics and optimal growth characteristics of strain

Ferroplasma acidiphilum Y^T. Strain Y^T possesses pleomorphic morphology with phenotypic characteristics summarized in table 2.4.

Table 2.4 - Characteristics of *Ferroplasma acidiphilum*

Characteristic	*Description*
Chemomixotrophic; chemoorganotrophic	Capable of oxidizing inorganic compounds such as ferrous iron or reduced sulfur to provide energy for growth. Also able to use organic compounds (i.e. yeast) as energy sources (Dopson et al., 2004).
Autotrophic*	There are conflicting results regarding the cellular carbon source.(Golyshina et al., 2000) report autotrophic behaviour, utilizing carbon dioxide as the sole carbon source. However, the strain has also been shown to possess a low organic carbon requirement (Dopson et al., 2004).
Aerobic/Anaerobic	Capable of growing in the presence or absence of oxygen (Dopson et al., 2004).
Mesophilic	An ideal temperature for growth is between 15-45 °C, with an optimum of approximately 35 °C (Golyshina et al., 2000).
Acidophilic	pH growth range is between 1.3-2.2, with an optimum of 1.7 (Golyshina et al., 2000).

*Conflicting results

There have been mixed reports regarding the organic-dependent nature of *F. acidiphilum* (Dopson et al., 2004). Therefore, it is crucial to analyze the effects of organic concentration on the growth and iron oxidizing capabilities of *F. acidiphilum*. It is also vital to study the growth kinetics in the presence of its phenotypically similar strains, *Leptospirillum sp.* and *A. ferrooxidans*, as well as the redox potential of *F. acidiphilum* as compared to the other stains of iron-oxidizers.

2.2. Jarosite Formation

As mentioned before, the three iron-oxidizing bacteria described oxidize iron via reaction 2.1. It is clear that due to hydrogen ion consumption, the pH of the solution

initially increases. However, as ferric iron accumulates, it undergoes a series of hydrolysis reactions, which thereby decrease the pH. This is shown in reactions 2.3-2.5.

$$Fe^{3+} + H_2O \Leftrightarrow FeOH^{2+} + H^+ \tag{2.3}$$

$$Fe^{3+} + 2H_2O \Leftrightarrow Fe(OH)_2^+ + H^+ \tag{2.4}$$

$$Fe^{3+} + 3H_2O \Leftrightarrow Fe(OH)_3 + H^+ \tag{2.5}$$

Therefore, it is clear that pH plays a vital role on the extent of the oxidation and hydrolysis reactions. More importantly, there is a reaction in competition with the hydrolysis reaction that produces solid ferric hydroxysulphates, known as jarosite. The chemical formula for jarosite is $MFe_3(SO_4)_2(OH)_6$, where $M=K^+$, Na^+, NH_4^+, Ag^+, or H_3O^+ (Jensen & Webb, 1995). Equation 2.6 shows the formation of jarosite.

$$3Fe^{3+} + M^+ + 2HSO_4^- + 6H_2O \rightarrow MFe_3(SO_4)_2(OH)_6 + 8H^+ \tag{2.6}$$

Since these iron oxidizing microorganisms are usually cultured in 9K medium developed by Silverman and Lundgren (Silverman & Lundgren, 1959) in a laboratory setting, there is a high concentration of NH_4^+ ions. Therefore, it is safe to conclude that jarosite produced in laboratory experiments are mostly ammoniojarosites with the formula $NH_4Fe_3(SO_4)_2(OH)_6$.

Jarosite formation has adverse effects on many applications such as biological gas desulphurization. Some of the effects include the blockage of pumps, valves, pipes, etc, and the creation of kinetic barriers due to the small diffusion of reactants and products through the precipitation zone (Jensen & Webb, 1995).

In biofuel cell applications, jarosite formation interferes with fuel cell stability, electron transfer, and electrolyte operation in the cathode electrode. Furthermore, the solid precipitate hinders the flow of ferric iron fuel through the flow channels. Therefore,

minimization of jarosite precipitation can lead to better fuel cell operation and efficiency, further prolonging the electrode life and power generation.

As mentioned above, due to the abundance of NH_4^+ ions in the 9K medium, the jarosite produced in laboratory experiments most closely correspond to ammoniojarosites with the chemical formula $NH_4Fe_3(SO_4)_2(OH)_6$.

A recent study has been conducted in order to characterize the composition of different types of jarosite produced biologically by using X-ray diffraction. It was found that ammoniojarosite has an elemental weight composition of 14.6% NH_4^+, 29.1% Fe, and 11.2% S (Sasaki & Konno, 2000).

Jarosite formation is a very important phenomenon that need be investigated when assembling the microbial biofuel cell system. Jarosite accumulation has been shown to impede the electron transfer capabilities of electrodes as well as disrupt flow channels in the fuel cell. Minimizing the occurrence of jarosite, while maintaining a high oxidation rate of ferric iron in the bioreactor, is vital in ensuring efficient fuel cell operation. Thus, this phenomenon must be carefully analyzed in order to arrive at operating conditions that provide maximal bacterial oxidation rates while yielding minimum jarosite precipitation.

2.3. Organic Metabolites

A major factor that hinders bioreactor and fuel cell efficiency alike is the accumulation of organics. These organics arise as the iron oxidizing organisms in the biofuel cell system excrete some of their metabolites or simply release them as biomass accumulates and cells die. This high organic accumulation is believed to repress the ribulose diphosphate (RuDP) carboxylase enzyme, which is responsible for carbon

dioxide fixation (Tabita & Lundgren, 1971). This inhibitory effect occurs at a certain threshold concentration reported to be equal to or above 250 ppm total organic carbon, TOC (Drogui et al., 2003).

For the bioreactor used in this study, the metabolic pathways of the chemolithotrophic iron-oxidizing bacteria (*A. ferrooxidans* and *Leptospirillum* sp.) appear to be fairly standard. The bacteria possess a Calvin cycle, an N_2-fixation pathway, possibly a hexose monophosphate pathway, glycolytic enzymes and an incomplete citric acid cycle. Aconitase, isocitrate dehydrogenase, fumarase and malic dehydrogenase are present but succinate and α-ketoglutarate dehydrogenase activities are very low.

Incomplete citric acid cycles are a feature of chemolithotrophs and this is thought to be because the cycle is directed towards providing carbon skeletons for the synthesis of amino acids rather than functioning as a catabolic pathway (Ingledew, 1982). Succinate is necessary for some important anabolic reactions (haem, methionine and lysine biosynthesis) and it is not clear how this compound can be formed unless it is by reduction of fumarate. Furthermore, poly(β-hydroxybutyrate) has been reported as being a major storage product. The metabolic skeleton is shown in figure 2.2.

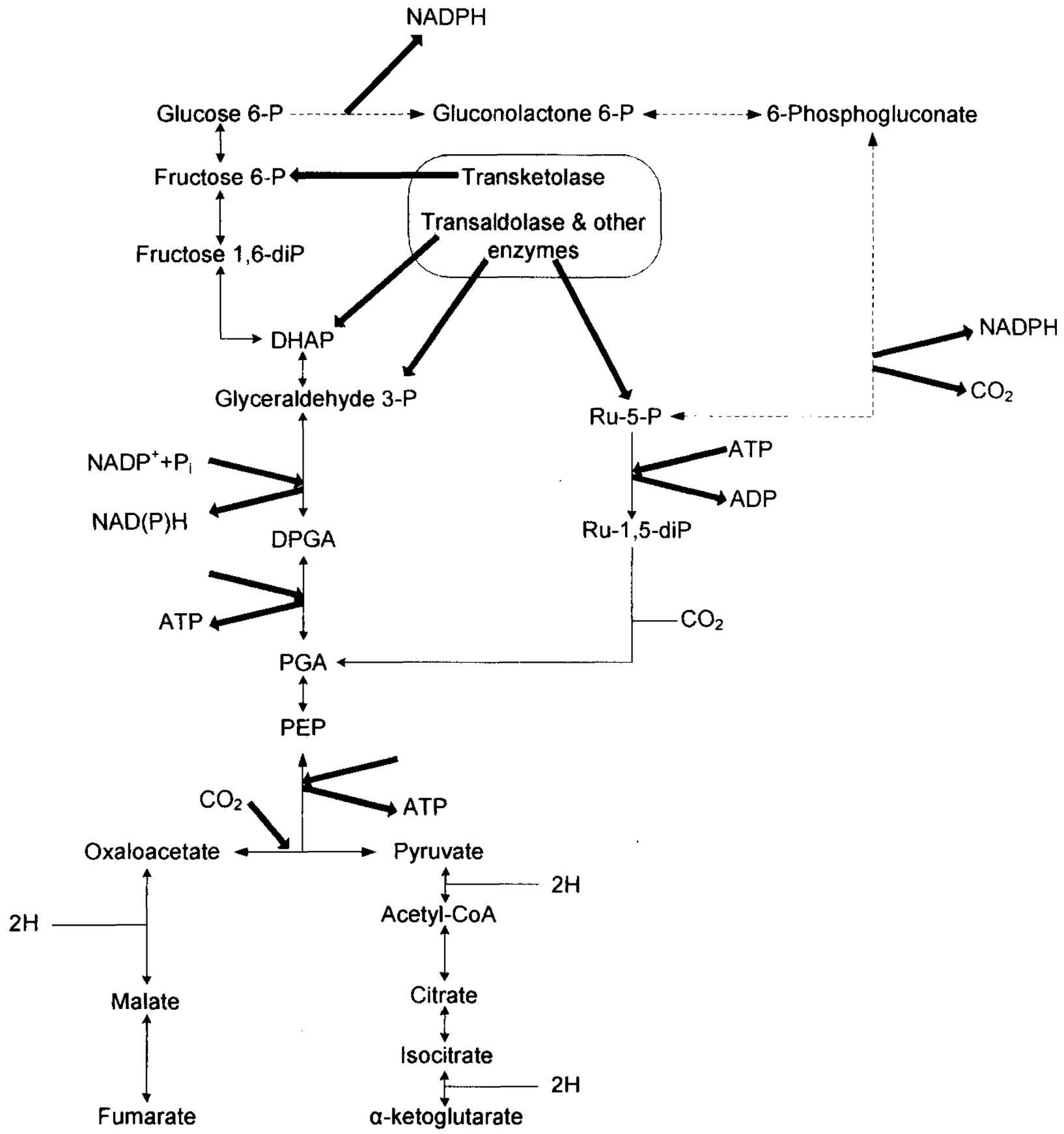

Figure 2.2 - Metabolic skeleton of chemolithotrophic iron-oxidizing bacteria (Ingledew, 1982)

In the microbial biofuel cell system, the accumulation of these organics poses adverse effects on the bioreactor viability and long-term stability. Organics, whether arising from metabolic waste or dead biomass, lead to slower bacterial growth and eventually diminish the oxidation capabilities of the microbes in the system. A slower oxidation of iron in the bioreactor translates into a slower reduction in the cathodic compartment of the fuel cell. This in turn leads to a lower current and power generation, thus decreasing the fuel cell efficiency. It is thus important to study mixotrophic microorganisms that rely on simultaneous iron-oxidation and organic consumption for

metabolism and thrive under acidophilic environments with other iron-oxidizing bacteria, such as *F. acidiphilum*. Such studies would provide promising insight into controlling the organic concentration in the biofuel cell system.

2.4. Bioreactor Configuration

The bioreactor is a vital unit of the microbial biofuel system. Firstly, the bioreactor must maintain a high oxidation rate of ferrous iron in order to maintain a steady rate of reduction of ferric iron in the cathodic compartment of the fuel cell. This in turn will yield a high, constant current, voltage and power generation. Secondly, the reactor must allow for maintenance of a maximal biomass concentration and ferrous iron oxidation rate while ensuring minimal jarosite precipitation; this is heavily dependent on sustaining constant and favorable operating conditions. Table 2.5 shows the different kinetic data associated with the reactor types in which iron oxidation occurs.

Table 2.5 - Iron oxidation kinetics in different reactor configurations

Reactor Type	*Iron Oxidation rate g Fe^{2+} L^{-1} h^{-1}*	*Reference*
Inverse fluidized-bed reactor	1.3-1.7	(D. Karamanev, 1991); (D. G. Karamanev & Nikolov, 1988)
Rotating biological contactor	0.3	(Olem & Unz, 1977)
Circulating-bed	1.6	(Armentia & Webb, 1992)
Reaction cell	6	(Nemati & Webb, 1997)
Shake flask	0.2	(Armentia & Webb, 1992)
Agitated reactor	1.2	(Breed & Hansford, 1999)

It is important to note that efficiency studies in a bioreactor setting that is continuously regenerated with ferrous ions have not been analyzed. Moreover, it is vital for fuel cell systems to provide a substrate that is free from solid particulates, such as jarosite, and organics, which pose problems for the microbes as well as the reduction

efficiency at the cathode. These byproducts are continually accumulated by microbial iron oxidation.

It is recommended to use an agitated reactor with a bubble reactor type configuration due to its design flexibility and high oxidation rates. This will also give a thorough analysis of the jarosite accumulation and further limiting factors.

2.5. Fuel Cell

An important aspect of the microbial biofuel cell system is the fuel cell itself. The cathode material has to be carefully selected in order to ensure maximum reduction efficiency which in turn gives better fuel cell operation. Given the byproducts of iron oxidation, which hinder the mass transfer characteristics of the electrode, it is vital to work with a material that provides maximal mass transfer.

In order to efficiently produce current, there is a need to have maximum mass transfer between the species to be reduced and the cathode electrode. Therefore, the study of porous electrodes is a matter of increasing interest (Carta et al., 1991). In this study, carbon felt is used as the cathode electrode, since it has provided promising results (Oren & Soffer, 1983) owing to its favorable physico-chemical characteristics: high chemical stability, large specific surface area, good fluid permeability and high electric conductivity, together with continuity of the electronic contact throughout the electrode (Carta et al., 1991).

A more important aspect of carbon felt is its mass transfer characteristics, which influence the rate of reduction at the cathode electrode and in turn affects current flow and fuel cell efficiency. It is important to further study the mass transfer characteristics of

carbon felt electrodes and compare them with those of other alternative electrode materials.

There are many geometric configurations and materials that are commonly used as electrode material. All these configurations are assessed in a flow-by mode (the current flow is perpendicular to that of the electrolyte), namely bundles of loose fibres with liquid flow parallel to the fibres, carbon cloth with flow parallel to the cloth and carbon felt with liquid flow through the felt (Schmal et al., 1986). In summary, the configurations which will be studied in the flow-by mode are:

i) Bundles of carbon fibres with liquid flow parallel to the fibres.

ii) Cloth, woven of carbon fibre yarn, with liquid flow parallel to the cloth.

iii) Felt made of carbon fibres with liquid flowing through the felt in the longitudinal direction.

To gain a better understanding of the mass transfer characteristics of all the configurations, all studies and results assumed that solution flows through the material at a steady uniform velocity and that no back-mixing takes place (plug flow) (Schmal et al., 1986). The mass transfer characteristics of these alternatives, and the suitability of carbon felt as the most suitable electrode material will now be investigated.

A popular tool for comparing electrodes is the polarization curve, which plots current versus electrode potential. This is used in order to obtain the limiting current of the electrode at the specified conditions. As the current density increases, there can be polarization when the ions are transported faster across the electrodes than are transported in the cell solutions to the electrode surface: this results in a very quick cell voltage increase. The "limiting current" is the maximum allowed current density to avoid this

steep cell voltage increase (Vatistas et al., 1991). Furthermore, All the studies investigated deal with the reduction of ferric ions in the cathodic electrode in a flow-by mode using limiting current conditions, and thus the mass transfer data in flow systems are represented in the form $Sh = (const)\mathrm{Re}^{\alpha}\, Sc^{\beta}$ (Carta et al., 1991).

2.5.1. Carbon Fibre

The first configuration to be analyzed is the carbon multi-fibre configuration as shown in figure 2.3. The fibres are arranged in parallel bundles with parallel fluid flow. Figure 2.4 shows some polarization curves for bundles of 200 000 fibres at various flow rates.

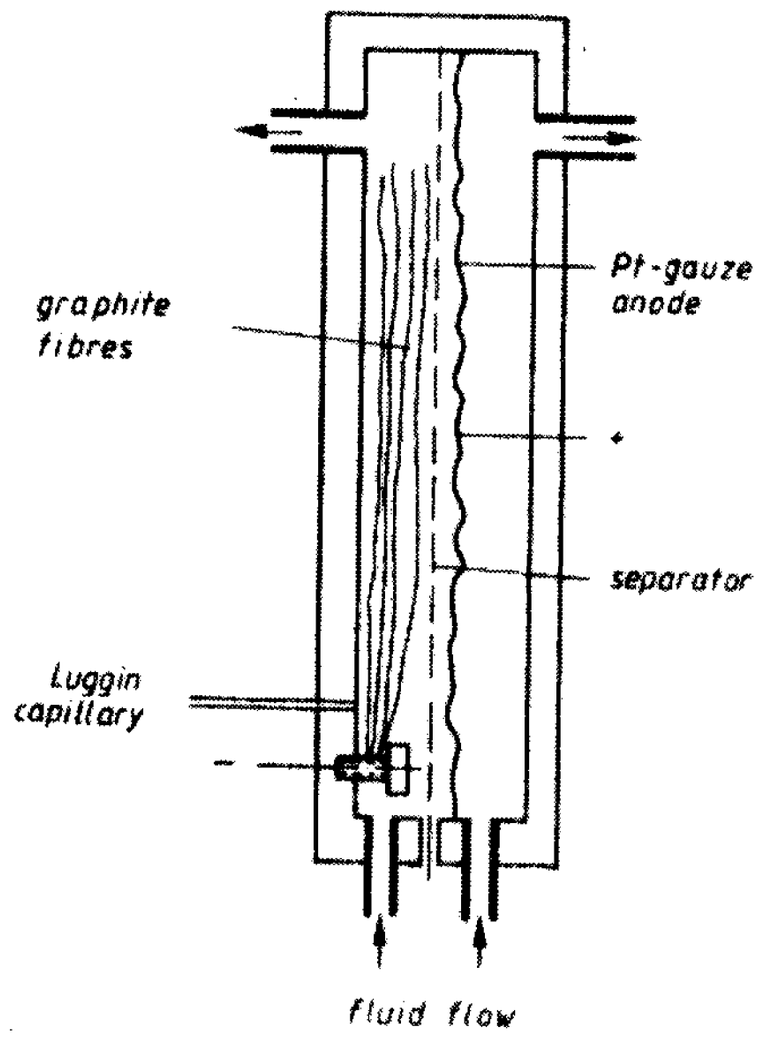

Figure 2.3 - Multi-fibre cell configuration (Schmal et al., 1986)

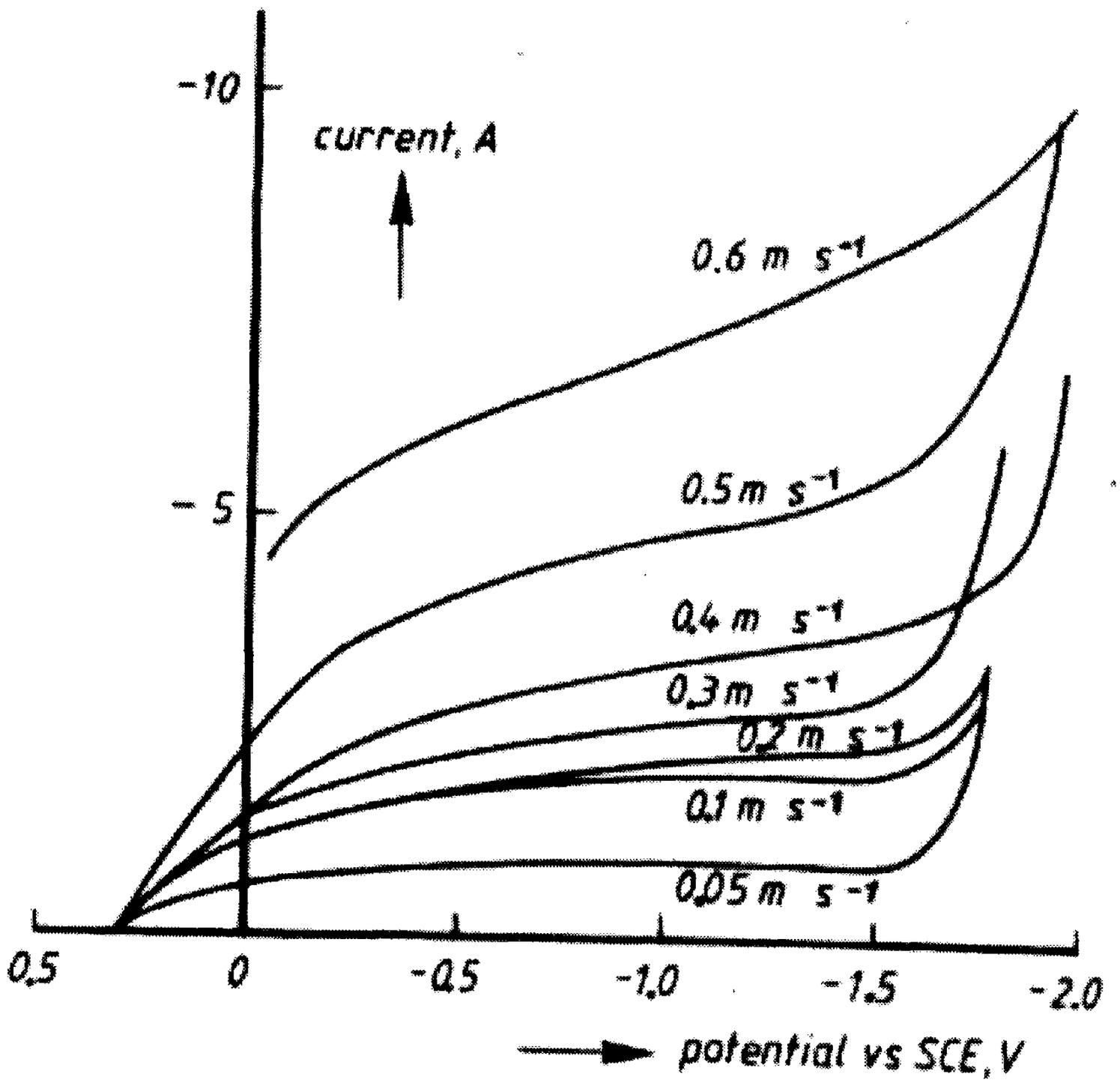

Figure 2.4 - Polarization curves for bundles of 200 000 fibres at various flow rates (Schmal et al., 1986)

This reveals that although the current is not constant at higher flow rates, most of the electrode is operating under limiting current conditions (Schmal et al., 1986). The relation between Sh and Re for the data measured at velocities up to 0.02 ms^{-1} is given below.

$$Sh = 7\,\mathrm{Re}^{0.4} \quad (0.04 \le \mathrm{Re} \le 0.2) \tag{2.7}$$

Figure 2.5 shows the mean characteristic length, λ, values calculated from measured concentrations plotted as a function of flow rate for different geometric configurations (with electrode length of 8.3 cm). The mean characteristic length of the electrode is a good indication of its mass transfer capabilities; an increase in the surface area of the electrode should lead to a decrease in λ. It can be seen that the increase in the

number of fibres in a bundle and thus in electrode surface area has relatively little influence on mass transfer: a 50-fold increase in specific surface area causes λ to decrease by a factor of only about 3 (Schmal et al., 1986). Therefore, most of the fibres do not take part in the reaction, owing to the flow between the parallel fibres being non-uniform and proceeding in preferred stream patterns (channeling) (Schmal et al., 1986).

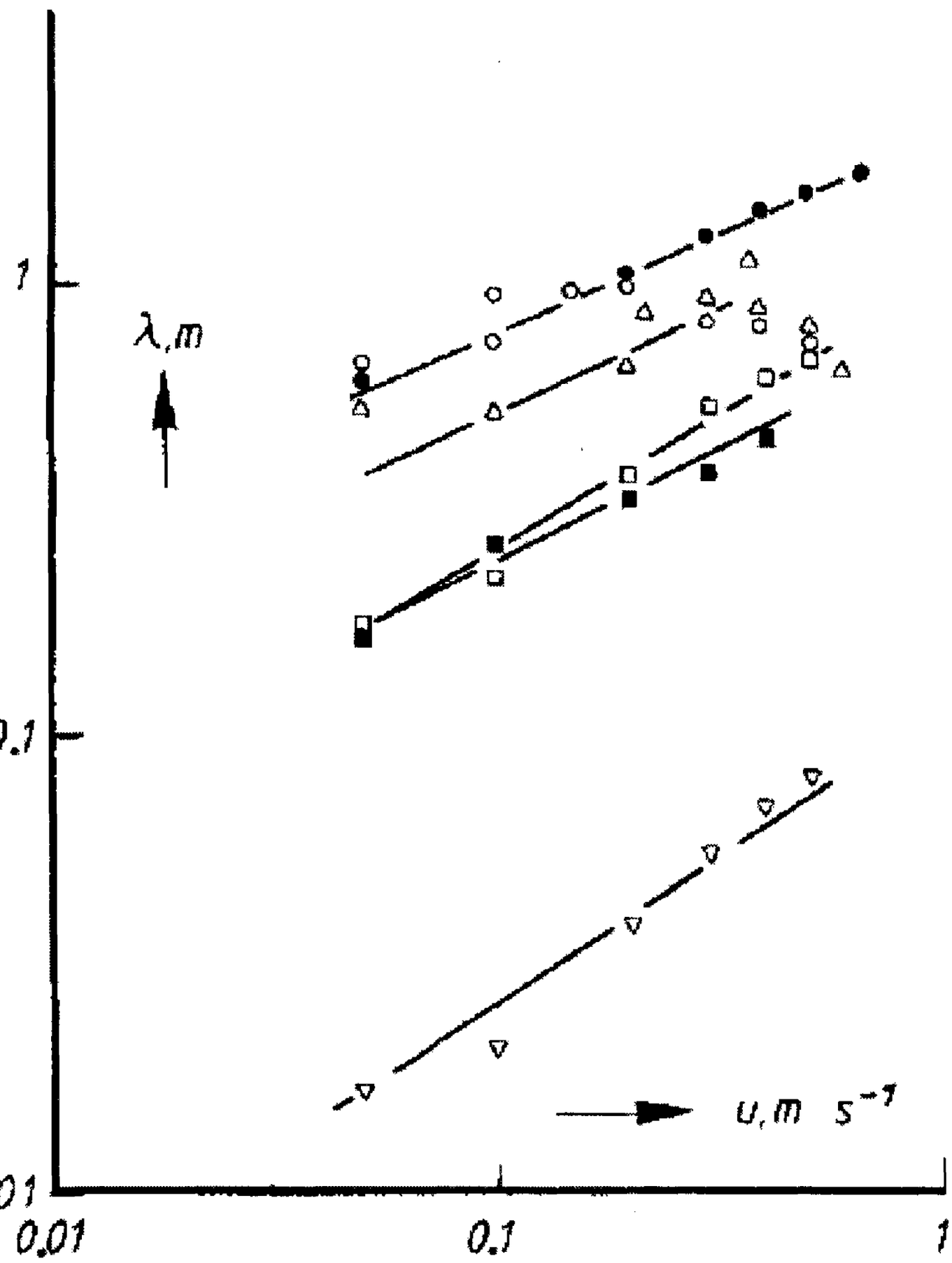

Figure 2.5 - Mean characteristic length as a function of electrolyte flow rate for different configurations: ● 10 000 fibres, ○ 50 000 fibres, Δ 200 000 fibres, □ 500 000 fibres (Schmal et al., 1986)

2.5.2. Carbon Cloth

Recently, the use of cloth fibres as electrodes was considered (Schmal et al., 1986). This is due to the fact of the use of the material in the production of light weight reinforced plastics and of the availability of this inexpensive material. Only until recently, studies on the mass transfer between a flowing liquid and a carbon cloth were conducted.

Carbon cloths are composed of long carbon fibres, 5 to 7 μm in diameter joined together in a woven bundle. As in traditional weaving there are several ways to set the bundles. Commonly, there are 2 modes of carbon cloth used; 'cloth' type (cloth 3257) and 'serge' type (cloth 3872), which are shown in figure 2.6.

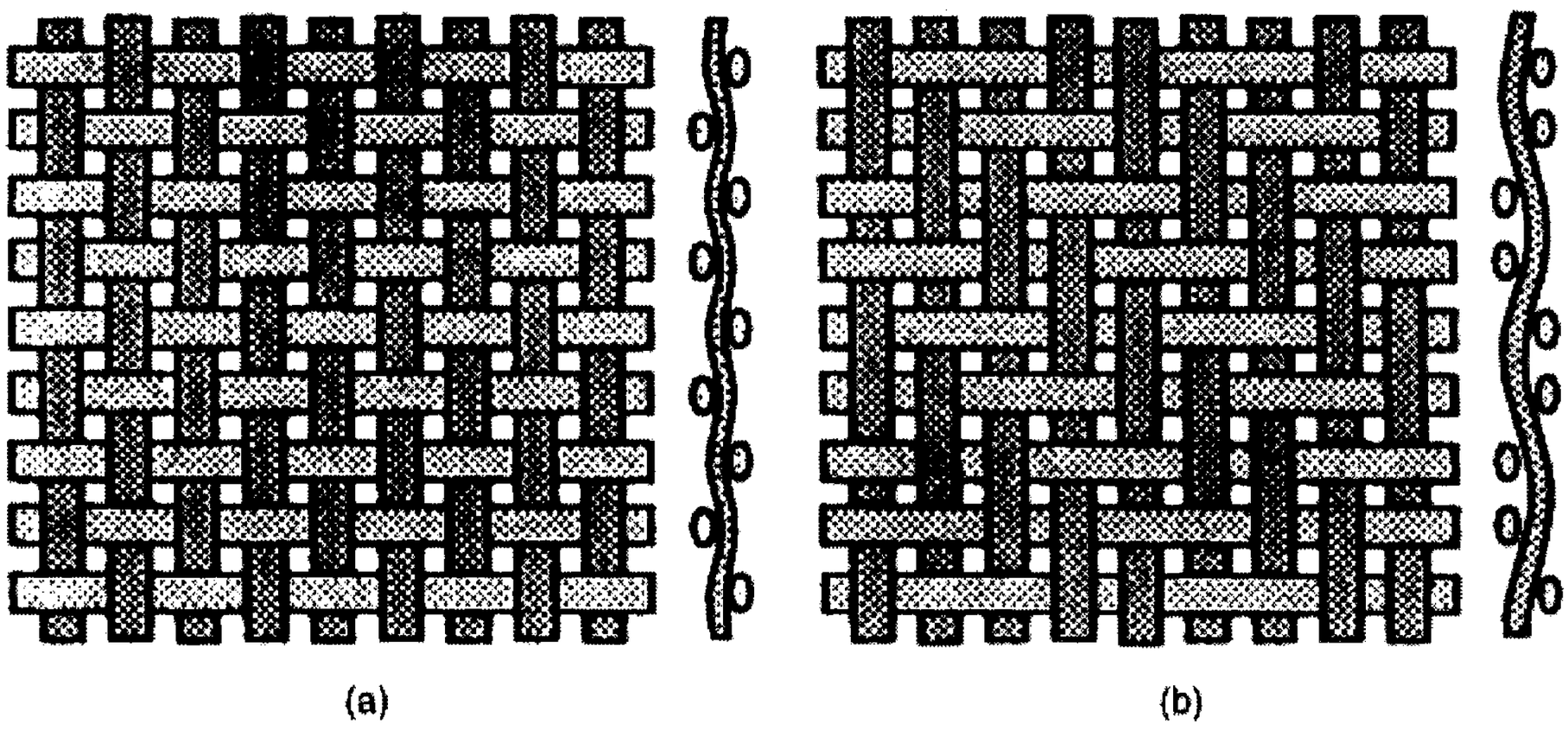

Figure 2.6 - 'cloth' type carbon cloth (a) and 'serge' type carbon cloth (b) (Coeuret et al., 2002)

'Cloth' type contains approximately 48000 fibres per bundle while 'serge' type contains 3000 fibres per bundle (Coeuret et al., 2002). Mass transfer studies of carbon cloths produced the following relationship between Sh and Re:

$$\overline{Sh} \cdot Sc^{-1/3} = 0.38\,\mathrm{Re}^{0.76} \quad (10 \le \mathrm{Re} \le 1000) \tag{2.8}$$

Figure 2.7 (a) and (b) show the polarization obtained with the cloth type and serge type carbon cloths in flow-by mode. These results indicate that even the smallest flow

velocities were sufficiently high to ensure that the reaction current at the external surface of the cloth was larger that the reaction current corresponding to the inner surface of the bundles (Coeuret et al., 2002).

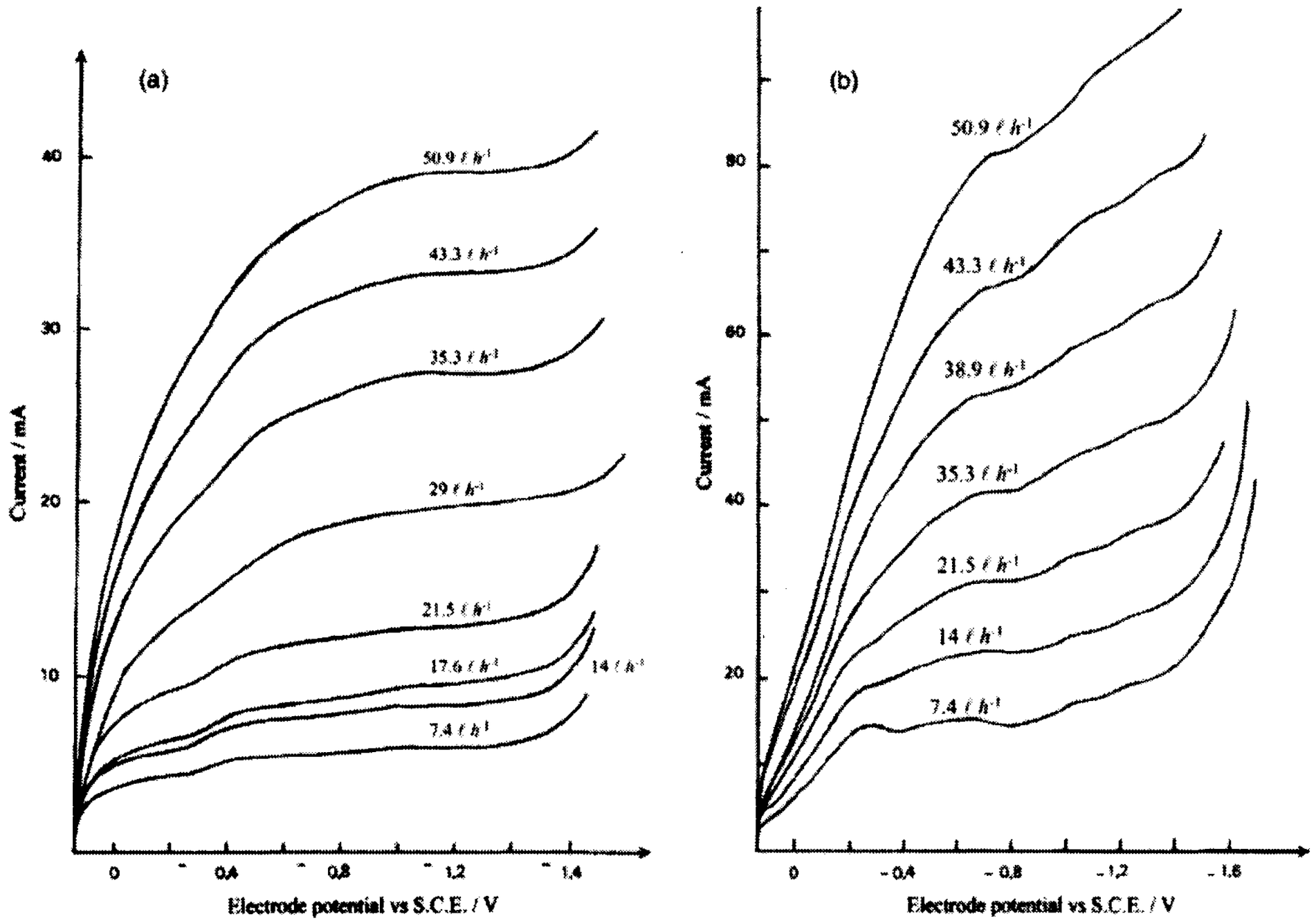

Figure 2.7 - Polarization curve obtained in flow-by mode of (a) cloth type and (b) serge type (Coeuret et al., 2002)

Even if they are made of long fibres, carbon cloths do not possess good electrode properties owing to the existence of double porosity, and electrical conduction problems (Coeuret et al., 2002). The structure of the bundles prevents percolation by the electrolyte; the movement of electroactive species into or out of the bundle is due essentially to molecular diffusion (Coeuret et al., 2002). Thus, the apparent surface area (projected area) can only be considered as an active electrode area, hence the use of such a material is not recommended as an electrode (Coeuret et al., 2002).

Therefore, it can be concluded that the mass transfer for fibre bundles and cloth under comparable conditions is much lower owing to channeling (Schmal et al., 1986).

2.5.3. Carbon Felt

Carbon felt as an electrode material, is used in a flow-by configuration under limiting current conditions. Such an arrangement (with the current flow perpendicular to that of the electrolyte) has been adopted to allow the use of an electrode that is thin in the current direction and long in the flow direction so that a high product conversion is achieved and a more or less uniform distribution of the potential inside the reactor is maintained (Storck et al., 1982).

Figure 2.8 shows a scanning electron microscope image of carbon felt as an anisotropic texture of cylindrical fibres furrowed by shallow grooves.

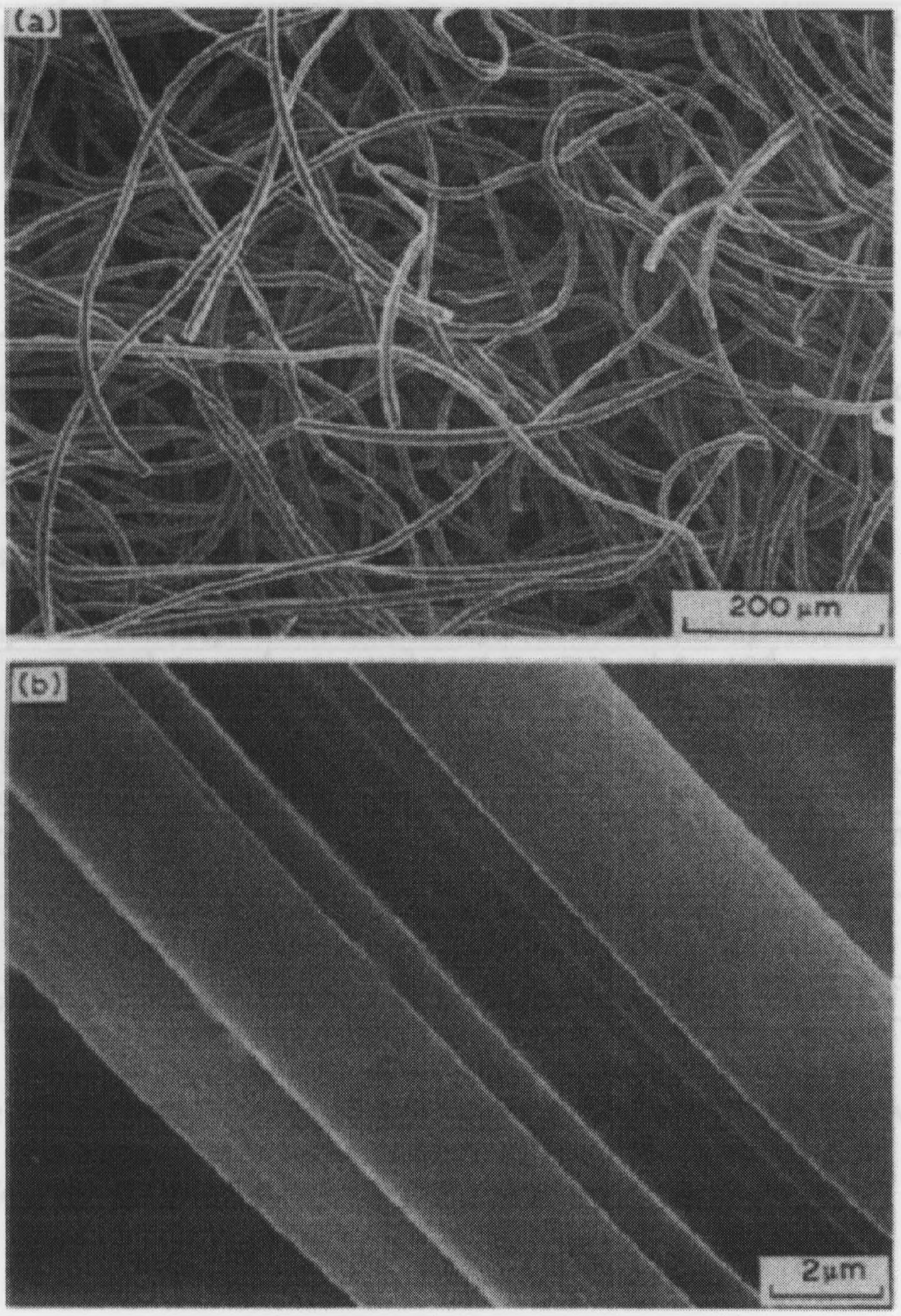

Figure 2.8 - Scanning electron micrographs for carbon felt: (a) material texture; (b) details of the fibre (Carta et al., 1991)

No significant microporosity was detected in the fibres (Carta et al., 1991). The overall porosity, θ, was calculated as $\theta = (\rho_R - \rho_A)/\rho_R$ where ρ_R is the true density of a common felt sample used in laboratory experiments, and ρ_A is the apparent density. The physical properties of carbon felt are summarized in table 2.6.

Table 2.6 - Physical properties of the carbon felt (Carta et al., 1991)

Fibre diameter	d_f	$(11.0 \pm 0.5) \times 10^{-6}$ m
Apparent density	ρ_A	122 kg m^{-3}
True density	ρ_R	2100 kg m^{-3}
Porosity	Θ	0.94

Most studies conducted on carbon felt involve the reduction of ferricyanide ions and cupric ions, which closely resemble the ferric sulfate used in this study. The characteristics of these electrolytes are summarized in table 2.7.

Table 2.7 - Composition and properties of the electrolyte (Carta et al., 1991)

Composition	$5 \times 10^{-4} - 2 \times 10^{-3}$ M $K_3Fe(CN)_6$ 0.1 M $K_4Fe(CN)_6$ 1 M KNO_3	$5 \times 10^{-4} - 1 \times 10^{-3}$ M $CuSO_4$ 0.1 M H_2SO_4
Kinematic viscosity	$v = 0.914 \times 10^{-6}$ m^2 s^{-1}	$v = 1.024 \times 10^{-6}$ m^2 s^{-1}
Diffusion coefficient of relevant ions	$D = 7.6 \times 10^{-10}$ m^2 s^{-1}	$D = 7.5 \times 10^{-10}$ m^2 s^{-1}
Conductivity	$\gamma_o = 8.8$ Ω^{-1} m^{-1} $\gamma = 8.1$ Ω^{-1} m^{-1}	$\gamma_o = 9.2$ Ω^{-1} m^{-1} $\gamma = 8.4$ Ω^{-1} m^{-1}
Schmidt number	1203	1365

Figure 2.9 shows a few typical current-potential, or polarization, curves at steady state for the flow-by carbon felt electrode in ferric ion solution.

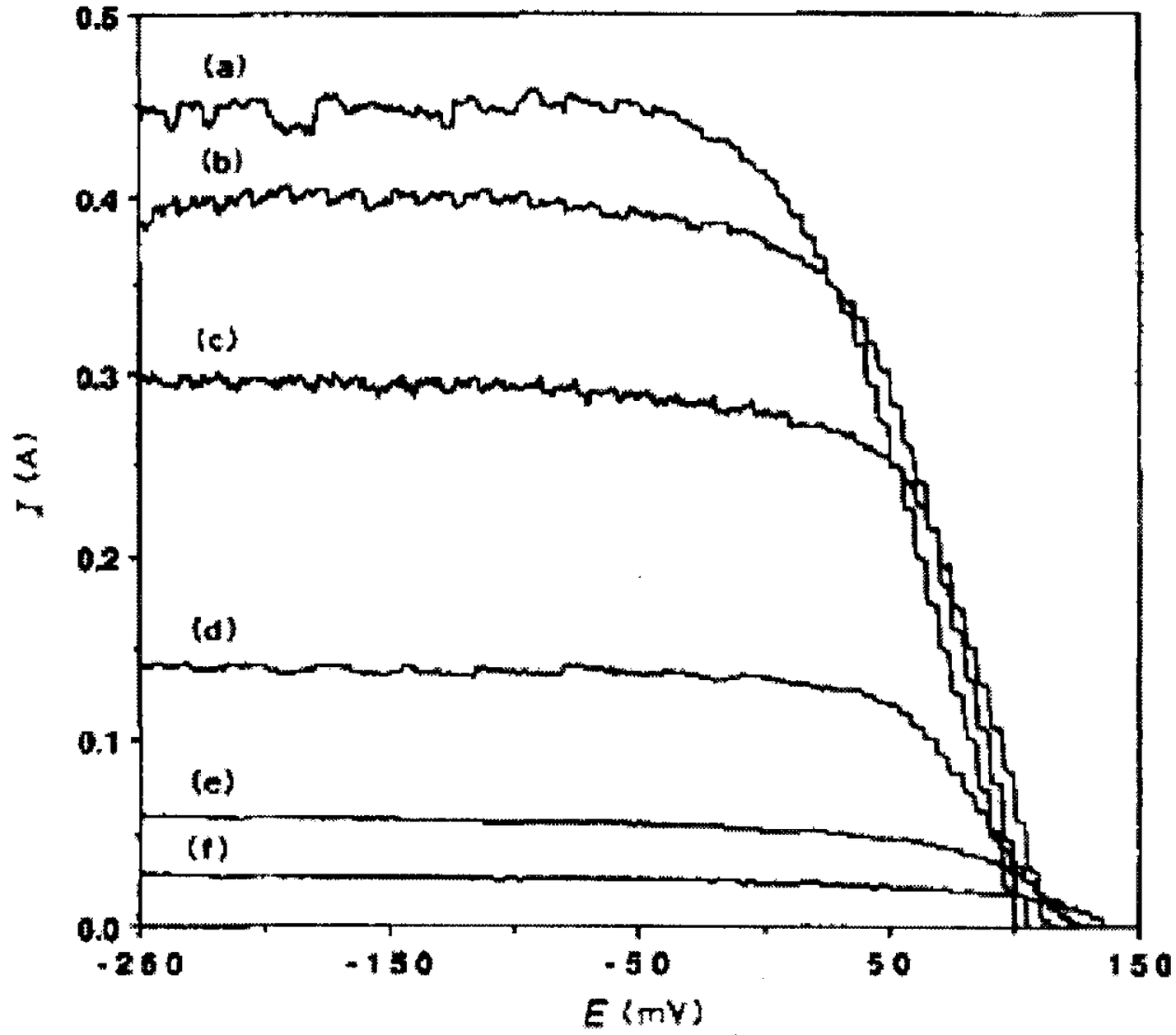

Figure 2.9 - Polarization curves for the reduction of ferricyanide ions in solution of $2x10^{3}$ M $K_3Fe(CN)_6$, 0.1 M $K_4Fe(CN)_6$, 1 M KNO_3 at several electrolyte velocities, u: (a) $8.1x10^{-2}$; (b) $5.8x10^{2}$; (c) $3.7x10^{-2}$; (d) $1.3x10^{-2}$; (e) $0.55x10^{-2}$; (f) 0.39x10-2 ms^{-1} (Carta et al., 1991).

The curve gives a well defined value of the limiting current (I_{lim}) so that the reaction conversion, X, can be obtained from the following limiting current equation (given a faradic efficiency of one).

$$X = \frac{I_{\lim}}{nFQ_L C_{in}} \tag{2.9}$$

where Q_L is the electrolyte flow rate and C_{in} is the initial concentration of electrolyte.

Furthermore, the cathodic reduction can be expressed in terms of conversion using the following equation.

$$X = \frac{C_{in} - C_{out}}{C_{in}} \tag{2.10}$$

where C_{out} is the final concentration of electrolyte in the cathodic compartment of the fuel cell. From the values of X the effective mass transfer coefficient is calculated as (Newman, 1976):

$$ak_m = -\frac{u}{l}\ln(1-X) \tag{2.11}$$

where 'a' is the specific electrode area, 'u' is the linear velocity of the electrolyte and 'l' is the length of the electrode.

Figure 2.10 shows the ak_m values for the reduction of ferric and cupric ions. At higher velocities, the data for both systems agree well, show only a small scatter and do not depend on the electrode length (Vatistas et al., 1991). Therefore beyond 0.5 x 10^{-2} m s^{-1} plug flow conditions are actually verified and equation 2.11 gives the true mass transfer coefficient from the bulk of the solution in the pores to the fibre surface (Carta et al., 1991).

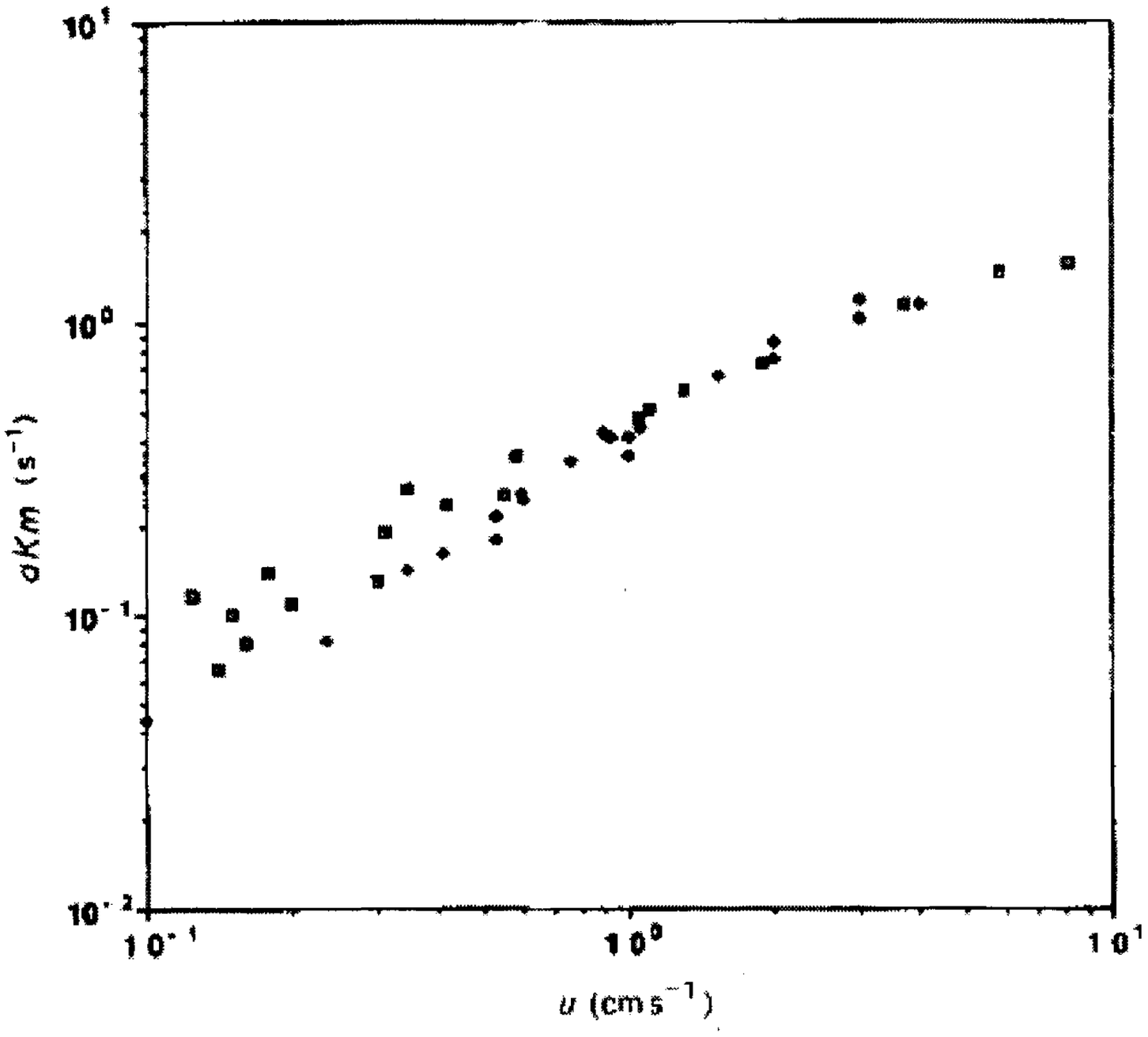

Figure 2.10 - Effective mass transfer coefficient as a function of electrolyte velocity; □ data from $[Fe(Cn)_6]^{-3}$ reduction; ♦ data from $[Cu^{2+}]$ reduction (Carta et al., 1991)

As mentioned earlier, mass transfer data in flow systems are represented in the form $Sh = (const)\mathrm{Re}^{\alpha}\, Sc^{\beta}$. There are many approaches to define the specific area, a_s, and the characteristic dimension, d_h. The following correlation is used:

$$d_h = 4\theta / a_s \tag{2.12}$$

Although the specific area is the most important parameter when the electrochemical reaction is kinetically limited (Carta et al., 1991), a strong effect of pore size is obtained when the reaction is diffusion controlled. The following relationship is obtained for evaluating the area per unit volume (a_v), electrode porosity, and specific area:

$$a_s = a_v(1-\theta) = \frac{4}{d_f}(1-\theta) \tag{2.13}$$

For the various studies evaluated, the following correlation is obtained for carbon felt sample electrodes (given characteristics in table 2.7) with the Sc value included in the constant term:

$$Sh = 3.19\,\mathrm{Re}^{0.69} \tag{2.14}$$

The studies for the mass transfer at carbon felt electrodes confirm the good mass transfer performance of the carbon felt electrode. Moreover, the high porosity of the felt allows a high electrolyte conductivity inside the pores and thus, if the electrolyte has a sufficiently high conductivity, the ohmic drop remains low (Carta et al., 1991).

2.6. Conclusions

Therefore, there are a few factors that must be investigated in order to arrive at a more efficient biofuel cell system. Firstly, the issue of jarosite precipitation must be addressed in that optimal operating conditions must be obtained while not comprising the iron-oxidizing capabilities of the bacteria. Primarily, the most popular iron-oxidizing bacteria for this study, *A. ferrooxidans,* were investigated. Results of this study will give insight into the more appropriate microbe and conditions that are most suitable for fuel cell applications.

Secondly, it is vital to study the organic metabolite accumulation that causes hindered bacterial operation. A solution to this problem is to study the influence of mixotrophic bacteria (*F. acidiphilum*) cultured with other chemolithotrophic strains (*A. ferrooxidans* and *Leptospirillum* sp.) in order to control the organic concentration. Finally, it is important to set up a biofuel cell system with a viable bioreactor and fuel cell

configurations in order to analyze the stability and efficiency of the system and to further analyze the limiting factors that can obscure prolonged fuel cell activity.

Nomenclature

a, b	Fitting parameters
a_s	Specific electrode area, m^2
a_v	Area per specific volume, $m^2\ m^{-3}$
AMD	Acid mine drainage
C	Concentration of electrolyte in cathodic compartment, M
d_h	Characteristic dimension
D	Diffusion coefficient, $m^2\ s^{-1}$
d_f	Fibre diameter
E_a	Activation Energy, kJ mol^{-1}
F	Faraday's constant, $6.6485309x10^4$ C mol^{-1}
Q_l	Electrolyte flow rate, $m^3\ s^{-1}$
I_{lim}	Limiting current, A
k_m	Mass transfer coefficient
l	Length of electrode, m
n	Number of electrons transferred in the half-reaction
Re	Reynolds number
Sc	Schmidt number
Sh	Sherwood number
T	Temperature, °C
T_{MIN}	Minimum temperature of operation, °C
T_{MAX}	Maximal temperature of operation, °C

TOC	Total organic carbon, ppm (mg/L)
v	Kinematic viscosity, $m^2 s^{-1}$
X	Conversion

Greek Letters

γ	Conductivity, $\Omega^{-1} m^{-1}$
θ	Porosity
ρ_A	Apparent density, kg m^{-2}
ρ_R	True density, kg m^{-3}
μ	Linear velocity of electrolyte, m s^{-1}

References

Ahonen, L., & Tuovinen, O. H. (1989). Microbiological oxidation of ferrous iron at low temperatures. *Applied and Environmental Microbiology, 55*(2), 312-316.

Armentia, H., & Webb, C. (1992). Ferrous sulfate oxidation using Thiobacillus *ferrooxidans* cells immobilized in polyurethane foam support particles. *Applied Microbiology and Biotechnology, 36*(5), 697-700.

Breed, A. W., & Hansford, G. S. (1999). Effect of pH on ferrous-iron oxidation kinetics of *Leptospirillum ferrooxidans* in continuous culture. *Biochemical Engineering Journal, 3*(3), 193-201.

Carta, R., Palmas, S., Polcaro, A. M., & Tola, G. (1991). Behavior of a carbon felt flow by electrodes. Part I: Mass transfer characteristics. *Journal of Applied Electrochemistry, 21*(9), 793-798.

Coeuret, F., Vilar, E. O., & Cavalcanti, E. B. (2002). Carbon fiber cloth as an electrode material: electrical conductivity and mass transfer. *Journal of Applied Electrochemistry, 32*(10), 1175-1182.

Dopson, M., Baker-Austin, C., Hind, A., Bowman, J. P., & Bond, P. L. (2004). Characterization of *Ferroplasma* isolates and *Ferroplasma* acidarmanus sp. nov., extreme acidophiles from acid mine drainage and industrial bioleaching environments. *Applied and Environmental Microbiology, 70*(4), 2079-2088.

Drobner, E., Huber, H., & Stetter, K. O. (1990). Thiobacillus *ferrooxidans*, a facultative hydrogen oxidizer. *Applied and environmental microbiology, 56*(9), 2922-2923.

Drogui, P., Mercier, G., & Blais, J.-F. (2005). Bioproduction of Ferric Sulfate Used during Heavy Metals Removal from Sewage Sludge. *J. Environ Qual, 34*, 816-824.

Edwards, K. J., Bond, P. L., Gihring, T. M., & Banfield, J. F. (2000). An Archaeal iron-oxidizing extreme acidophile important in acid mine drainage. *Science (Washington, D. C.), 287*(5459), 1796-1799.

Franzmann, P. D., Haddad, C. M., Hawkes, R. B., Robertson, W. J., & Plumb, J. J. (2005). Effects of temperature on the rates of iron and sulfur oxidation by selected bioleaching bacteria and archaea: Application of the Ratkowsky equation. *Minerals Engineering, 18*(13-14), 1304-1314.

Golyshina, O. V., Pivovarova, T. A., Karavaiko, G. I., Kondrat'eva, T. F., Moore, E. R. B., Abraham, W.-R., et al. (2000). *Ferroplasma acidiphilum* gen. nov., sp. nov., an acidophilic, autotrophic, ferrous-iron-oxidizing, cell-wall-lacking, mesophilic member of the Ferroplasmaceae fam. nov., comprising a distinct lineage of the Archaea. *International Journal of Systematic and Evolutionary Microbiology, 50*(3), 997-1006.

Ingledew, W. J. (1982). Thiobacillus *ferrooxidans*. The bioenergetics of an acidophilic chemolithotroph. *Biochimica et biophysica acta, 683*(2), 89-117.

Jensen, A. B., & Webb, C. (1995). Ferrous sulfate oxidation using Thiobacillus *ferrooxidans*: a review. *Process Biochemistry (Oxford), 30*(3), 225-236.

Karamanev, D. (1991). Model of the biofilm structure of Thiobacillus *ferrooxidans*. *Journal of Biotechnology, 20*(1), 51-64.

Karamanev, D. G., & Nikolov, L. N. (1988). Influence of some physicochemical parameters on bacterial activity of biofilm: ferrous iron oxidation by Thiobacillus *ferrooxidans*. *Biotechnology and Bioengineering, 31*(4), 295-299.

Nemati, M., Harrison, S. T. L., Hansford, G. S., & Webb, C. (1998). Biological oxidation of ferrous sulfate by Thiobacillus ferrooxidans: a review on the kinetic aspects. *Biochemical Engineering Journal, 1*(3), 171-190.

Nemati, M., & Webb, C. (1997). A kinetic model for biological oxidation of ferrous iron by Thiobacillus *ferrooxidans*. *Biotechnology and Bioengineering, 53*(5), 478-486.

Newman, J. (1976). *Simultaneous reactions at disk and porous electrodes* (No. Report): Lawrence Berkeley Lab.,Univ. California,Berkeley,CA,USA. FIELD URL:.

Nyavor, K., Egiebor, N. O., & Fedorak, P. M. (1996). The effect of ferric ion on the rate of ferrous oxidation by Thiobacillus *ferrooxidans*. *Applied Microbiology and Biotechnology, 45*(5), 688-691.

Okereke, A., & Stevens, S. E., Jr. (1991). Kinetics of iron oxidation by Thiobacillus *ferrooxidans*. *Applied and Environmental Microbiology, 57*(4), 1052-1056.

Okibe, N., Gericke, M., Hallberg Kevin, B., & Johnson, D. B. (2003). Enumeration and characterization of acidophilic microorganisms isolated from a pilot plant stirred-tank bioleaching operation. *Applied and environmental microbiology, 69*(4), 1936-1943.

Olem, H., & Unz, R. F. (1977). Acid mine drainage treatment with rotating biological contactors. *Biotechnology and Bioengineering, 19*(10), 1475-1491.

Oren, Y., & Soffer, A. (1983). Graphite felt as an efficient porous electrode for impurity removal and recovery of metals. *Electrochimica Acta, 28*(11), 1649-1654.

Rawlings, D. E., Tributsch, H., & Hansford, G. S. (1999). Reasons why \"*Leptospirillum*\"-like species rather than Thiobacillus *ferrooxidans* are the dominant iron-oxidizing bacteria in many commercial processes for the biooxidation of pyrite and related ores. *Microbiology (Reading, United Kingdom), 145*(1), 5-13.

Sasaki, K., & Konno, H. (2000). Morphology of jarosite-group compounds precipitated from biologically and chemically oxidized Fe ions. *Canadian Mineralogist, 38*(1), 45-56.

Schmal, D., Van Erkel, J., & Van Duin, P. J. (1986). Mass transfer at carbon fiber electrodes. *Journal of Applied Electrochemistry, 16*(3), 422-430.

Silverman, M. P., & Lundgren, D. G. (1959). Studies of the chemoautotrophic iron bacterium Ferrobacillus ferrooxidans. I. An improved medium and a harvesting procedure for securing high cell yields. *J. Bacteriol., 77*, 642-647.

Smith, J. R., Luthy, R. G., & Middleton, A. C. (1988). Microbial ferrous iron oxidation in acidic solution. *Journal - Water Pollution Control Federation, 60*(4), 518-530.

Storck, A., Enriquez-Granados, M. A., Roger, M., & Coeuret, F. (1982). The behavior of porous electrodes in a flow-by regime. I. Theoretical study. *Electrochimica Acta, 27*(2), 293-301.

Tabita, R., & Lundgren, D. G. (1971). Utilization of glucose and the effect of organic compounds on the chemolithotroph Thiobacillus *ferrooxidans*. *Journal of Bacteriology, 108*(1), 328-333.

Torma, A. E. (1977). *Advances in Biochemical Engineering, Vol. 6: New Substrates*.

Vatistas, N., Marconi, P. F., & Bartolozzi, M. (1991). Mass-transfer study of the carbon felt electrode. *Electrochimica Acta, 36*(2), 339-343.

CHAPTER 3

Formation of Jarosite during Fe^{2+} Oxidation by *Acidithiobacillus ferrooxidans*[*]

3.1. Introduction

A. ferrooxidans, recently renamed from *Thiobacillus ferrooxidans*, is a gram-negative bacterium, characterized by non-sporulating, rods, 0.5-0.6 μm wide by 1.0-2.0 μm long, with rounded ends, occurring singly or in pairs, rarely in short chains. They are also known to be motile by means of a single polar flagellum (Jensen & Webb, 1995). *A. ferrooxidans* is found naturally in acid mine drainage waters of iron and bituminous coal mines and is a dominant organism in biohydrometallurgy in the process of ore bioleaching (Jensen & Webb, 1995). Furthermore, it has been utilized in the processes of desulphurization of sour gases, treatment of acid mine drainage, and the desulphurization of coal.

A. ferrooxidans can obtain energy from the oxidation of different inorganic substances, the most common of which is ferrous sulfate. The overall biochemical reaction of the oxidation of ferrous ions is:

$$4Fe^{2+} + O_2 + 4H^+ \xrightarrow{A.f.} 4Fe^{3+} + 2H_2O \qquad (3.1)$$

This bioreaction is of great practical importance.

Ore bioleaching involves the dissolution of metal sulfides (MeS) by presumably an indirect mechanism, involving the oxidation of Fe^{2+} to Fe^{3+} by *A. ferrooxidans*

---

[*] A version of this chapter was published by the Minerals Engineering Journal

(reaction 3.1) in the liquid phase. Following this oxidation, the Fe^{3+} leaches the metal through a chemical reaction (Jensen & Webb, 1995):

$$2Fe^{3+} + MeS \rightarrow Me^{2+} + S^0 + 2Fe^{2+} \qquad (3.2)$$

Hydrogen sulfide is usually a component of many modern day gas streams such as biogas. It is a highly toxic component and is usually removed by means of hydrogen sulfide scrubbers and other mechanisms like the Claus process. *A. ferrooxidans* can be used to eliminate hydrogen sulfide from gas streams. This process first involves contacting H_2S-containing gases with a solution of ferric sulfate in an absorber. The solution absorbs H_2S and oxidizes it to elemental sulfur, while the ferric sulfate is reduced to ferrous sulfate (Nemati et al., 1998). This is shown in the following reaction:

$$H_2S + Fe_2(SO_4)_3 \rightarrow S + 2FeSO_4 + H_2SO_4 \qquad (3.3)$$

This reaction goes to completion very rapidly and the hydrogen disulfide is removed efficiently. Ferrous sulfate obtained from the first step is further treated by *A. ferrooxidans*, according to reaction 1 in order to oxidize ferrous iron to ferric iron in a bioreactor. This ferric iron obtained is recycled to the absorber for the first step and the cycle is repeated (Nemati et al., 1998).

The ability of *A. ferrooxidans* to oxidize ferrous ions is used in the treatment of acid mine drainage. In acid mine drainage, the main source of pollution is ferrous iron, with concentrations of up to 1 kg/m^3 (Jensen & Webb, 1995). In order to treat this problem, the oxidation of Fe^{2+} to Fe^{3+} (by *A. ferrooxidans*) must precede the precipitation of ferric iron as various insoluble oxyhydroxides (Jensen & Webb, 1995). In recent studies, *A. ferrooxidans* has proven to be efficient for the bacterial oxidation of ferrous iron in acid mine drainage.

Another application of the iron oxidation by *A. ferrooxidans* is the desulfurization of coal (Juszczak et al., 1995). It is based on the oxidation and dissolution of metal sulfides, which are naturally present in coal.

There are several factors that play a role in the rate of oxidation of ferrous ions by *A. ferrooxidans*. These factors include ferrous/ferric iron concentration, cell and oxygen concentrations, pH, temperature, and reactor type. Past studies have concluded that ferric ions competitively inhibit ferrous ion oxidation by *A. ferrooxidans*; an inhibitory effect that can be reduced by increasing cell concentration (Nyavor et al., 1996).

Moreover, the pH and temperature have significant effects on the oxidation kinetics of iron by *A. ferrooxidans*. Several studies have been conducted for the purpose of finding the optimum pH and temperature ranges for *A. ferrooxidans* operation. Some findings are as shown in table 3.1.

Table 3.1 - Optimum pH and Temperatures for *A. ferrooxidans* as reported by different sources

Source	*Optimum pH*
(Karamanev & Nikolov, 1988)	2.0
(Torma, 1977)	2.3
(Smith et al., 1988)	2.0-2.3
(Drobner et al., 1990)	2.0

Source	*Optimum Temperature (^oC)*
(Ahonen & Tuovinen, 1989)	28
(Okereke & Stevens, 1991)	30
(Smith et al., 1988)	25-30
(Nemati, 1996)	35

Therefore, the pH and temperature at which the bacterial operation and oxidation rate are at a maximum are approximately 2.0 and 30 ^oC, respectively.

3.1.1. Jarosite Formation

A. ferrooxidans is commonly grown on 9K medium developed by Silverman and Lundgren. The ferrous iron oxidation occurs via reaction 1.

Since there is consumption of hydrogen ions, the pH of the liquid media initially increases. However, this pH increase is counteracted by the hydrolysis of ferric iron:

$$Fe^{3+} + H_2O \Leftrightarrow FeOH^{2+} + H^+ \quad (3.4)$$

$$Fe^{3+} + 2H_2O \Leftrightarrow Fe(OH)_2^+ + H^+ \quad (3.5)$$

$$Fe^{3+} + 3H_2O \Leftrightarrow Fe(OH)_3 + H^+ \quad (3.6)$$

Therefore, it is quite visible that the pH of the system has effect on the extent of the oxidation and hydrolysis reactions. Furthermore, there is a reaction in competition with the hydrolysis reaction giving products of basic ferric hydroxysulphates with the formula $MFe_3(SO_4)_2(OH)_6$, where $M=K^+$, Na^+, NH_4^+, Ag^+, or H_3O^+ (Jensen & Webb, 1995). These hydroxysulphate precipitates are known as jarosite. The following is the formula for jarosite precipitation:

$$3Fe^{3+} + M^+ + 2HSO_4^- + 6H_2O \rightarrow MFe_3(SO_4)_2(OH)_6 + 8H^+ \quad (3.7)$$

Since the 9K medium contains a high concentration of NH_4^+ ions, the jarosites produced were ammoniojarosites with the formula $NH_4Fe_3(SO_4)_2(OH)_6$.

Jarosite formation has negative effects on many applications that require the use of *A. ferrooxidans*, especially in the process of biological gas desulphurization. Some of the effects include the diminishment of ferric iron used as the absorbent for hydrogen disulfide, blockage of pumps, valves, pipes, etc, and the creation of kinetic barriers due to the small diffusion of reactants and products through the precipitation zone (Jensen & Webb, 1995).

The precipitation of jarosite is widely used in the zinc industry to remove iron solubilized in the processing circuit (Dutrizac, 1999). The precipitation reaction is greatly accelerated by the presence of jarosite seed, and the rate increases in a nearly linear manner with increasing seed additions (Dutrizac, 1999).

Also, in the process of coal desulfurization, the formation of jarosite on the surface of the biooxidized metal sulfide particle significantly decreases the rate of bioleaching by deactivating the surface. Jarosite formation in coal desulfurization results in residual sulfur, which cannot be removed, from coal. Furthermore, jarosite formation in immobilization matrices limits the amount of biomass retention since ferric iron deposits occupy most of the available space (Jensen & Webb, 1995).

As mentioned above, due to the abundance of NH_4^+ ions in the 9K medium, the jarosites produced in these experiments most closely corresponds to ammoniojarosites, $NH_4Fe_3(SO_4)_2(OH)_6$.

A recent study has been conducted in order to characterize the composition of different types of jarosite produced biologically by using x-ray diffraction. It was found that ammoniojarosite has an elemental weight composition of 14.6% NH_4^+, 29.1% Fe, and 11.2% S (Sasaki & Konno, 2000).

3.1.2. Purpose of this Study

Several studies have been conducted in order to determine the importance of jarosite formation in bioreactors. For example, jarosite precipitation has been directly related to the number of attached cells (Pogliani & Donati, 2000). However, no studies have dealt directly with determining the amount of jarosite formation under varying cultivation condition. The main goal of this study to investigate jarosite precipitation

under different conditions, by varying pH and temperature. The results will be of significant importance for determining the cultivation conditions for minimal jarosite precipitation.

3.2. Materials and Methods

This experiment deals with the effects of two parameters, pH and temperature, on iron oxidation and jarosite formation. Therefore, the experiment was divided into two parts, dealing with varying pH and temperature.

3.2.1. Equipment

For this procedure, the bacteria were grown in 11 x 250 ml Erlenmeyer flasks with the appropriate medium. The pH of each trial was adjusted using sulfuric acid and monitored using a pH meter (Orion Model No. 420A). The bacteria were allowed to grow in a Rotary flask shaker with speed and temperature adjustment (New Brunswick Scientific Model No. G-25 R). For the ferric and total iron analyses, we used a spectrophotometer (Varian Cary 50) with the appropriate procedure (Karamanev et al., 2002). Lastly, filter paper with pore size 25 μm was used to separate the jarosite produced in each flask.

3.2.2. Chemicals

All the chemicals used in this study were of analytical grade, including 100% H_2SO_4, components of the 9K medium, sulfosalicylic acid and ammonium hydroxide (30%).

3.2.3. pH Effect

For the first part of the experiment, the effect of varying pH on jarosite formation, was tested in order to find the optimal range of pH in which the bacteria operate efficiently with minimal jarosite precipitation.

Eleven 250 ml Erlenmeyer flasks were used, one for each pH in the range of 1.0-3.0 in intervals of 0.2 pH. 100 ml of 9K medium was added into each of the 11 flasks. The desired pH in each flask was obtained by adding 100% H_2SO_4 drop wise, with continuous agitation and pH measurement. Further, 20 ml of *A. ferrooxidans* inoculum was added to each flask. The inoculum contained an average of 10^8 cells per milliliter. The flasks were then covered with pieces of aluminum foil. Finally, the flasks were placed in the rotary shaker at ambient temperature with a rotation speed of 260 rpm. The Fe^{3+} and Fe_{total} concentrations in the flasks are measured initially, at 22 hours and at 46 hours. The ferrous and ferric iron concentrations were measured using sulfosalycilic acid as an indicator (Karamanev et al., 2002).

When more than 90% of Fe^{2+} was oxidized, the flasks were removed from the shaker in order to measure the jarosite precipitation. Firstly, the liquid in each flask was filtered using a vacuum flask and filter paper (pore size 25 μm). The solids on the filter paper were then returned back to the corresponding flask by washing them with distilled water. This was done in order to combine the filtered jarosite and that attached to the wall of the flask. Approximately 10 ml of 50% H_2SO_4 were then added to each jarosite and distilled water mixture in order to dissolve the jarosite (suspended and on the walls). Finally, the total iron concentration was measured using the sulfosalycilic method and the

volume of mixture in each flask was measured using graduated cylinders in order to obtain the total mass of jarosite present.

3.2.4. Temperature Effect

For the second part of the experiment, the appropriate pH range obtained from the first part, displaying the optimum pH, was selected in order to test for the optimum temperature. This allows us to obtain the optimum pH and temperature combination in which the bacterial iron oxidation rate is maximal with minimum jarosite formation.

To start this part of the experiment, we selected the appropriate optimal pH, with minimal jarosite precipitation, from the first part of this experiment. We then selected the appropriate number of 250 ml flasks in order to have pH intervals of 0.1. We then followed the same procedure as the first part except we set the flask shaker temperature consecutively to 25 °C, 30 °C, 35 °C, and 40 °C.

The mean ferrous iron oxidation rate (in g/L·hr) was determined by subtracting the Fe^{3+} concentration at 22 hours from the initial, and dividing the result by 22 hours. This gives more accurate results since the oxidation does not go to completion in any of the samples at 22 hours, thus the mean oxidation rate can be accurately compared for all the samples at this time.

3.2.5. Analytical Procedures

The analysis of ferrous and ferric iron concentrations at different times in the bacterial samples was done using a precise quantitative method, which is not affected by the presence of iron or *A. ferrooxidans* in solution. The method utilizes a spectrophotometer for the colorimetric measurement of red-colored ferric-sulfosalicylate

complex, which gives the concentration of Fe^{3+} in solution. Ammonia is then added, causing the 5-sulfosalicylic acid (SSA) to form a yellow complex with all the iron ions, which gives the concentration of total iron in solution (Karamanev et al., 2002).

3.3. Results and Discussions

This experiment consisted of two parts analyzing the effect of pH and temperature on jarosite precipitation. For each parameter, we will discuss the data and observations.

3.3.1. pH

Several experimental runs were performed testing the effect of the various pHs, range from 1.0-3.0 in 0.2 intervals, taking samples initially, at 22 and at 46 hours. The temperature was kept constant at 22 °C. The observations of oxidation progression with time for the various pHs are given in Table 3.2.

Table 3.2 - Observations of Fe^{2+} Oxidation at various pHs

	Time (hrs)		
pH	***0***	***22***	***46***
1.00	light yellow	Light yellowish lime	light yellowish lime with no visible solids on wall or suspended
1.20	Darker yellow	darker yellowish lime	darker yellowish lime with no visible solids on wall or suspended
1.39	Darker yellow	darker yellowish lime	dark yellowish lime with no visible solids on wall or suspended
1.60	Darker yellow	dark yellowish lime	light orange pekoe with no visible solids on wall or suspended
1.80	dark yellow	light orange pekoe	darker orange pekoe with some residue on walls but no suspended visible solids

2.01	light orange	darker orange pekoe	darker orange pekoe with some whitish muck and visible solids on wall and suspended
2.19	Darker orange	darker orange pekoe	darker orange pekoe with more whitish muck and more visible solids on wall and suspended
2.41	Darker orange	darker orange pekoe	darker orange pekoe with more whitish muck and more visible solids on wall and suspended
2.58	Darker orange	darker orange pekoe	darker orange pekoe with more whitish muck and more visible solids on wall and suspended
2.81	Darker orange	darker orange pekoe	darker orange pekoe with more whitish muck and more visible solids on wall and suspended
2.96	dark orange	dark orange pekoe	dark orange pekoe with most whitish muck and most visible solids on wall and suspended

Therefore, the jarosite formation was only observed at the 46-hour period with jarosites precipitating on the walls, in suspension with the fluid and the bottom of the flasks, possessing a yellowish-brown color. The 2.96 pH flask was found to have the most precipitation of jarosites while flasks of pH 1.0-1.6 displayed no visible jarosite precipitation.

From Figure 3.1, it can be seen that over the course of the experiment, conducted at room temperature of 22 ˚C, *A. ferrooxidans* reached a degree of oxidation as high as 100%. Therefore, the mass of jarosite was examined at the end of the 46-hour period in which the bacteria efficiently oxidized most of Fe^{2+} into Fe^{3+}.

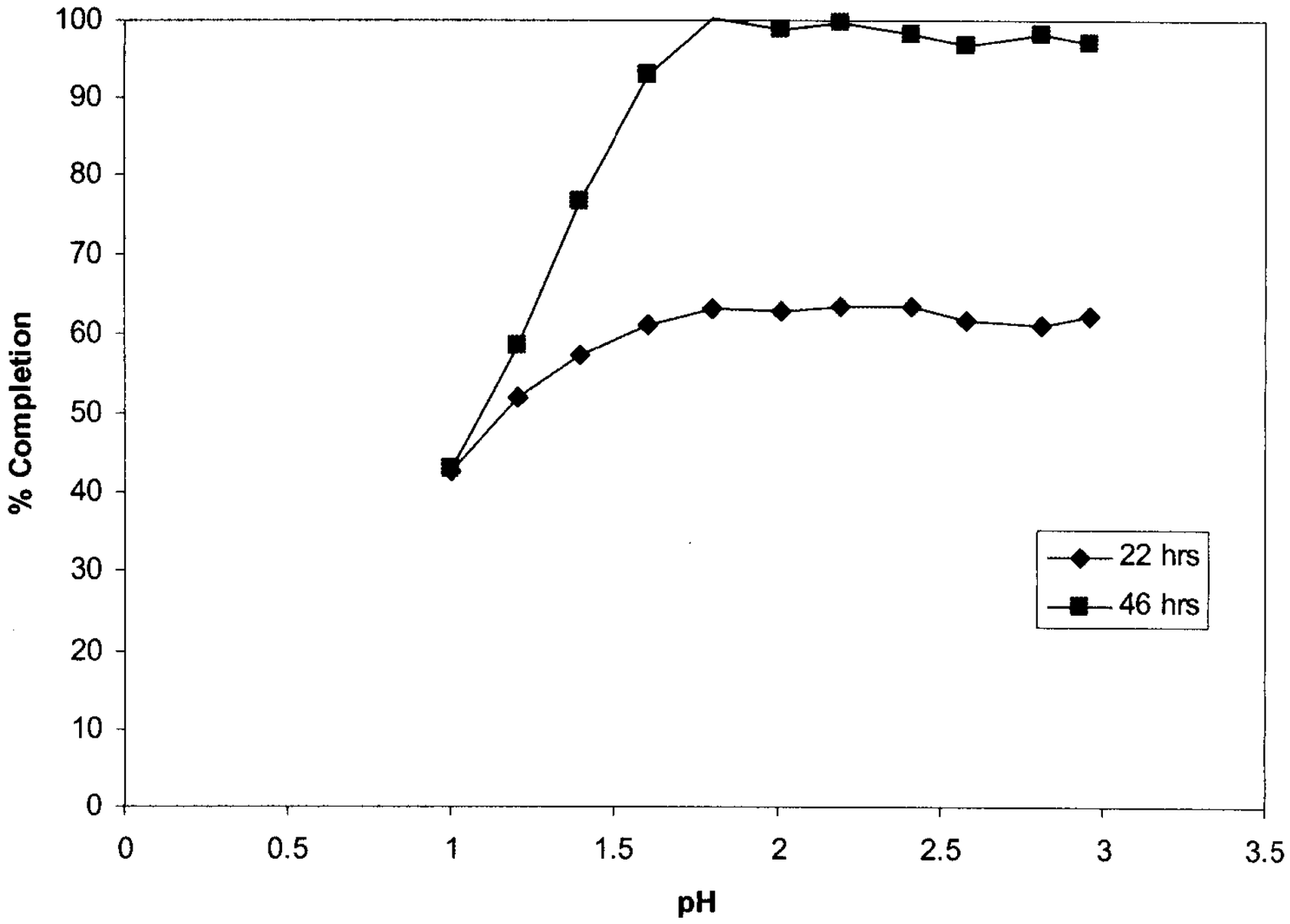

Figure 3.1 - Percent Completion of Fe^{2+} Oxidation vs. pH at Different Times

Figure 3.2 shows further analysis of jarosite mass produced at 46 hours and oxidation rate of *A. ferrooxidans*. At the room temperature of 22 °C, pH of 1.6-2.0 produced the least amount of jarosite (between 0-0.025 g/L·h) while still maintaining high Fe^{2+} oxidation rates of up to 0.127 g/L·h.

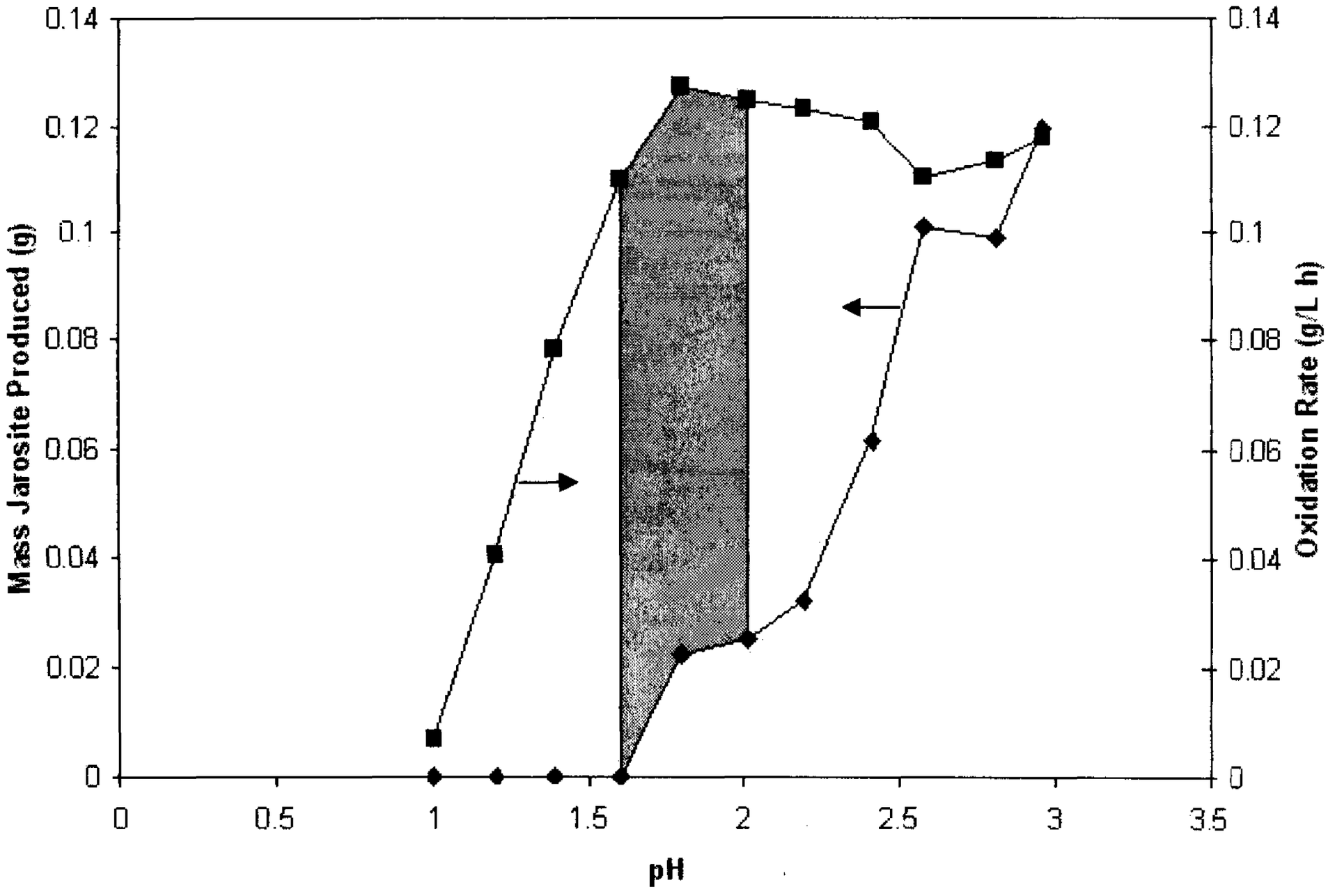

Figure 3.2 - Comparison of Jarosite Produced and Oxidation Rate vs. pH at 46 hrs

3.3.2. Temperature

The optimal pH at room temperature was determined to be in the range of 1.6-2.0. Using these pH values in 0.1 intervals and varying the temperature to 25, 30, 35, and 40 °C, the optimal pH and temperature combination was investigated. This will give the pH and temperature optimums for *A. ferrooxidans* with minimal jarosite deposition.

Figures 3.3-6 illustrate the relationship between oxidation rate of *A. ferrooxidans* and jarosite mass as a function of pH at different temperatures of 25, 30, 35, and 40 °C. At temperatures of 25 and 30 °C, the oxidation rate and the jarosite produced curves have opposite slopes at pH below 1.9-2.0. However, at temperatures of 35 and 40 °C, oxidation rate and jarosite mass both increase as pH increases. The pH yielding reasonable oxidation rates with little jarosite precipitation for all temperatures, was between 1.6 and

1.7. Figures 3.7 and 3.8 further show the effect of temperature and pH on the jarosite mass.

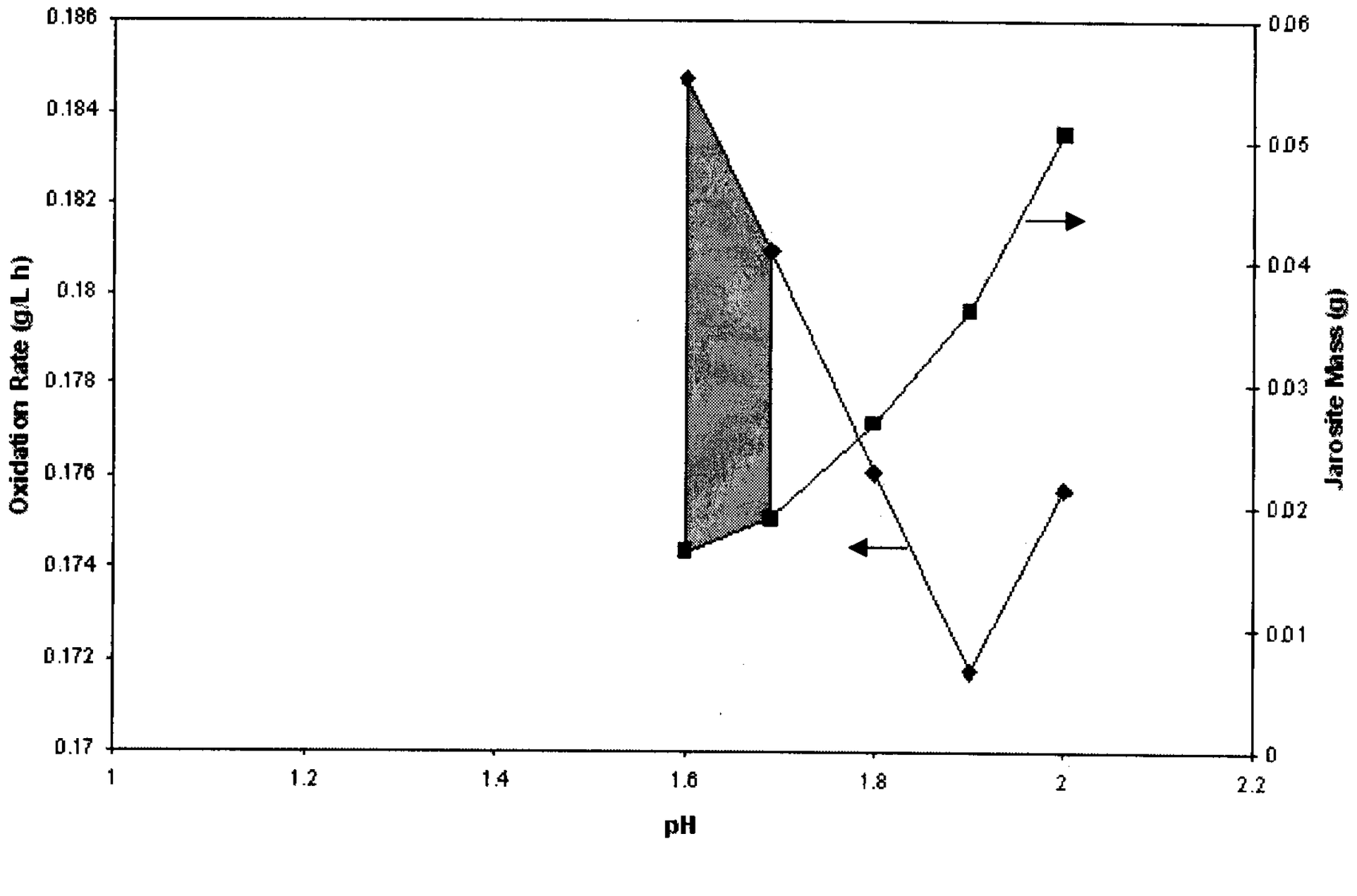

Figure 3.3 - Oxidation Rate and Jarosite Mass vs. pH at 25 °C

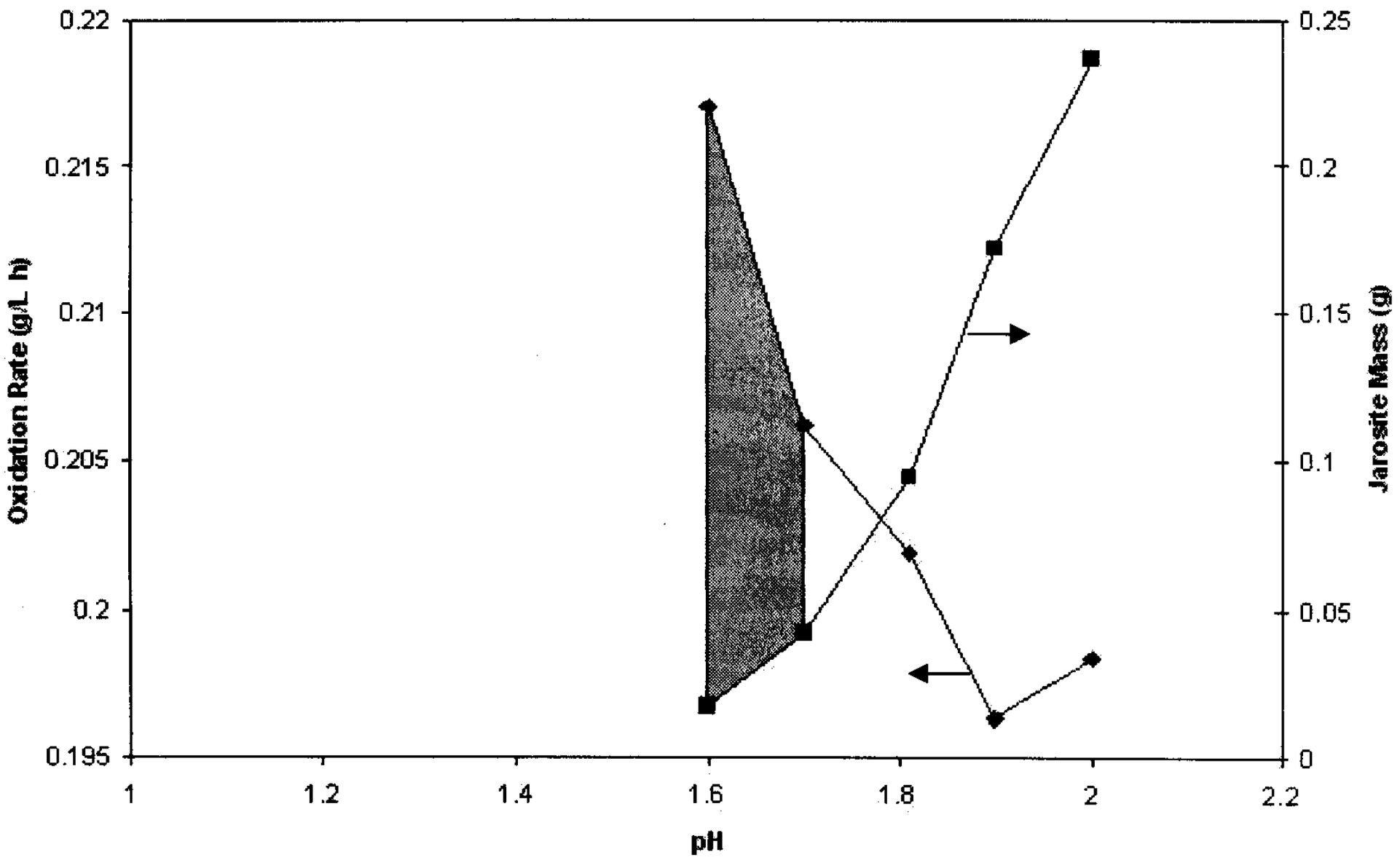

Figure 3.4 - Oxidation Rate and Jarosite Mass vs. pH at 30 °C

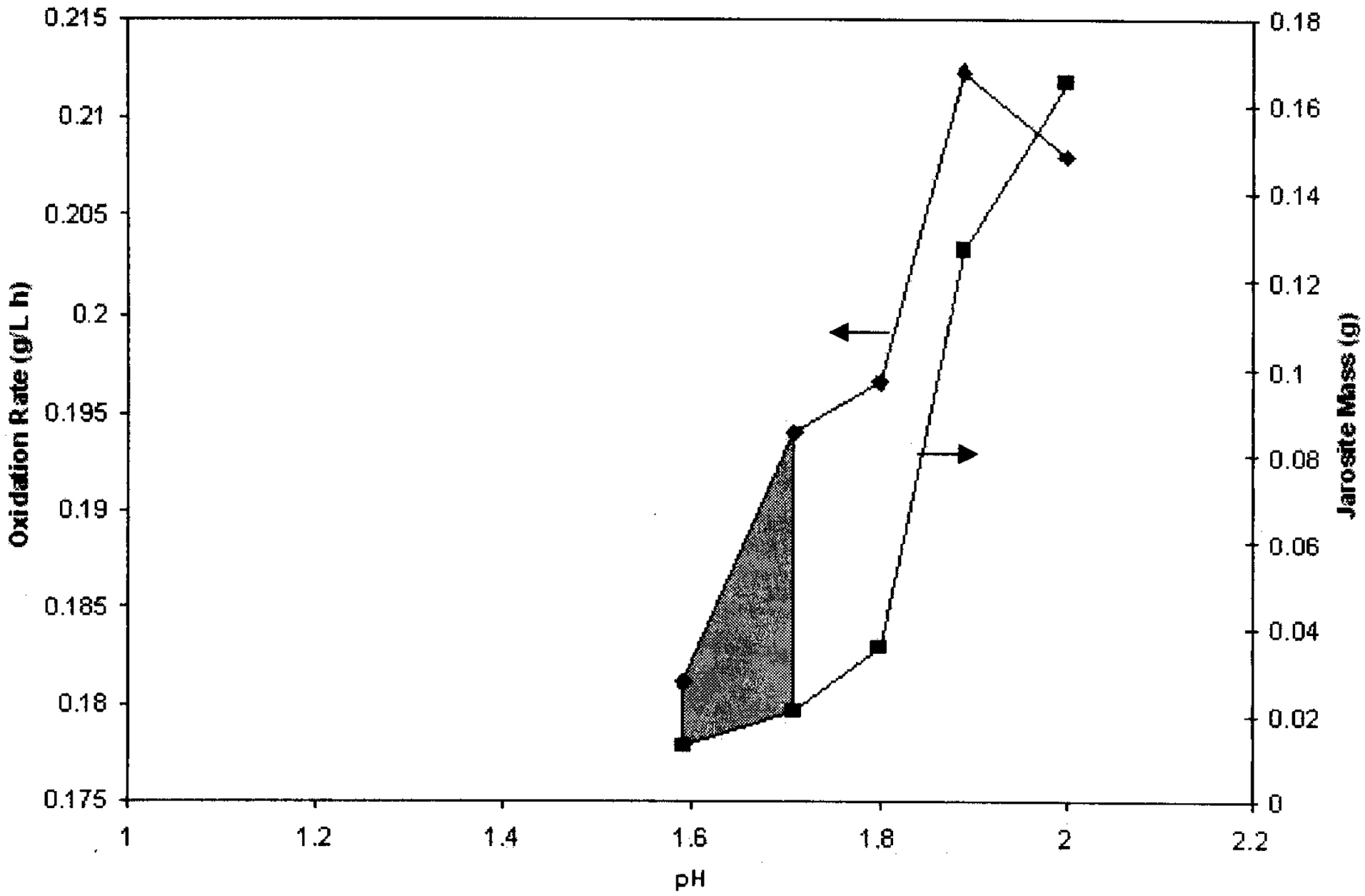

Figure 3.5 - Oxidation Rate and Jarosite Mass vs. pH at 35 °C

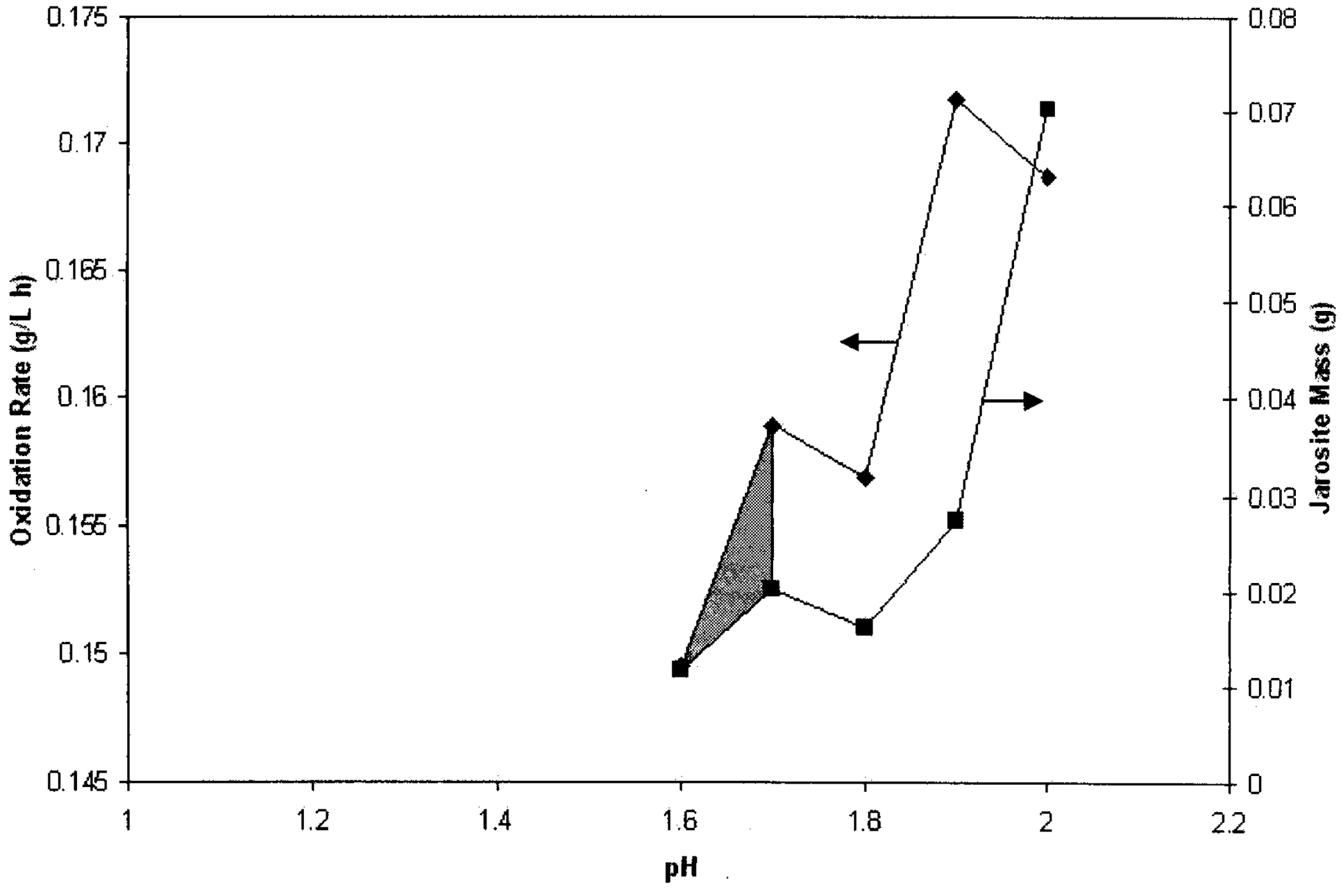

Figure 3.6 - Oxidation Rate and Jarosite Mass vs. pH at 40 °C

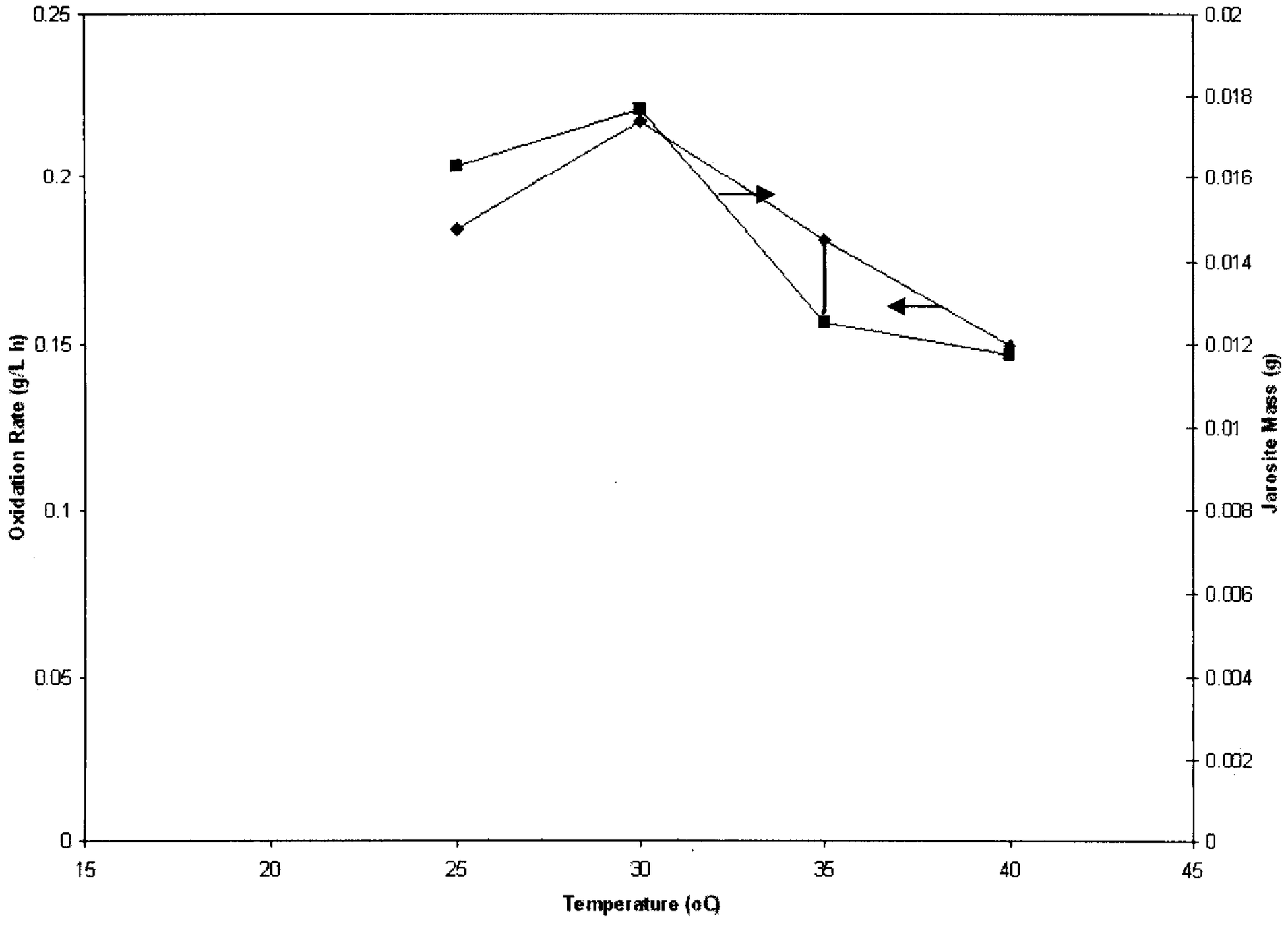

Figure 3.7 - Oxidation Rate and Jarosite Mass vs. Temperature at pH 1.6

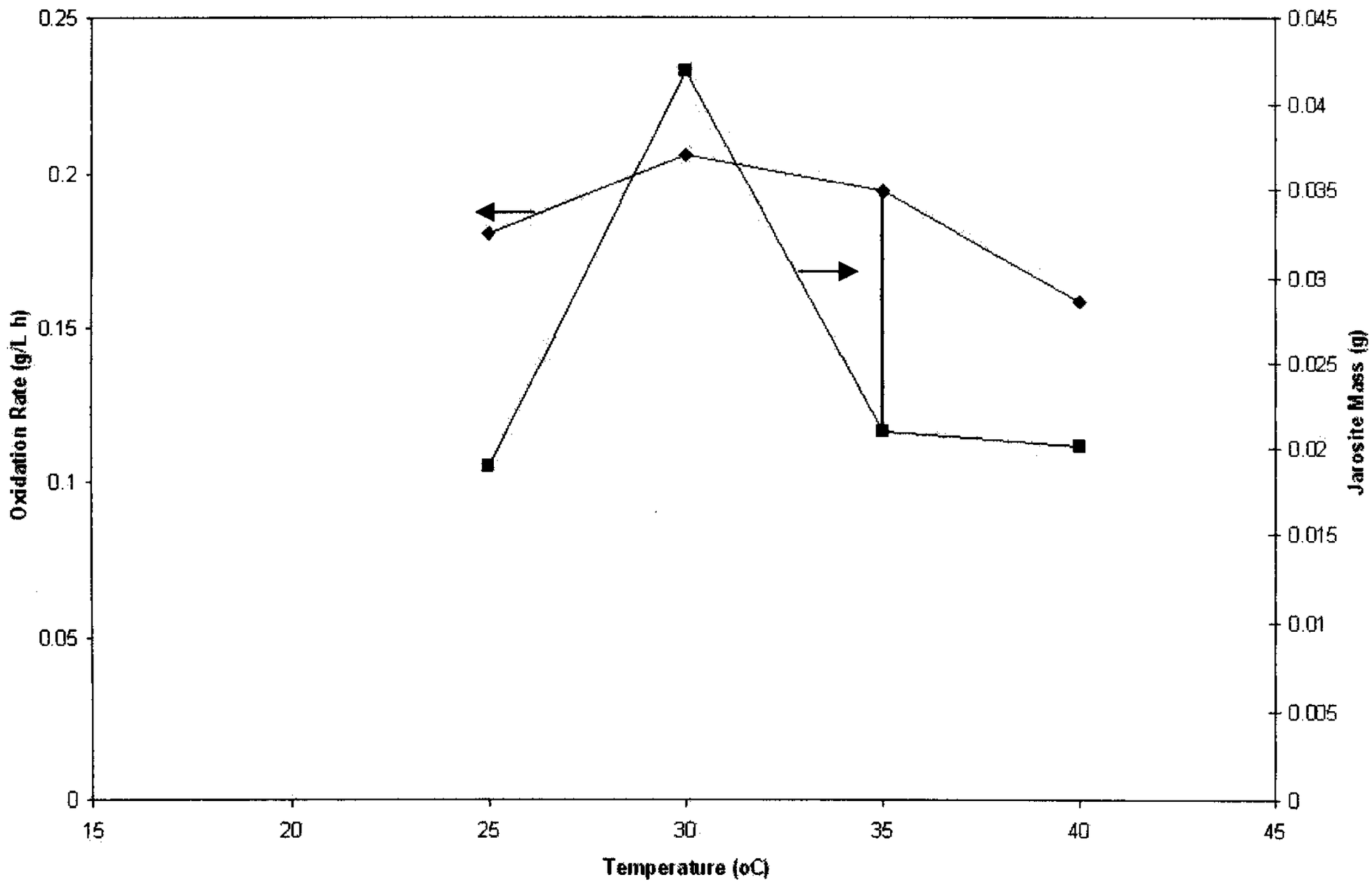

Figure 3.8 - Oxidation Rate and Jarosite Mass vs. Temperature at pH 1.7

From the analysis of figures 3.7 and 3.8 at pH of 1.6 and 1.7, respectively, it is clear that the Fe^{2+} oxidation rate and the jarosite produced are directly related, reaching a peak at 30 °C. The optimum operation temperature in both cases, however, was 35 °C, yielding relatively high oxidation rates of 0.181-0.194 g/L·h with low jarosite mass of 0.0125-0.0209 g. The oxidation rates attained at these conditions were consistent with values obtained by T. Das et al. at similar conditions giving an oxidation rate of 0.15 g/L·h with a reaction rate constant of 0.065 h^{-1} (Das et al., 1998).

3.4. Conclusions

The main purpose of this work was to investigate the operating conditions for the Fe^{2+} oxidation by *A. ferrooxidans*, under which minimal amount of jarosite precipitate is produced, while the Fe^{2+} and rates are still high with respect to pH and temperature. From

the experiments, we concluded that the optimal pH and temperature combination giving the least amount of jarosite is pH 1.6-1.7 at a temperature of 35 °C. These conditions yielded very appealing results, giving oxidation rates of 0.181-0.194 g/L·h, with small jarosite precipitation of 0.0125-0.0209 g. However, this jarosite precipitation remains relatively significant considering the total iron is only 5 g/L, thus it is unsuitable for use in a biofuel cell system. Therefore, it would be more beneficial to operate at even a lower pH. A promising microorganism is *Leptospirillum* sp., which is capable of operating at a lower pH of 1.0.

References

Ahonen, L., & Tuovinen, O. H. (1989). Microbiological oxidation of ferrous iron at low temperatures. *Applied and Environmental Microbiology, 55*(2), 312-316.

Das, T., Panchanadikar, V. V., & Chaudhury, G. R. (1998). Bio-oxidation of iron using Thiobacillus *ferrooxidans*. *World Journal of Microbiology & Biotechnology, 14*(2), 297-298.

Drobner, E., Huber, H., & Stetter, K. O. (1990). Thiobacillus *ferrooxidans*, a facultative hydrogen oxidizer. *Applied and environmental microbiology, 56*(9), 2922-2923.

Dutrizac, J. E. (1999). The effectiveness of jarosite species for precipitating sodium jarosite. *JOM, 51*(12), 30-32.

Jensen, A. B., & Webb, C. (1995). Ferrous sulfate oxidation using Thiobacillus *ferrooxidans*: a review. *Process Biochemistry (Oxford), 30*(3), 225-236.

Juszczak, A., Domka, F., Kolowski, M., & Wachowska, H. (1995). Microbial desulfurization of coal with Thiobacillus *ferrooxidans* bacteria. *Fuel, 74*(5), 725-728.

Karamanev, D. G., & Nikolov, L. N. (1988). Influence of some physicochemical parameters on bacterial activity of biofilm: ferrous iron oxidation by Thiobacillus *ferrooxidans*. *Biotechnology and Bioengineering, 31*(4), 295-299.

Karamanev, D. G., Nikolov, L. N., & Mamatarkova, V. (2002). Rapid simultaneous quantitative determination of ferric and ferrous ions in drainage waters and similar solutions. *Minerals Engineering, 15*(5), 341-346.

Nemati, M. (1996). *An evaluation of ferrous sulphate oxidation, using immobilised Thiobacillus ferrooxidans.* University of Manchester Institute of Science and Technology, Manchester.

Nemati, M., Harrison, S. T. L., Hansford, G. S., & Webb, C. (1998). Biological oxidation of ferrous sulfate by Thiobacillus ferrooxidans: a review on the kinetic aspects. *Biochemical Engineering Journal, 1*(3), 171-190.

Nyavor, K., Egiebor, N. O., & Fedorak, P. M. (1996). The effect of ferric ion on the rate of ferrous oxidation by Thiobacillus *ferrooxidans*. *Applied Microbiology and Biotechnology, 45*(5), 688-691.

Okereke, A., & Stevens, S. E., Jr. (1991). Kinetics of iron oxidation by Thiobacillus *ferrooxidans*. *Applied and Environmental Microbiology, 57*(4), 1052-1056.

Pogliani, C., & Donati, E. (2000). Immobilisation of Thiobacillus *ferrooxidans*: importance of jarosite precipitation. *Process Biochemistry (Oxford), 35*(9), 997-1004.

Sasaki, K., & Konno, H. (2000). Morphology of jarosite-group compounds precipitated from biologically and chemically oxidized Fe ions. *Canadian Mineralogist, 38*(1), 45-56.

Smith, J. R., Luthy, R. G., & Middleton, A. C. (1988). Microbial ferrous iron oxidation in acidic solution. *Journal - Water Pollution Control Federation, 60*(4), 518-530.

Torma, A. E. (1977). *Advances in Biochemical Engineering, Vol. 6: New Substrates.*

CHAPTER 4

Biokinetic Characterization of *Ferroplasma acidiphilum*[†]

4.1. Introduction

Acidophilic ferrous iron-oxidizing microorganisms have been implicated in the production of acid mine drainage (AMD), whereby metal sulfides are solubilized by oxidative dissolution, releasing metals and acid (Dopson et al., 2004).

The discharge of AMD causes considerable environmental damage via the release of metal rich acidic effluents into groundwater. It was initially thought that the most important microorganism implicated in AMD was *Acidithiobacillus ferrooxidans* (Dopson et al., 2004). However, recent advances in molecular phylogenic techniques have shown that other species are numerically dominant at certain acid-generating sites.

Examples of these microorganisms are archaea of the genus *Ferroplasma*. There are four different strains of *Ferroplasma* isolated from various environments. *Ferroplasma acidarmanus*, strain Fer1, is found in Iron Mountain, California (Edwards et al., 2000). This strain coexists with bacterial strains of *A. ferrooxidans* and *Leptospirillum* sp. in their natural environment. Fer1 has been known to require yeast extract for growth, but can also grow heterotrophically on yeast extract as the sole energy source (Edwards et al., 2000). It is described as capable of chemolithotrophic growth and heterotrophic growth in the presence of SO_4 (Baumler et al., 2005).

[†] A version of this chapter is being prepared for submittal to the appropriate journal

Ferroplasma acidiphilum, strain Y^T, was isolated from a pilot plant bioreactor for biooxidation of a gold-bearing aresenopyrite-pyrite concentrate (Golyshina et al., 2000). *F. acidiphilum* Y^T was described as being obligatory aerobic and autotrophic, as it is only capable of growth on Fe(II) or Mn(II) with the addition of a small concentration of organic carbon as a growth factor. *F. acidiphilum* Y^T has been reported to be incapable of growth on organic carbon alone and is not capable of aerobic growth on reduced inorganic sulfur compounds (Golyshina et al., 2000). However, more recent studies have classified the organism as a mixotrophic strain that displays inconclusive results for being autotrophic since it has been shown to use low amounts of organics for its carbon source (Dopson et al., 2004).

Another member of the genus *Ferroplasma* is strain MT17, isolated from a South African pilot scale bioleaching reactor oxidizing a polymetallic sulfide concentrate at 45 ^{o}C (Okibe et al., 2003). This isolate was described as unable to grow in the absence of organic carbon but capable of chemomixotrophic growth on yeast extract either with Fe(II) or the reduced inorganic sulfur compound tetrathionate. MT17 was also reported to grow on yeast extract alone and was described as heterotrophic. It was also capable of anaerobically oxidizing yeast extract coupled to the reduction of Fe(III), but it was not ascertained if this was coupled to growth (Dopson et al., 2004).

The final isolate, strain DR1, was cultured from a separate pilot scale biooxidation plant in South Africa and was shown to be similar to the genus *Ferroplasma*. No phenotypic characterization of this isolate has been published (Dopson et al., 2004).

Extensive studies have been conducted using strains MT17, DR1 and Fer1. However, apart from the studies of (Golyshina et al., 2000)., little work has been done in

analyzing strain Y^T, specifically the iron oxidation nature of the strain. In this study, we will further study the kinetics and growth characteristics of strain *Ferroplasma acidiphilum* Y^T. The phenotypic characteristics of strain Y^T are summarized in table 2.4 (Golyshina et al., 2000; Dopson et al., 2004).

4.1.1. Iron Oxidation

F. acidiphilum, like *A. ferrooxidans,* can obtain energy from the oxidation of different inorganic substances, the most common of which is ferrous sulfate. The overall biochemical reaction of the oxidation of ferrous ions is:

$$4Fe^{2+} + O_2 + 4H^+ \xrightarrow{F.a.} 4Fe^{3+} + 2H_2O \qquad (4.1)$$

Physiologically, *F. acidiphilum* obtains energy by oxidation of the ferrous iron in the pyrite (FeS_2) using oxygen as a terminal electron acceptor. This process produces sulfuric acid as a by-product which leads to further acidification of its environment. The reaction is as follows (Edwards et al., 2000):

$$FeS_2 + 14Fe^{3+} + 8H_2O \rightarrow 15Fe^{2+} + 2SO_4^{2+} + 16H^+ \qquad (4.2)$$

The rate of iron oxidation of *F. acidiphilum* has not been widely investigated. Past studies have emphasized on measuring protein concentration as a measure of cell growth (Golyshina et al., 2000). However, it is important to obtain optimal operating conditions for *F. acidiphilum* in a reactor setting by analyzing the rate of iron oxidation as a measure of cell growth.

The study in chapter 3 with *Acidithiobacillus ferrooxidans* has stressed the importance of various factors when studying the rate of iron oxidation. Such factors include pH, temperature, and jarosite formation. Another important factor is also organic

concentration, which is a result of metabolite accumulation. This has adverse effects on cell growth. Given the organic-dependent nature of *F. acidiphilum* reported in literature (Dopson et al., 2004), it is crucial to analyze the effects of organic concentration on the iron oxidizing capabilities of *F. acidiphilum*.

A recent study has examined the effects of temperature on the rates of iron oxidation by *F. acidiphilum* by employing the Ratkowsky equation (Franzmann et al., 2005). This equation describes the relationship of microbial activity to temperature:

$$\sqrt{\frac{1}{Time}} = b(T - T_{MIN})(1 - e^{(c(T-T_{MAX})})) \tag{4.3}$$

Here T is the temperature, "time" is generally the generation time or the time taken to reach a specific condition, T_{MIN} is the theoretical extrapolated minimum temperature for growth, T_{MAX} is the theoretical extrapolated maximal temperature for growth, and "b" and "c" are fitting parameters (Franzmann et al., 2005). Table 4.1 shows the results generated for *F. acidiphilum* using Fe^{2+} as a substrate.

Table 4.1 - Temperature values and constants for *F. acidiphilum* derived from Ratkowsky equation and activation energy derived from Arrhenius plot

T_{MIN} (°C)	T_{OPT} (°C)	T_{MAX} (°C)	"b"	"c"	E_a (kJ/mol)
12.7 ± 6.1	39.6	47.2 ± 0.7	0.00431 ± 0.0149	0.3453 ± 0.03546	79 ± 19

4.1.2. Jarosite Formation

F. acidiphilum is commonly grown on modified 9K medium developed by Silverman and Lundgren (Golyshina et al., 2000). The ferrous iron oxidation occurs via reaction 1. As ferric ions accumulate, hydrolysis reactions occur which result in an increase in pH. However , there is a reaction in competition with the hydrolysis reaction

giving products of basic ferric hydroxysulphates with the formula $MFe_3(SO_4)_2(OH)_6$, where $M=K^+$, Na^+, NH_4^+, Ag^+, or H_3O^+ (Jensen & Webb, 1995).

In chapter 3, studying the affects of jarosite on *A. ferrooxidans*, a bacteria that shares the same niche as *F. acidiphilum*, revealed that the main parameter affecting the jarosite formation was pH. Several experiments yielded results showing oxidation rates as high as 0.181-0.194 g/L·h, with low jarosite precipitation of 0.0125-0.0209 g at conditions of pH 1.6-1.7 with an operating temperature of 35 °C.

4.1.3. Organic Requirement

Several studies have indicated the requirement of an organic nutrient (yeast extract or vitamins) as a growth factor for *F. acidiphilum* growth (Golyshina et al., 2000). This requirement raises questions as to how the bacteria satisfy this nutritional requirement in acid mine solutions. The yeast extract requirement and ability to grow chemoorganotrophically (Dopson et al., 2004) is consistent with previous findings with *T. acidiphilum, Picrophilus* sp., and all *Ferroplasma* sp., which grow mixotrophically (Baumler et al., 2005).

A requirement for oligopeptides has been reported for *T. acidiphilum*, but individual fractions of oligopeptides from yeast extract would not support growth (Smith et al., 1975). It was speculated that yeast extract may: contain or scavenge a micronutrient, protect the organism from the high H^+ gradient, or participate with ion transporters (Smith et al., 1975). The requirement for an exogenous organic molecule indicates that *F. acidiphilum* may be dependent upon other organisms in acid mine solutions (Baumler et al., 2005).

4.1.4. Metabolite Accumulation

It is well documented the *F. acidiphilum* is able to grow in AMD environments shared by *A. ferrooxidans* and *Leptospirillum* sp. (Baumler et al., 2005), for example in Iron Mountain, California (Edwards et al., 2000). In the absence of these organisms, yeast extract is needed as an organic source for *F. acidiphilum* growth (Golyshina et al., 2000).

Organics arise as bacterial cell excrete intermediates of their metabolic pathway into the medium. With time, these organics accumulate and limit the bacterial growth rate of the chemolithotrophic bacteria, *Leptospirillum* sp. and *A. ferrooxidans*. It is reported that organic concentrations in excess of 250 ppm of organic carbon inhibit iron-oxidizing by the aforementioned chemolithotrophs (Drogui et al., 2005). It is suggested that these organics at the threshold concentration repress the enzyme responsible for CO_2 fixation, ribulose diphosphate (RuDP) (Tabita & Lundgren, 1971). Furthermore, table 4.2 gives some concentration reported in literature of different organics that pose inhibitory effects on the chemolithotrophic iron oxidizing bacteria, *A. ferrooxidans*.

Table 4.2 - Inhibitory concentrations of organic compounds for *A. ferrooxidans* (Frattini et al., 2000)

Inhibitory Concentrations (mM)				
Glucose	**Cellobiose**	**Galacturonic Acid**	**Citric Acid**	**SDS**
70	15	50	130	0.3

AMD bacterium possesses a Calvin cycle, an N_2-fixation pathway, possibly a hexose monophosphate pathway, glycolytic enzymes and an incomplete citric acid cycle. Aconitase, isocitrate dehydrogenase, fumarase and malic dehydrogenase are present but succinate and α-ketoglutarate dehydrogenase activities are very low. In complete citric acid cycles are a feature of chemolithotrophs and this is thought to be because the cycle is

directed towards providing carbon skeletons for the synthesis of amino acids rather than functioning as a catabolic pathway (Ingledew, 1982). Succinate is necessary for some important anabolic reactions (haem, methionine and lysine biosynthesis) and it is not clear how this compound can be formed unless it is by reduction of fumarate. Furthermore, poly(β-hydroxybutyrate) has been reported as being a major storage product in a major AMD bacterium, *A. ferrooxidans*. The metabolic skeleton is shown in figure 4.1.

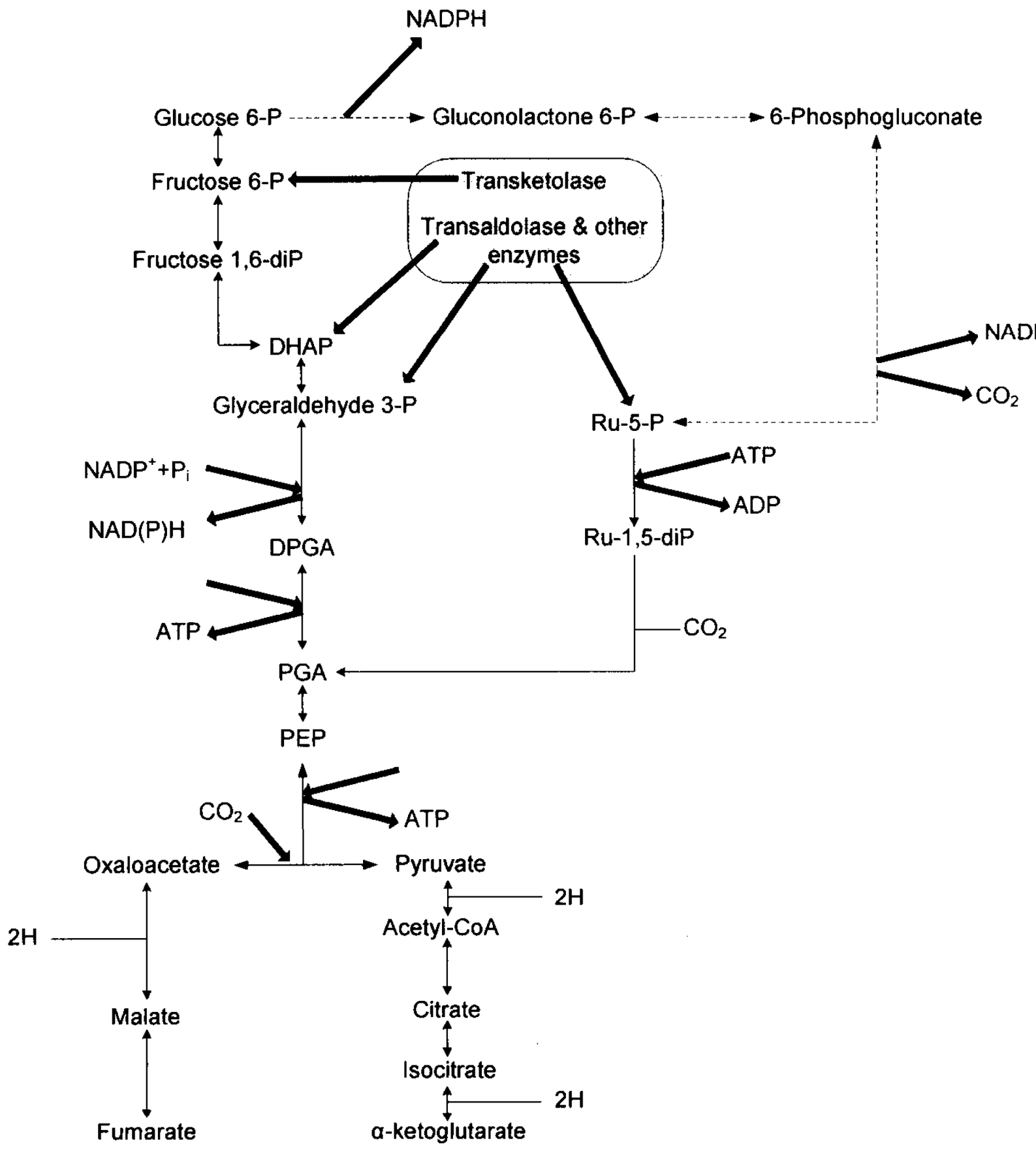

Figure 4.1 - Metabolic skeleton of chemolithotrophic iron-oxidizing bacteria (Ingledew, 1982)

It is speculated that organics, from the metabolic pathway of organisms that share the environment, are used as growth factors by *F. acidiphilum*. It is even reported that *F. acidiphilum* is capable of mixotrophic growth and minor organic carbon requirement (Dopson et al., 2004). However, extensive studies have been inconclusive as to the specific organic that is utilized by *F. acidiphilum* (Golyshina et al., 2000). Nonetheless, it is vital to study the effects of organic accumulation on the growth rate of *F. acidiphilum*.

4.1.5. Purpose of this Study

The main goal of this study is to perform a thorough kinetic characterization of the mixotroph *Ferroplasma acidiphilum*. Firstly, it is important to find the optimal yeast concentration which promotes organic consumption. Using this information, the next step is to find the optimal conditions that minimize jarosite precipitation while not comprising iron oxidation. Once obtaining the optimal conditions for *Ferroplasma* iron oxidation, it is important to analyze the organic dependence of the organism and its growth kinetics. The next and final step involves the characterization of *Ferroplasma* growth and organic dependence in a mixed culture with the chemolithotrophic *Leptospirillum* sp. microorganism, resembling the organisms' natural environment. This will give valuable insight into the capability of *Ferroplasma* to control the organic levels in conjunction with chemolithotrophic iron oxidizing strains.

4.2. Materials and Methods

This experiment deals with the effect of various factors on the iron-oxidation capabilities and organic dependence of the strain *Ferroplasma acidiphilum*. Therefore, the experiment was divided into various parts.

4.2.1. Equipment

The pH of each trial was adjusted using sulfuric a cid and monitored using a pH meter (Orion Model No. 420A). For the shake flask experiments, the bacteria were allowed to grow in a rotary flask shaker with speed and temperature adjustment (New Brunswick Scientific Model No. G-25 R). For the ferric and total iron analyses, we used a spectrophotometer (Varian Cary 50) with the appropriate procedure (Karamanev et al., 2002). For the jarosite measurement, filter paper with pore size 25 um was used to separate the jarosite produced in each flask.

For the TOC measurement, we used a Tekmar Dohrmann Apollo 9000 TOC analyzer, which uses a combustion-based analyzer of organic carbon. Moreover, to measure microbial concentration, we used a Zeiss Axioskop 40 upright microscope, and viewed 5 ul samples under 100x magnification, which are calibrated according to the viewing area in relation to the pixel area.

4.2.2. Chemicals and Microorganisms

All the chemicals used in this study were of analytical grade, including 100% H_2SO_4, components of the 9K medium, sulfosalicylic acid, ammonium hydroxide (30%) and the chemical constituents of the FISH buffers.

The strain *Ferroplasma acidiphilum* was obtained from Deutshe SammLung von Mikroorganism (DSM12658). *Leptospirillum* sp. was obtained from AMD in Iron Mountain, California.

4.2.3. Yeast Effect

The first part of the experiment involves finding the optimal yeast concentration in which iron oxidation and organic consumption occur in conjunction. As a starting basis, 0.02% (w/v) yeast concentration, pH of 1.7 and temperature of 35 °C were used since they were reported to give optimal bacterial growth (Golyshina et al., 2000). This allowed us to test for both the appropriate and limiting organic concentrations along with a better understand of the organic dependence of the organism with respect to organic accumulation/consumption.

Six 250 mL Erlenmeyer flasks were used, one for each yeast concentration in the range of 0% - 2% (w/v) in ten-fold intervals. 225 mL of modified 9K medium along with the varying yeast concentrations (by adding the appropriate volume of 10% (w/v) yeast solution) were added to each flask. The desired pH of 1.7 was obtained by adding 100% H_2SO_4 drop wise, with continuous agitation and pH measurement. Further, 20 mL of *F. acidiphilum* inoculum was added to each flask. The inoculum contained an average of 10^9 cells per milliliter. The flasks were then covered with pieces of glass wool in order to provide proper aeration and preventing major evaporation. Finally, the flasks were placed in a rotary shaker at 35 °C with a rotation speed of 260 rpm. The Fe^{3+} and Fe_{total} concentrations in the flasks were measured initially and at appropriate time intervals throughout the course of oxidation. Furthermore, a 30 mL sample from each flask was also obtained periodically throughout the oxidation for TOC measurement (using a combustion based TOC analyzer) in order to analyze the organic accumulation/consumption at various yeast concentrations.

4.2.4. pH Effect

After obtaining an optimal yeast concentration for iron oxidation purposes, the second part of the experiment involves finding an optimum pH at which minimal jarosite precipitation occurs while not compromising iron oxidation.

Eight 100 mL Erlenmeyer flasks were used, one for each pH range of 0.3-2.5 in intervals of 0.3 pH. 100 mL of modified 9K medium and the appropriate yeast concentration were added into each of the eight flasks. The desired pH in each flask was obtained by adding 100% H_2SO_4 drop wise, with continuous agitation and pH measurement. Further, 5 mL of *F. acidiphilum* inoculum was added to each flask. The inoculum contained an average of 10^9 cells per milliliter. The flasks were then covered with glass wool. Finally, the flasks were placed in a rotary shaker at 35 °C with a rotation speed of 260 rpm. The Fe^{3+} and Fe_{total} concentrations in the flasks were measured initially and at appropriate time intervals throughout the course of oxidation.

When the iron oxidation was near completion, the flasks were removed from the shaker in order to measure jarosite precipitation. Firstly, the liquid in each flask was filtered using a vacuum flask and filter paper (pore size 0.45 μm). The solids on the filter paper were then returned back to the corresponding flask by washing them with distilled water. This combines the filtered jarosite with that deposited on the flask walls. Approximately 10 mL of 50% H_2SO_4 were then added to each flask in order to dissolve the jarosite and resuspend the wall deposits. Finally, the total iron concentration was measured using the sulfosalycilic method and the volume of mixture of each flask was measured using graduated cylinders in order to obtain the total mass of jarosite present.

4.2.5. Temperature Effect

For the third part of the experiment, the appropriate pH range and yeast concentration from earlier findings, were selected in order to test for the optimum temperature. This allows us to obtain the optimum yeast, pH and temperature combination in which the bacterial iron oxidation is maximal with minimal jarosite formation and the appropriate organic concentration.

To start this part of the experiment, we selected an optimal pH range and yeast concentration that yields maximal oxidation with minimal jarosite precipitation from earlier experiments. We then selected the appropriate number of 100 mL flasks in order to have pH intervals of 0.1. We then followed the same procedure as the first part except we set the flask shaker temperature consecutively to 25 °C, 35 °C, 40 °C and 50 °C.

The mean ferrous iron oxidation rate (in g/L·hr) was determined by calculating the concentration of iron oxidized and dividing it by the time period in which the oxidation occurred. This calculation is performed during the exponential phase growth of the bacteria.

4.2.6. Organic Effect

The next step of the experiment is a further examination of the organic requirement of the organism. In step 1, it is determined which yeast concentration yields the best results in terms of iron oxidation. However, in order to closely examine the organic dependence of the organism, there must be a comparison with the a culture at optimal yeast concentration, found in experiment 1, and other scenarios in which yeast and/or iron are used as limiting factors.

This experiment involves inoculating three different 100 mL flasks with 5 mL of 10^9 bacteria per milliliter. The first flask contains 100 mL of modified 9K solution with the optimal yeast concentration. Flask two contains 100 mL of modified 9K solution but with no yeast added. Finally, the third flask contains 100 mL of Fe-free modified 9K solution containing the appropriate amount of yeast extract.

In order to measure biomass, a 5 μL sample is analyzed and cells are counted using a phase contrast microscope. Like the first experiment, TOC is measured using a TOC analyzer. This experiment will allow us to further analyze the extent of the bacteria's organotrophic and mixotrophic capabilities.

4.2.7. Substrate Concentration Effect

After thoroughly evaluating *Ferroplasma* iron oxidizing and growth capabilities in terms of pH, temperature and organic concentration, it is important to characterize the bacterial growth rate. In classic Monod kinetics, this is accomplished by evaluating the growth curve of the organism through variation of the substrate concentration, in this case, ferrous iron.

In this experiment, using the optimal conditions obtained earlier, we examined the substrate effect of 5 g/L, 10 g/L, 20 g/L and 40 g/L in an inverse fluidized bed bioreactor setting. The inverse fluidized bed reactor is a 1.5 L vessel which contains 2-3 mm low density polyethylene balls with a smooth surface in order to prevent the formation of biofilm and limit jarosite build-up due to the lack of a rough surface for immobilization. The reactor was constructed using pelxiglass and contained an inner draft tube that was aerated using a perforated nozzle. The outer diameters of the reactor and the draft tube were 6 cm and 3 cm, respectively. Also, the height of the reactor was 55 cm, while the

height of the draft tube was 45 cm. The reactor configuration is shown in figure 4.2. This is in order to improve the mixing and aeration in order to provide a more thorough study of the bacteria in a batch regime. The reactors were filled with 1.2 L of modified 9K medium (Fe^{2+} concentration modified accordingly) with the appropriate yeast concentration, then inoculated with 45 mL of 10^9 bacteria per milliliter. To measure iron oxidation, Fe^{3+} and Fe_{total} measurements are performed using the sulfosalycilic acid method. Also, biomass concentration was also measured using cell counts under a phase contrast microscope.

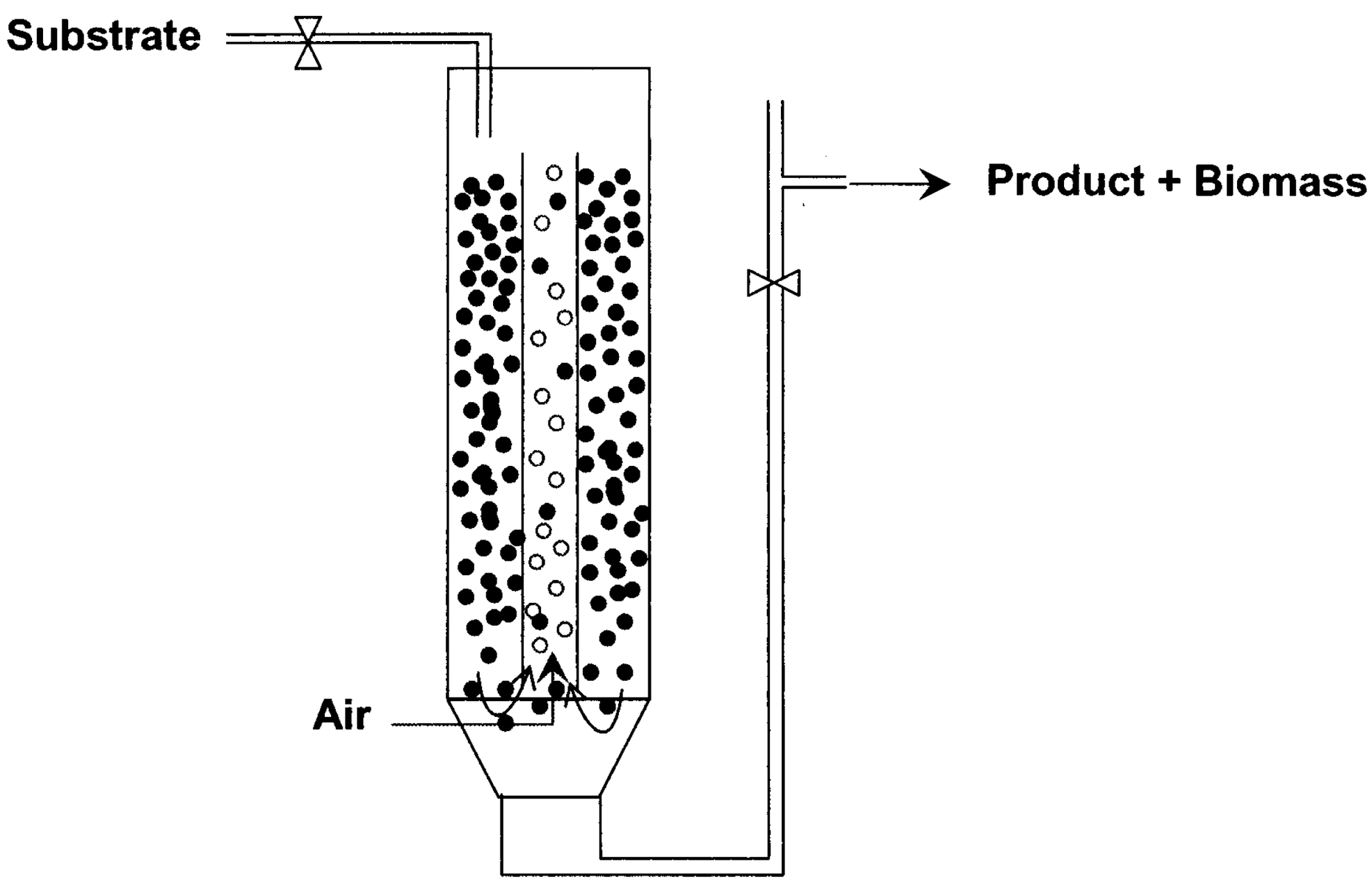

Figure 4.2 - Inverse fluidized bed reactor

4.2.8. Mixed Culture Growth

This final part of the experiment was based on the compilation of the results produced in the earlier experiments. Bearing in mind the optimal conditions uncovered earlier, we inoculated 1.2 L of 9K medium (not containing yeast) with 20 mL of the

chemolithotrophic iron-oxidizer *Leptospirillum* sp. and the mixotroph *F. acidiphilum* in a 1.5 L inverse fluidized bed reactor (shown in figure 4.2). Iron oxidation, biomass concentration and TOC are measured on periodically using the sulfosalycilic acid, microscope count method, and TOC analyzer, respectively. Also, a 10 mL sample is taken at each reading for the purpose of performing fluorescent in situ hybridization (FISH) in order to quantify and qualitatively identify each strain with time.

This is the most important experiment since the results address the mixotrophic organism's ability to live in conjunction with its chemolithotrophic counterpart in a reactor setting while utilizing the chemolithotrophic organism's organic deposits as its organic requirement for growth; thus controlling the organic concentration at a level below the lethal threshold of chemolithotrophic bacteria.

4.2.9. Analytical Procedures

The analysis of ferrous and ferric iron concentrations at different times in the bacterial samples was done using a precise quantitative method, which is not affected by the presence of iron or *A. ferrooxidans* in solution. The method utilizes a spectrophotometer for the colorimetric measurement of red-colored ferric-sulfosalicylate complex, which gives the concentration of Fe^{3+} in solution. Ammonia is then added, causing the 5-sulfosalicylic acid (SSA) to form a yellow complex with all the iron ions, which gives the concentration of total iron in solution (Karamanev et al., 2002).

4.2.10. Fluorescent in situ hybridization (FISH)

For FISH analysis, 10 mL samples were centrifuged and resuspended with freshly prepared 4% paraformaldehyde/phosphate buffered saline (PBS; 130 mM sodium

chloride, 10 mM sodium phosphate buffer, pH 7.2) solution. The fixed samples were stored at 4 °C for 1-3 hours. Following fixation, the samples were centrifuged and washed with PBS buffer to remove the fixative. The cells were then resuspended in a PBS/96% ethanol solution (1:1, v/v), and stored at -20 °C prior to hybridization.

Prior to hybridization, the fixed samples or control cells were partially homogenized by vortexing. Ten microliter aliquots of each sample were spotted to each of three wells on a CLEARCELL slide ER-203B-2 (Erie Scientific, Portsmouth, NH). The samples on the slides were dried at room temperature, then dehydrated and permeabilized by passing through a 50%, 80% and 96% ethanol series (3 min each). Samples were air dried again at room temperature. For each slide, a master mix resuspended in 1.7 mL Eppendorf centrifuge tubes was made by adding 100 µl of hybridization buffer, 0.9 M NaCl, 20 mM Tris/HCl (pH 7.4), 0.01% SDS (w/v), containing 100 ng of labeled probe, in the presence of formamide (v/v according to table 4.3 for each probe). The mixture was gently mixed. A 25 µL aliquot of master mix containing the probe was applied to each well on a slide. A cover glass (22 x 50 mm, FISHERfinest) was placed on top of each slide. Slides were incubated for 90 min at 46 °C in a rotary shaker, but without shaking.

Table 4.3 - Probes used for FISH

Probe	*Nucleotide sequence (5' – 3')*	*Specificity*	*Formamide/NaCl (%/mM)*	*Reference*
LF655	CGCTTCCCTCTCCCAGCCT	*Leptospirillum* species	35/70	(Bond & Banfield, 2001)
FER656	CGTTTAACCTCACCCGATC	*Ferroplasma* genus	25/149	(Edwards et al., 2000)

After hybridization, washes were done in diffuse light to avoid bleaching of fluorescence. Cover glasses were removed from slides by dipping them in a Coplin staining jar filled with prewarmed wash buffer. Then, slides were immediately placed in a

wash buffer band incubated at 48 °C for 15 minutes. The buffer was composed of 20 mM Tris/HCl (pH 7.4), 0.01% SDS (w/v), 5 mM EDTA, and the appropriate concentration of NaCl obtained from table 4.3 for each probe. Slides were rinsed in distilled water to remove salts and SDS, and air-dried in a dark room at room temperature. The slides were then counterstained with 4',6-diamidino-2-phenylindole (DAPI; Sigma-Aldrich) working solution (200 ug/mL) for 10 minutes and then rinsed in sterile distilled water before being dried in the dark at room temperature. Each slide was mounted with the anti-fading agent Vectashield (Vector Laboratories, Burlingame, CA), covered with a cover glass, and observed after storage at -20 °C.

For viewing the slides, we used a Zeiss Axioskop 40 upright microscope with an HBO 50W UV light source. Probes LF655 and FER656 were labeled at the 5' end with Texas Red and Cy5 fluorescent dyes, respectively. To view the different fluorescently labeled probes and the nucleic acid specific DAPI dye, various filter sets were used. Chroma filter set C-73347, Zeiss filter sets 00 (488000-0000) and 50 (488050-0000) were used for viewing DAPI, Texas Red and Cy5, respectively.

4.3. Results and Discussions

As mentioned above, this study involved various parts with the overall goal of kinetically characterizing *Ferroplasma acidiphilum* in order to arrive at appropriate conditions of operation which promote organic consumption and minimize jarosite precipitation while not compromising iron-oxidation. Furthermore, this will lead us to attain the final goal of growing a mixed culture of the mixotroph with a chemolithotrophic iron oxidizer, *Leptospirillum*, with the aim of controlling the metabolite organic accumulation produced by the chemolithotroph.

4.3.1. Yeast Concentration

Several experimental runs were performed in order to obtain the optimal yeast concentration that yielded the optimal combination of iron oxidation and organic consumption. This was performed at a pH of 1.7 and temperature of 35 °C. The yeast concentrations examined were 0%, 0.0002%, 0.002%, 0.02%, 0.2% and 2% (w/v). Figure 4.3 shows the iron oxidation rate for the various concentrations.

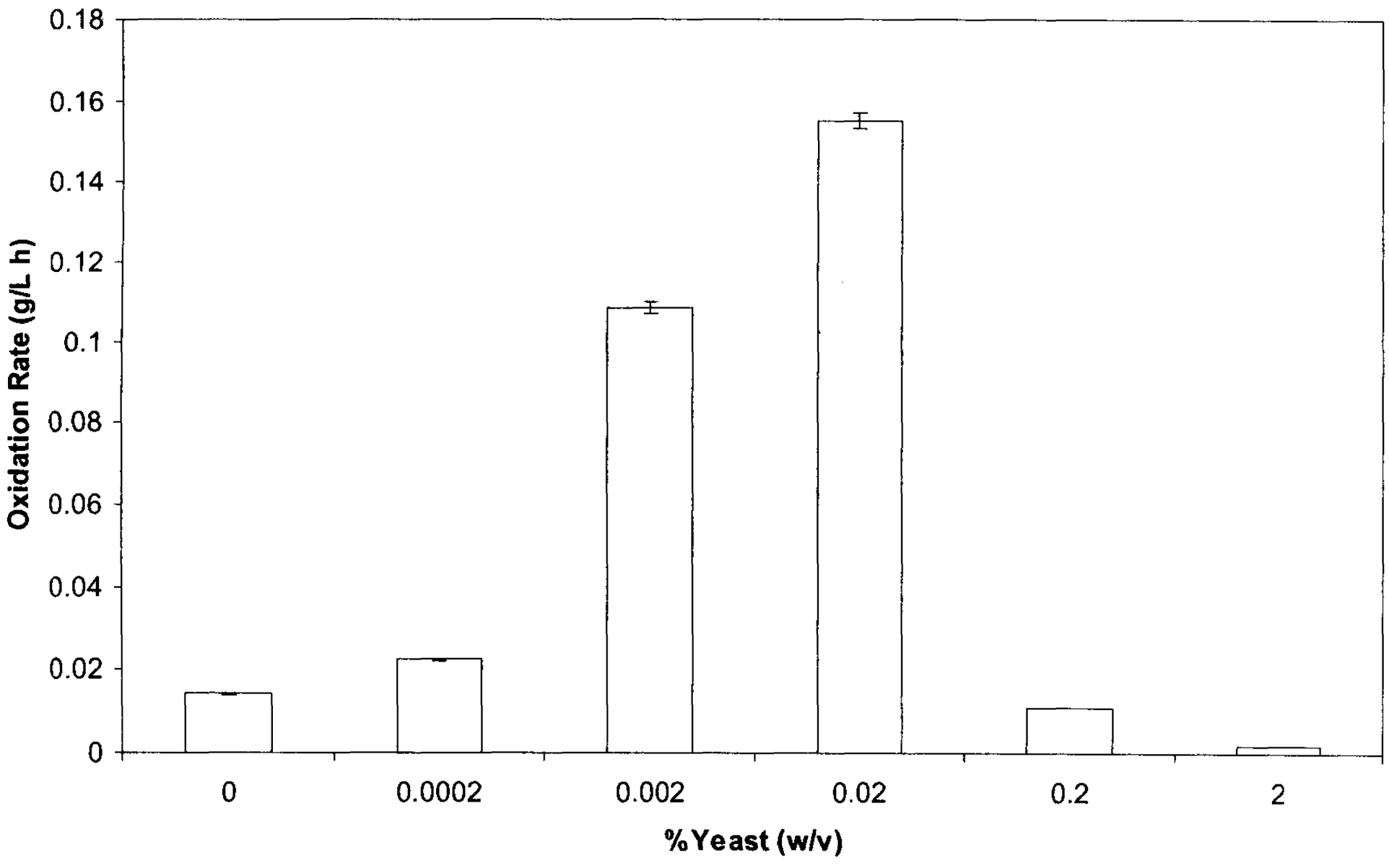

Figure 4.3 – Iron oxidation rates at different yeast concentrations

It is clear that the iron oxidation is greatly enhanced when the yeast concentration is 0.02% (w/v) and inhibited at concentrations of 0.2% (w/v) and above. Figure 4.4 shows the TOC in the system for the yeast concentrations of 0%, 0.0002%, 0.002% and 0.02% (w/v), which displayed oxidation. At concentrations of 0%, 0.0002% and 0.002% (w/v) yeast, the organic carbon rises to a level of approximately 45-50 ppm before being consumed by the bacteria until a plateau is reached around 20 ppm. Moreover, it is

apparent that at 0.02% (w/v) yeast, the bacteria utilize the available organic carbon, reaching a plateau at approximately 30 ppm toward the end of the oxidation; this is more clearly shown in figure 4.5. These results point to the organic dependence of *F. acidiphilum* as a mixotrophic organism. We will later examine in this study the organotrophic nature of the organism as well as its ability to control organic carbon alone and a mixed chemolithotrophic culture.

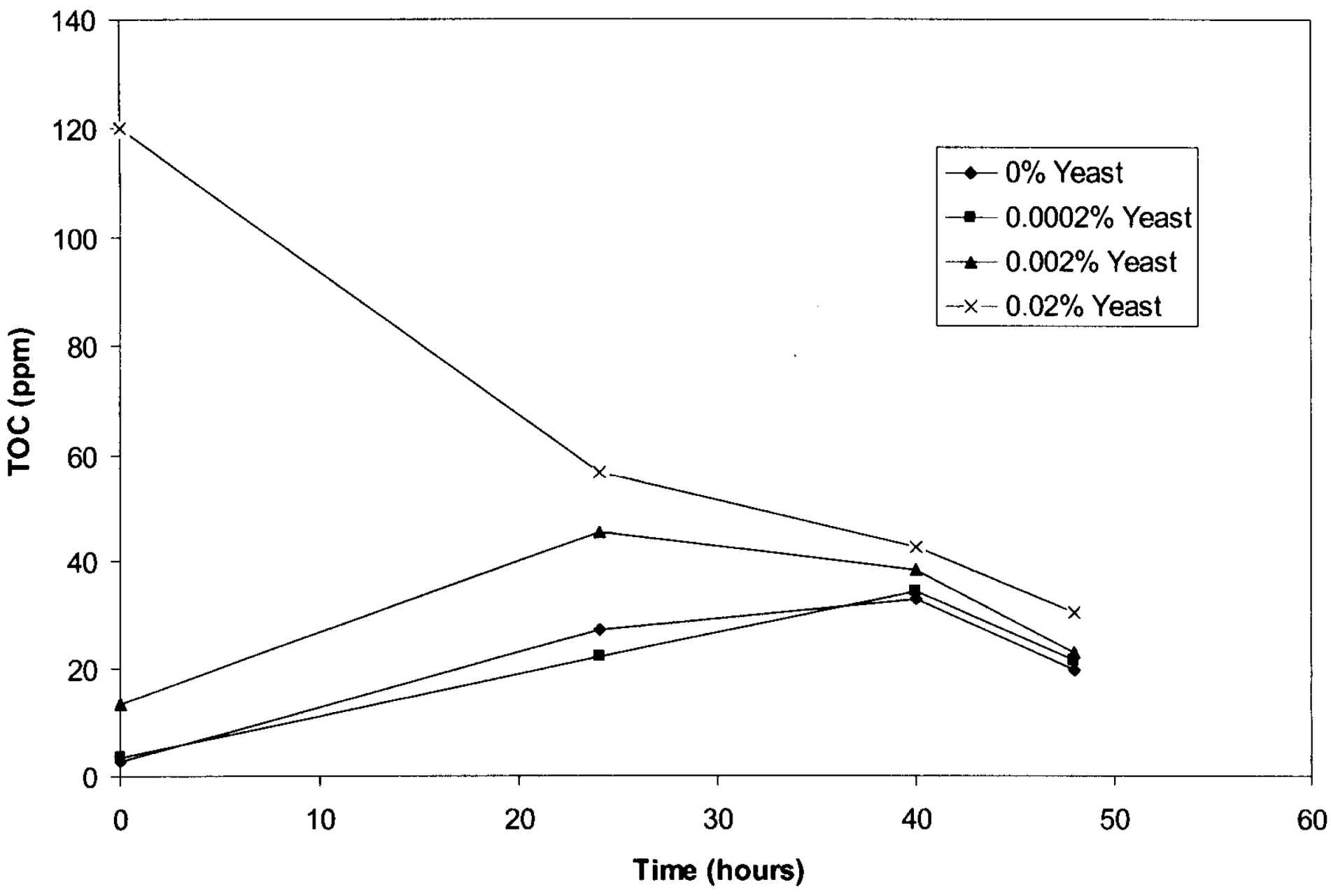

Figure 4.4 - TOC vs. time at various yeast concentrations

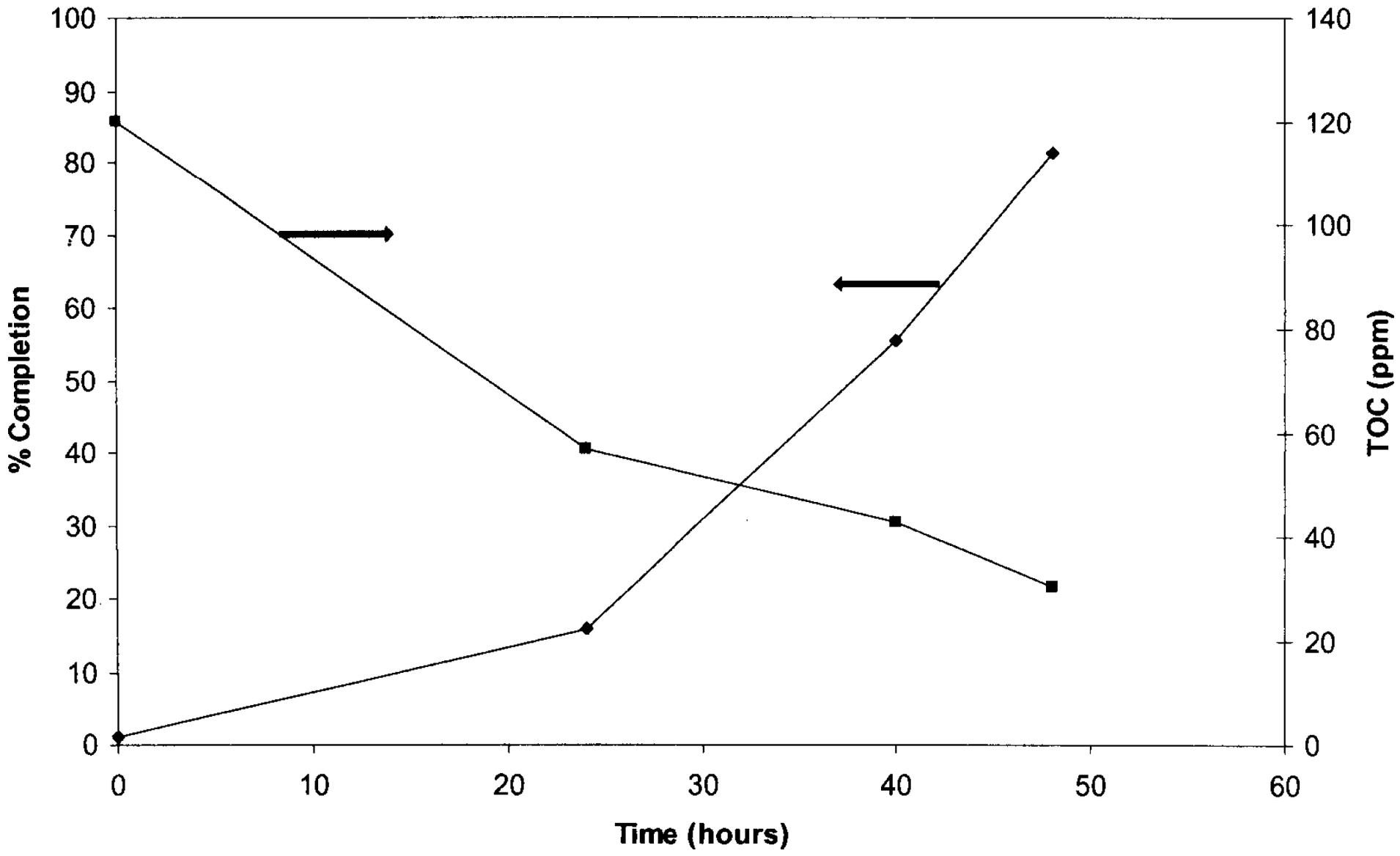

Figure 4.5 - Percent completion of oxidation and TOC vs. time

4.3.2. pH

Using the optimal yeast concentration of 0.02% (w/v) and the suggested temperature of 35 °C, the pH was varied between 0.3 and 2.5 in intervals of 0.3 and the oxidation rate was observed. The jarosite mass produced was measured at the end of the oxidation period in which the bacteria oxidized most of Fe^{2+} into Fe^{3+}. Figure 4.6 clearly indicated that at a pH range of 1.4-1.6, low jarosite mass was produced while still maintaining high iron oxidation rates.

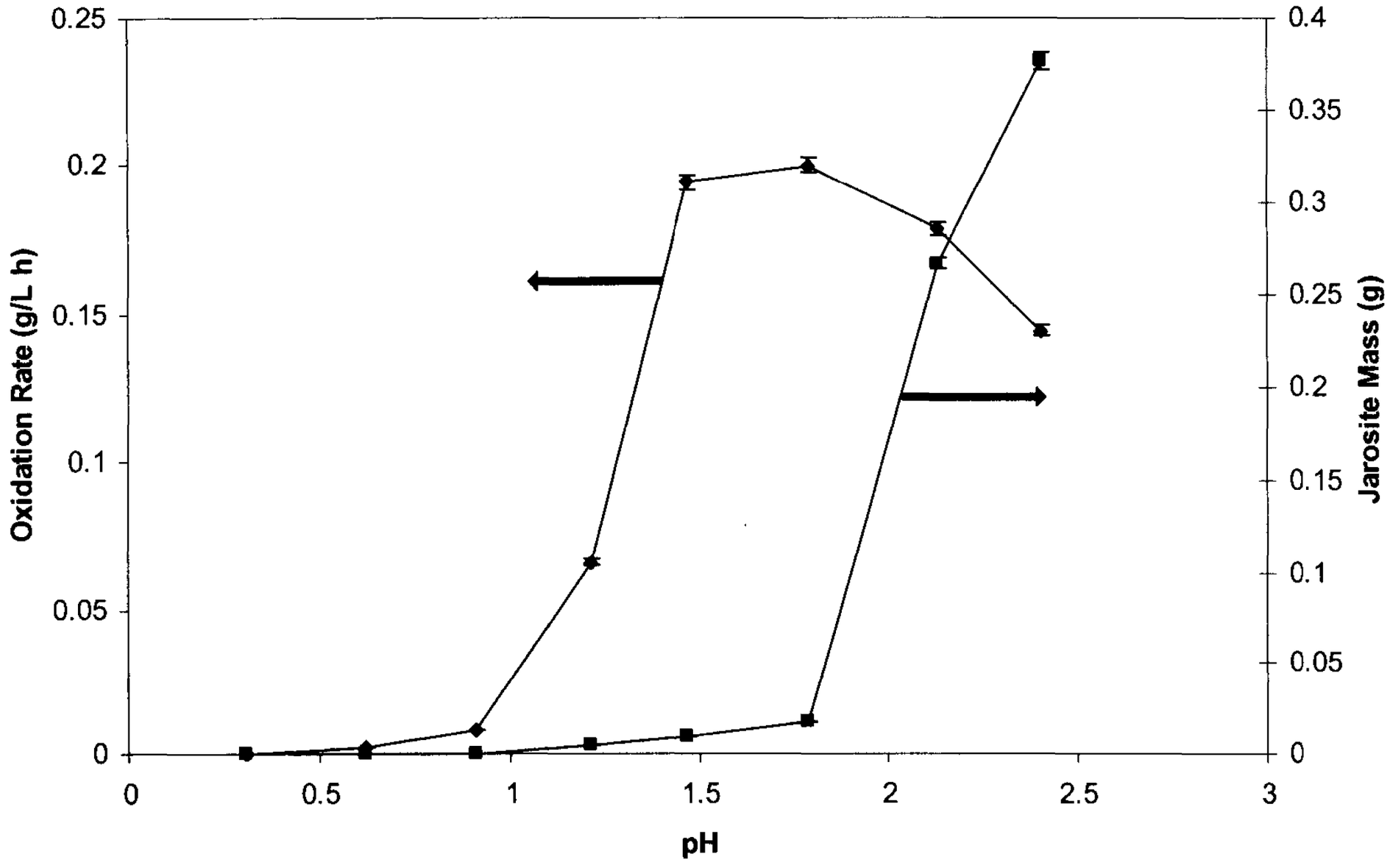

Figure 4.6 - Oxidation rate and jarosite mass vs. pH

4.3.3. Temperature

Using the pH range of 1.4-1.6 and yeast concentration of 0.02% (w/v) obtained earlier, the temperature is varied at 25 °C, 35 °C, 40 °C and 50 °C in order to yield the optimal temperature of operation. Figure 4.7 clearly shows that at pH of 1.6 and 35 °C, the oxidation rate is maximal. Furthermore, all pHs displayed thermal deactivation at 50 °C.

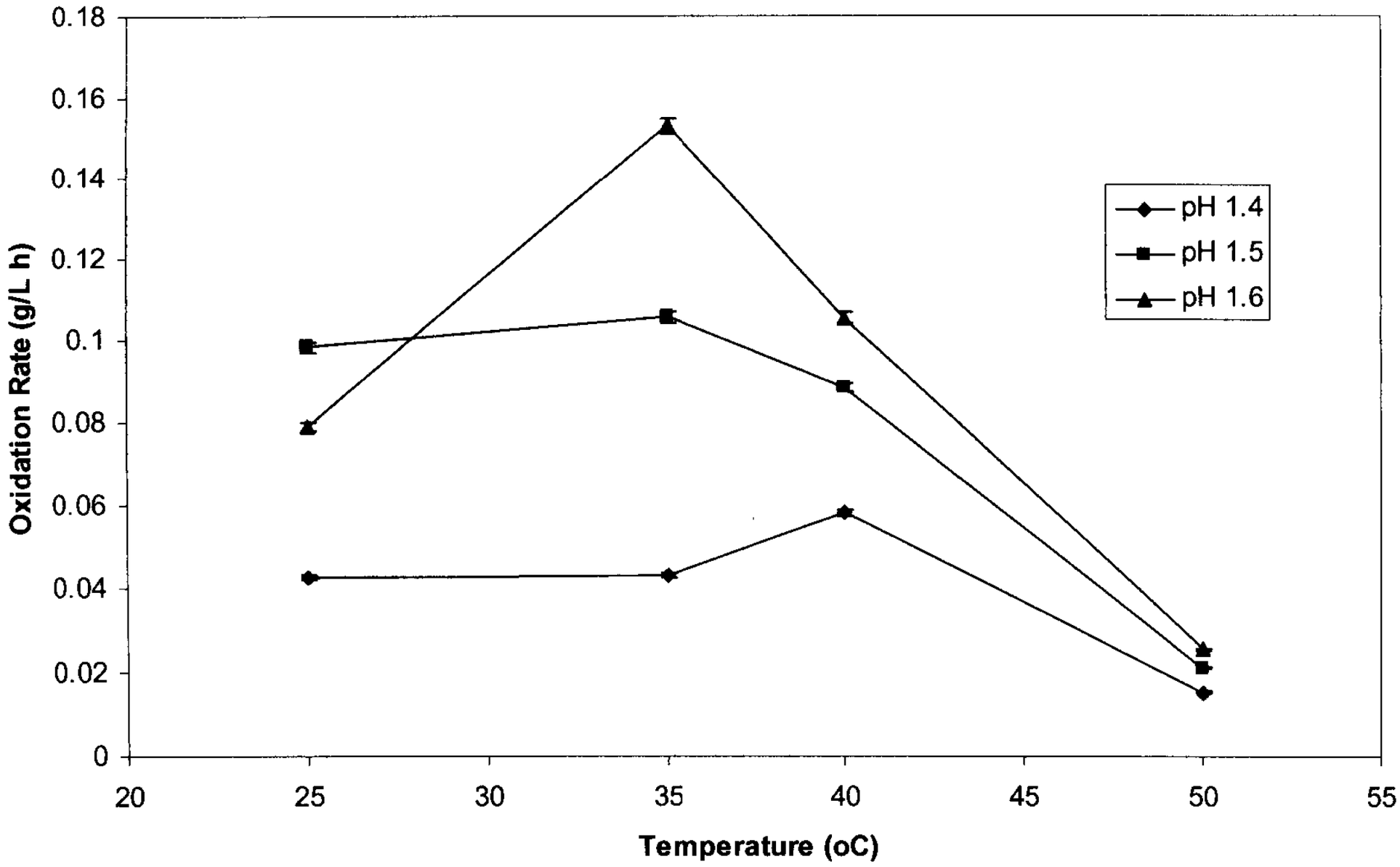

Figure 4.7 - Oxidation rate vs. temperature at different pHs

4.3.4. Organics

As mentioned before, the optimal yeast concentration was found to be 0.02% (w/v). It was also shown from Figure 4.5 that at this concentration, the amount of organic carbon decreases with time as the iron oxidation goes to completion until a plateau is reached. This indicates the mixotrophic behaviour of the organism. However, in order to further study the organic dependence and organotrophic characteristics of the organism, we analyzed *F. acidiphilum* growth at normal optimal conditions (pH 1.6, temperature of 35 ^{o}C and yeast concentration of 0.02% w/v), no yeast, and only yeast.

Figure 4.8 shows that biomass concentration increases the most with the normal culture (Fe + yeast), followed by the culture only provided with yeast. Cell growth was not encouraged in the absence of yeast. These biomass trends for the normal and only

yeast cultures are both inversely proportional to the TOC trend shown in figure 4.9. The organic carbon concentration as well as the cell growth both displayed very similar trends for the normal and only yeast cultures, with increasing biomass concentrations with time, and decreasing TOC that plateaus at approximately 20 ppm. This confirms the occurrence and similarity in trends of mixotrophic and organotrophic growth of the organism.

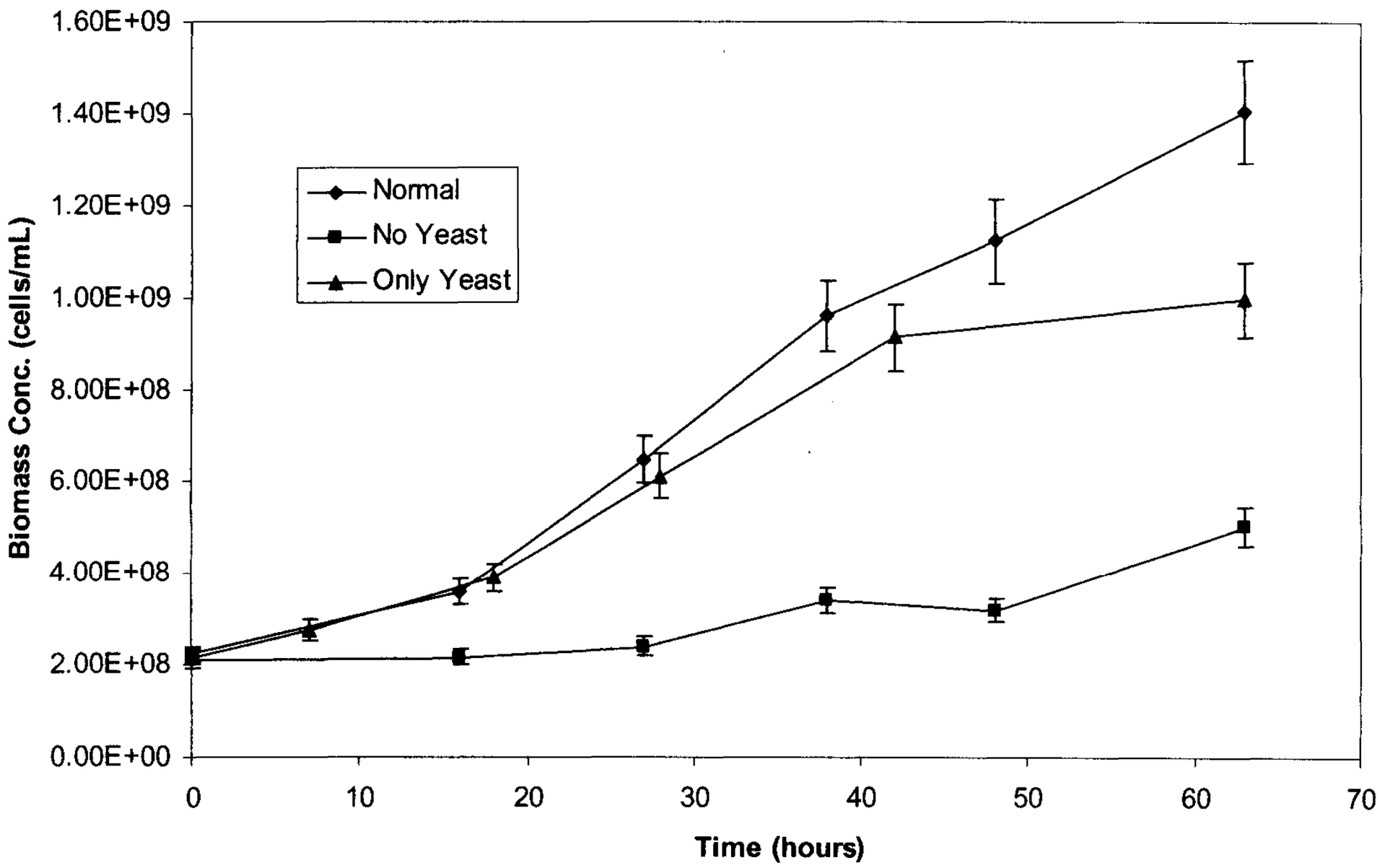

Figure 4.8 - Biomass concentration vs. time for various culture conditions

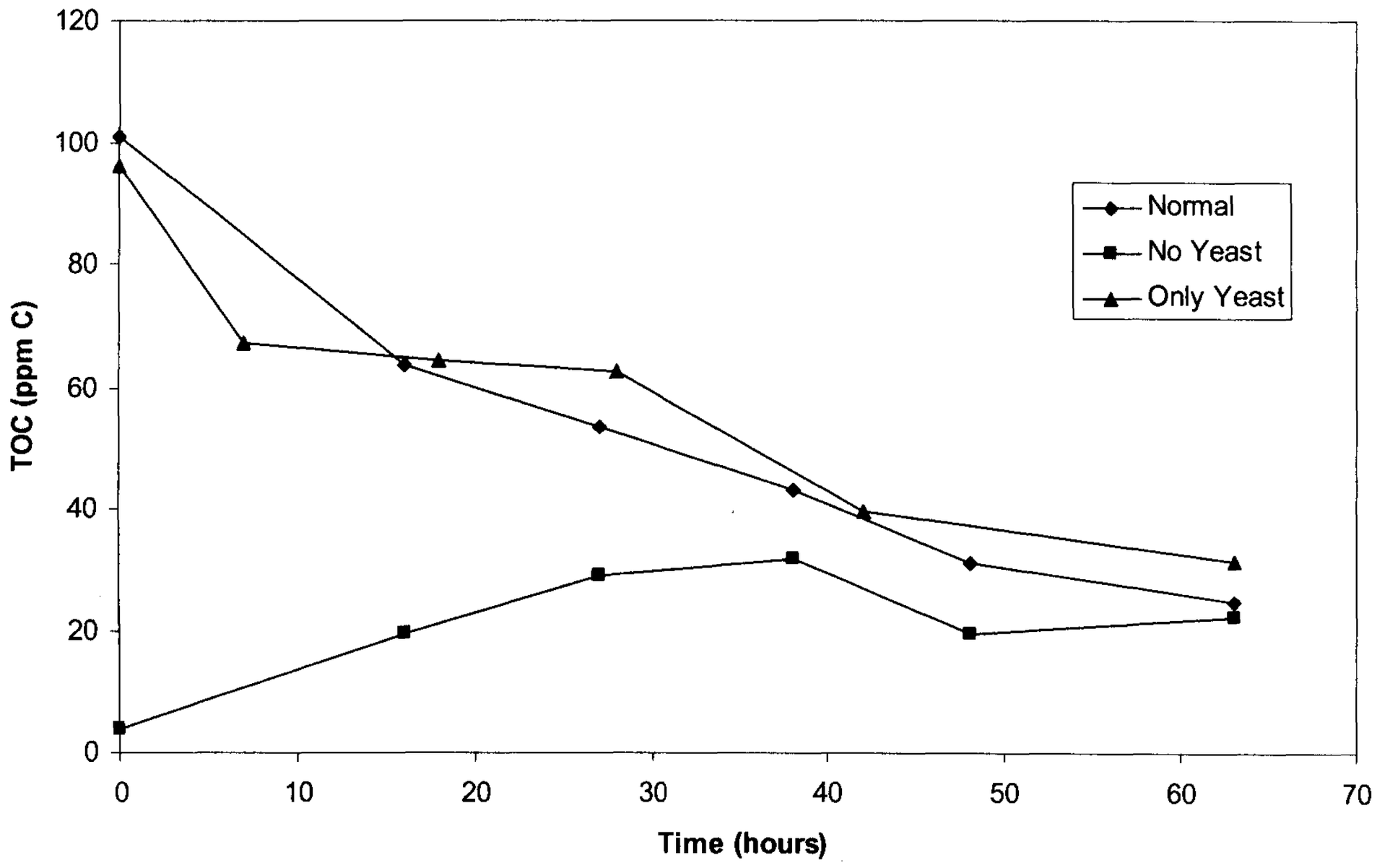

Figure 4.9 - TOC vs. time for various culture conditions

4.3.5. Fe^{2+} Concentration

The last step in characterizing *F. acidiphilum* is calculating the specific growth rate of the bacteria. This is accomplished by growing the bacteria under different substrate (ferrous iron) concentrations of 5 g/L, 10 g/L, 20 g/L and 40 g/L. The specific growth rate is obtained from equation 4.5 under exponential phase growth.

$$X = X_o e^{\mu t} \tag{4.5}$$

To isolate for specific growth rate, equation 4.6 is used.

$$\mu \cdot t = \ln\left(\frac{X}{X_o}\right) \tag{4.6}$$

The specific growth rate for different substrate concentrations is then used in a classic cell growth rate versus substrate concentration plot in order to give insight into the

organism's maximum specific growth rate and the concentration at which substrate inhibition occurs. This relationship follows the Monod kinetics given in equation 4.7.

$$\mu = \frac{\mu_{max} S}{K_s + S} \tag{4.7}$$

Figure 4.10 is a plot of biomass concentration versus time for the different substrate concentrations. It is clear that the lag time for bacterial growth increases accordingly with substrate concentration. Using the data from the exponential phase growth of the bacteria, Figure 4.11 provides a plot of $\ln(X/X_o)$ versus time in which the slope gives the growth rate constants. It is clear that as the substrate concentration increases above 5 g/L ferrous iron, the specific growth rate of the bacteria decreases. Figure 4.12 indicates the trend of specific growth rate versus substrate concentration, giving a maximum specific growth rate of 0.0351-0.042 h^{-1}, while displaying the trend in substrate inhibition above 20 g/L ferrous iron.

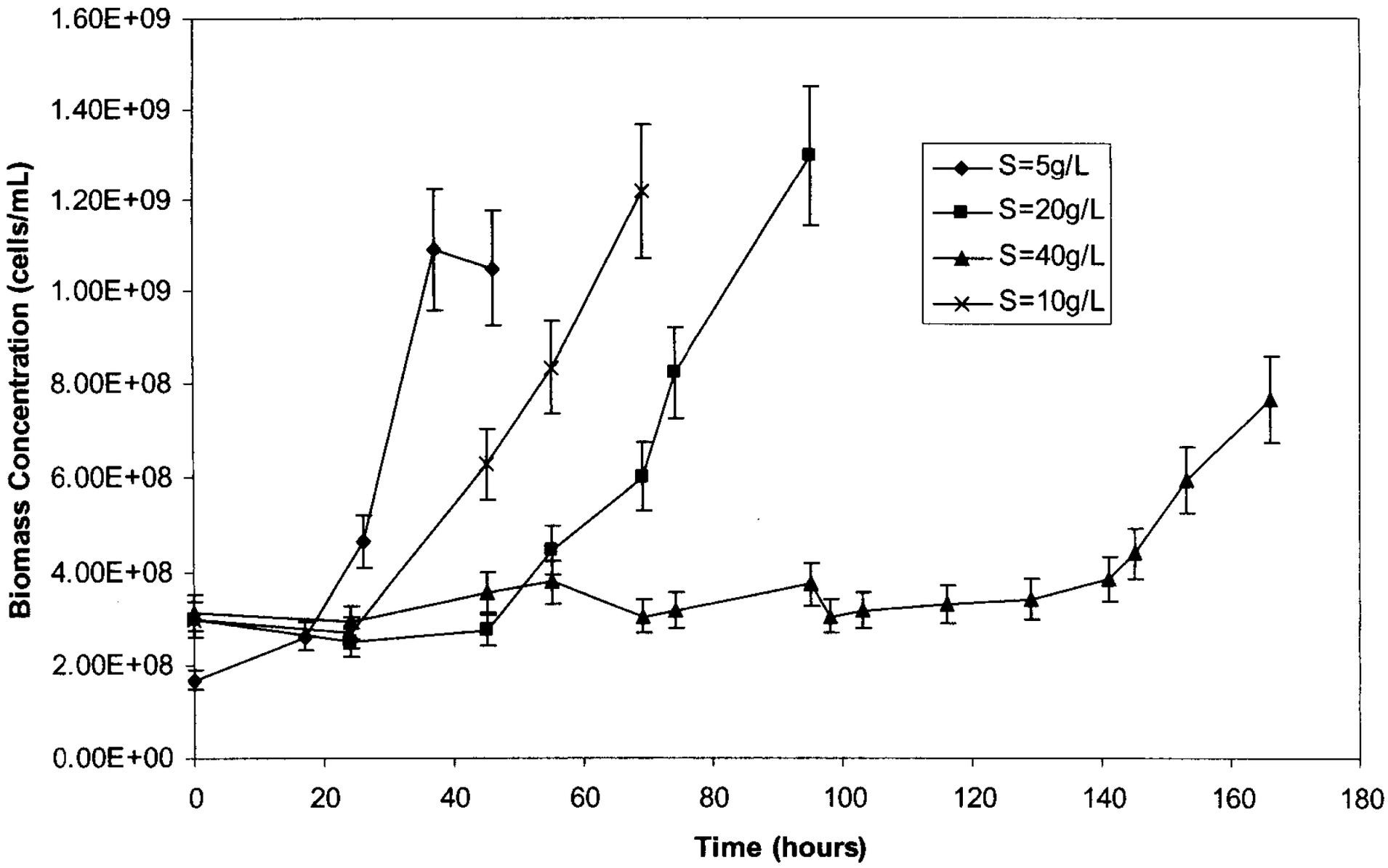

Figure 4.10 - Biomass concentration versus time for various substrate concentrations

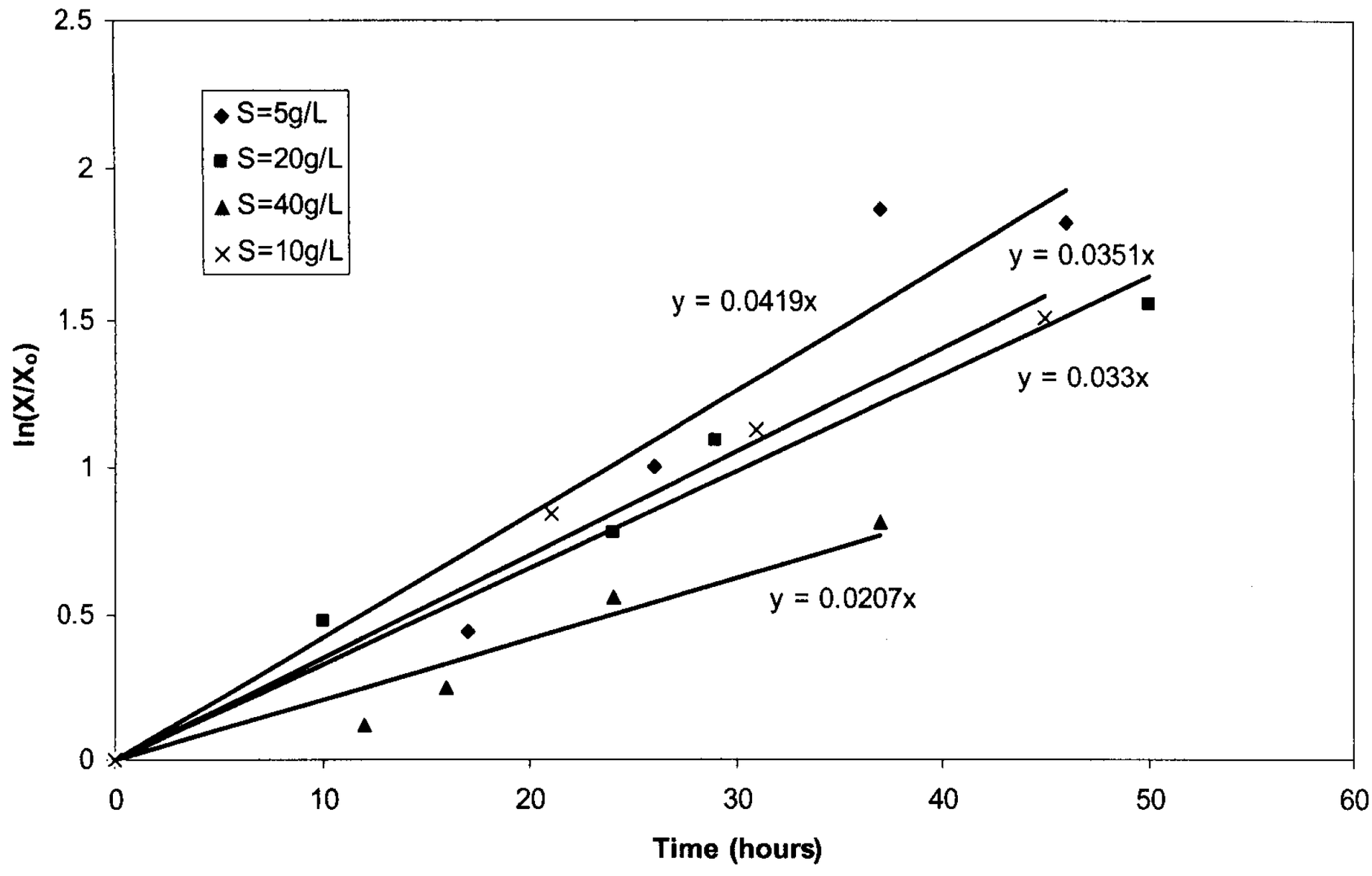

Figure 4.11 - ln(X/Xo) versus time for various substrate concentrations

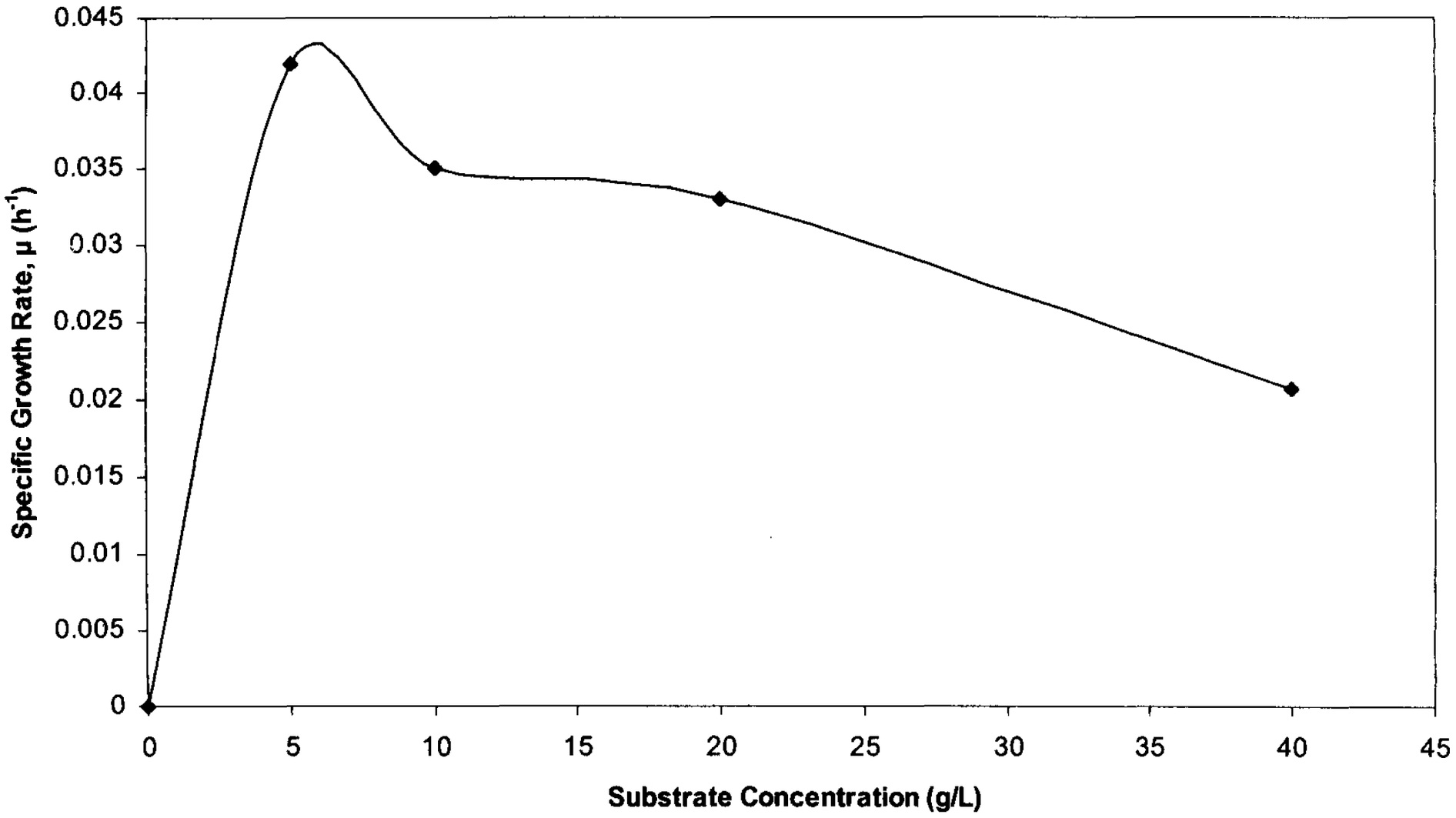

Figure 4.12 - Specific growth rate versus substrate concentration

4.3.6. Mixed Culture Growth

Now that *F. acidiphilum* has been successfully characterized, it is important to analyze the strain's capability to grow in a mixed culture with its chemolithotrophic counterpart, *Leptospirillum* sp., with the goal of utilizing the organic metabolite accumulation as its organic source for growth. This will in turn limit the organic accumulation and control its concentration below the threshold lethal level of 100 ppm TOC.

The mixed culture was grown in accordance to the optimal condition of both iron-oxidizing strains. Since the chemolithotrophic strain's optimal growth occurs at 40 °C and pH of 1.1, and the mixotroph prefers 35 °C at pH of 1.6, it was decided to culture both in yeast-free 9K media at pH of 1.3 and 38 °C.

Figure 4.13 shows the relationship between the biomass concentration of each strain and TOC of the solution versus time. At the beginning of the oxidation, it is clear

that the chemolithotroph *Leptospirillum* is dominant. However, as the oxidation progresses and both pH and organic levels rise, the *Ferroplasma* becomes more active and displays its mixotrophic capability by consuming the organics and lowering the TOC to the 20 ppm level, analogous to figure 4.5. As the oxidation goes to completion, the mixotroph becomes the dominant organism.

Figure 4.14 displays the results yielded from the FISH analysis by showing the percentage of each fluorescent probe that bound its respective bacteria. Furthermore, figure 4.15 gives the fluorescent images that accompany the results given. It shows the FISH images of the mixed culture throughout the course of the experiment.

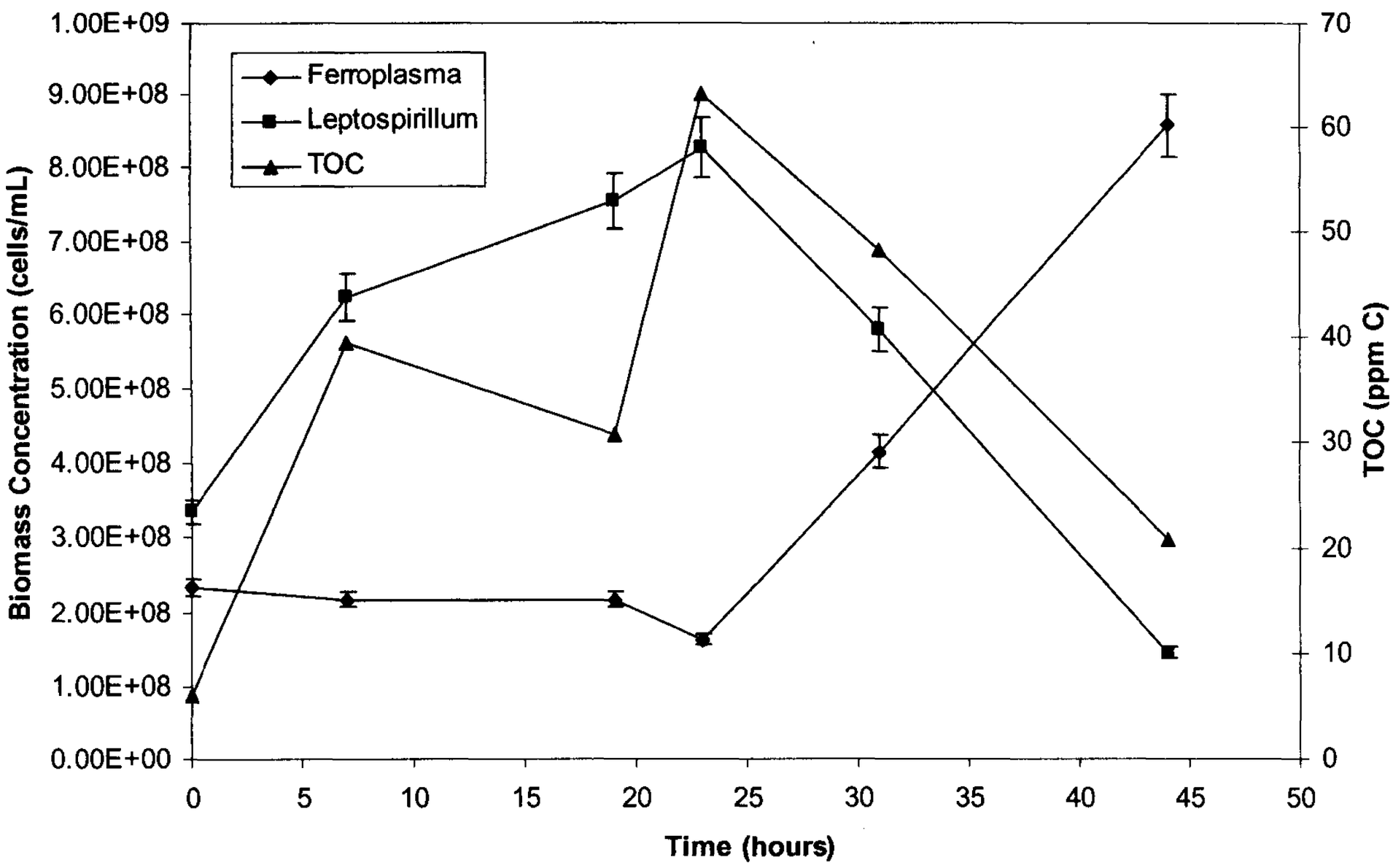

Figure 4.13 - Biomass concentration and TOC versus time for *Ferroplasma* and *Leptospirillum*

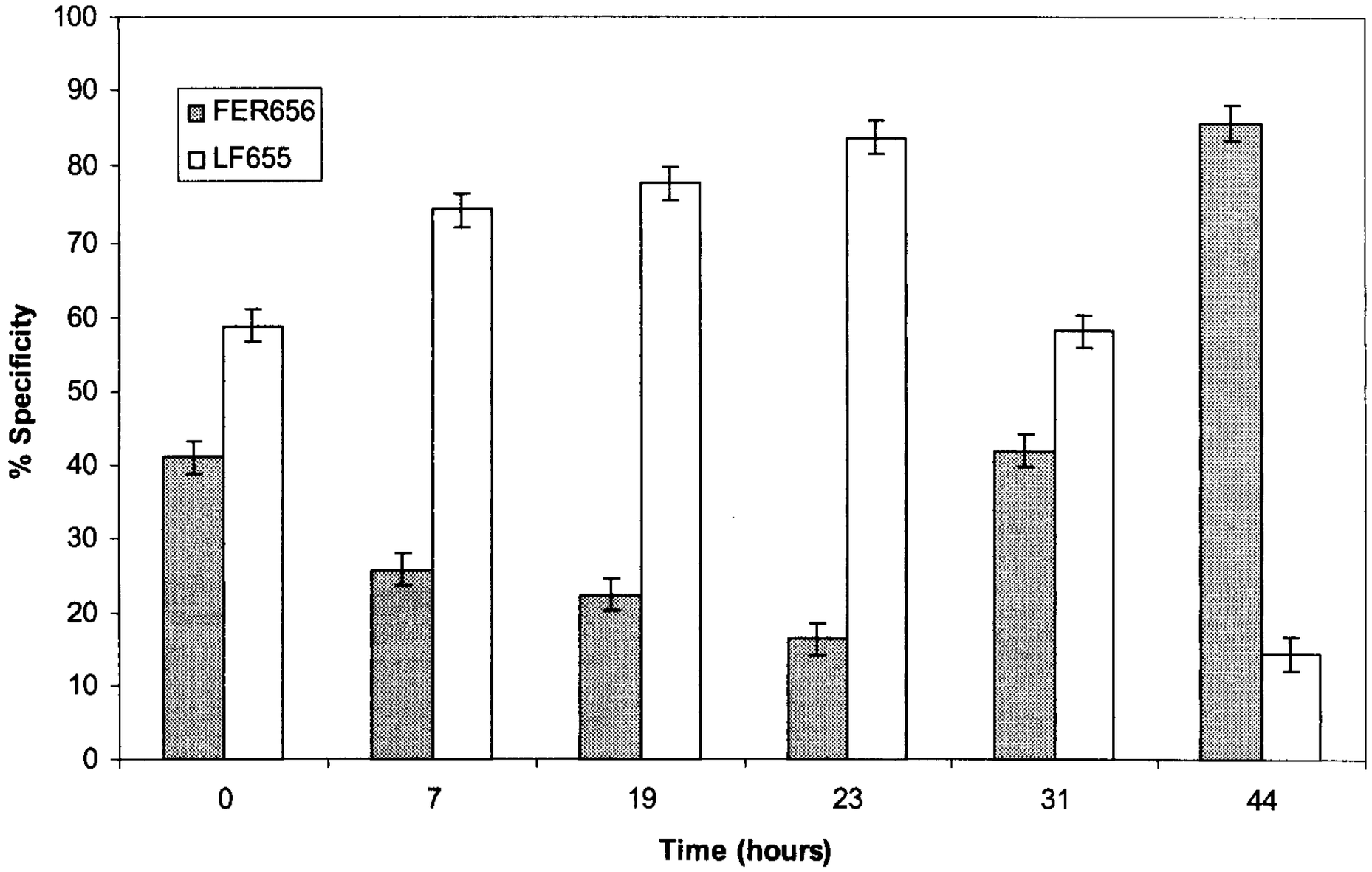

Figure 4.14 - Percent specificity versus time for FER656 and LF655 probes

Initial

a)

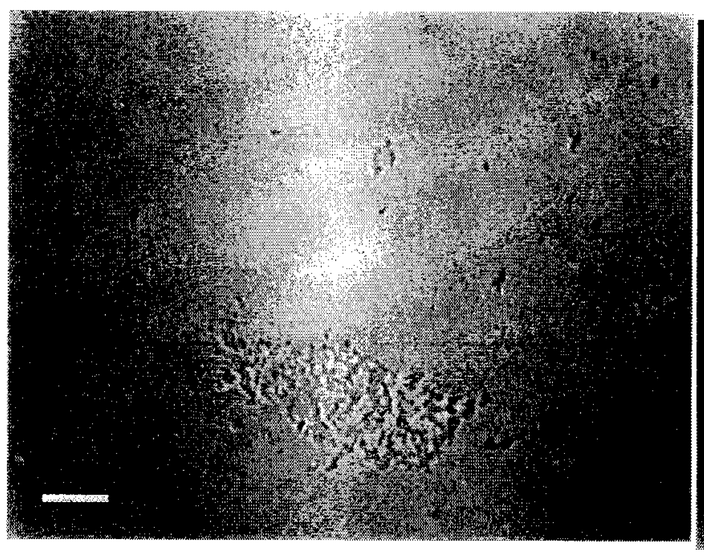

b)

c)

7 Hours

a)

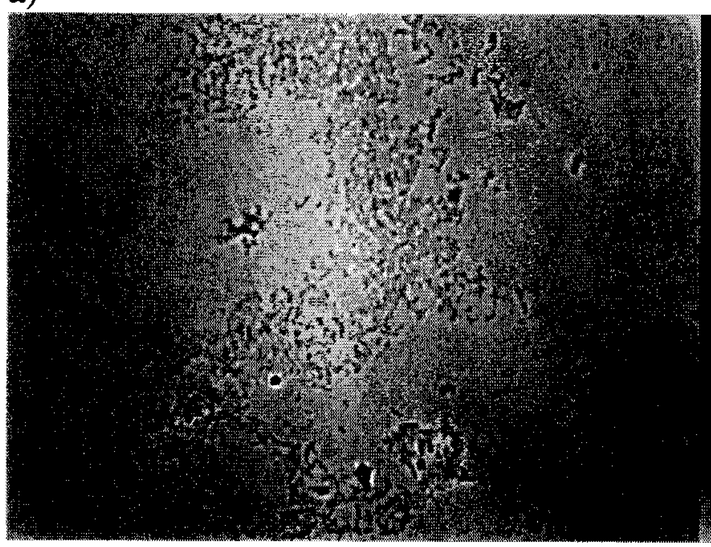

b)

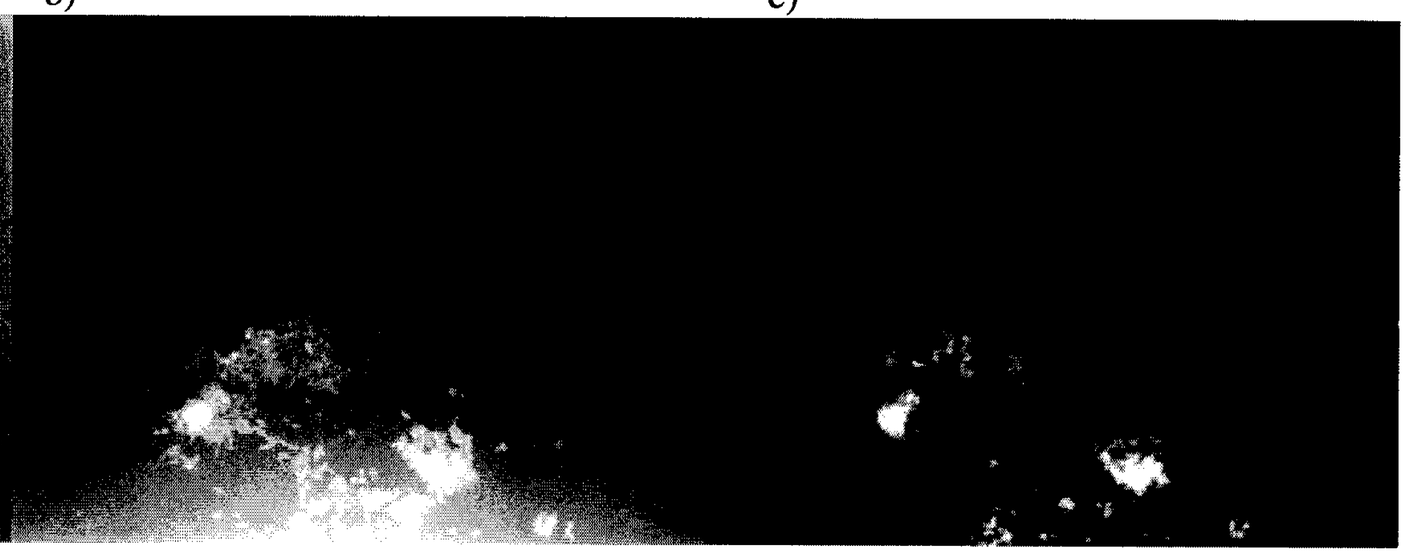

c)

19 Hours

a) b) c)

23 Hours

a) b) c)

31 Hours

a) b) c)

44 Hours

a) b) c)

Figure 4.15 – FISH images of mixed reactor through course of oxidation; a) normal phase contrast, b) DAPI stain for all organisms, c) LF655 stain for Leptospirillum

4.4. Conclusions

The main purpose of this study was to kinetically characterize the mixotroph *Ferroplasma acidiphilum* in order to evaluate its ability to effectively act as an iron-oxidizer and controller of organic concentration in solution. This also provides analysis with regards to its suitability to be used for biofuel cell applications, as a secondary iron-oxidizing organism that controls the organic levels below the threshold concentration lethal to its chemolithotrophic counterparts *A. ferrooxidans* and *Leptospirillum* sp.

In this study, we were able to successfully characterize optimal conditions for *F. acidiphilum* growth and iron oxidizing capabilities while limiting the jarosite precipitation and enhancing the organic consumption. *F. acidiphilum* was found to function optimally at a pH of 1.6 and a temperature of 35 ^{o}C, provided 0.02% (w/v) yeast concentration. Under these conditions, the maximum specific growth rate was found to be between 0.0351-0.042 h^{-1}. Furthermore, *F. acidiphilum* was shown to be able to consume organics mixotrophically and organotrophically, whereby decreasing the organics and maintaining the total organic carbon level at 20 ppm.

In closing, *F. acidiphilum* was also shown to be able to utilize the organic metabolite accumulation of the chemolithotroph *Leptospirillum* in a mixed culture. The organic buildup as a result of the initial domination of chemolithotrophic growth was effectively counteracted by the growth of *F. acidiphilum* in order to again bring the total organic carbon to a low of 20 ppm.

Therefore, *F. acidiphilum* is a very promising organism for use in conjunction with chemolithotrophs such as *Leptospirillum* sp. The issue of organic accumulation is effectively addressed by the mixotrophic growth of *F. acidiphilum*. However, due to *F.*

acidiphilum's relatively high pH requirement in comparison with Leptospirillum, jarosite formation is still a limiting factor, as with *A. ferrooxidans* which strives at a similar pH.

Nomenclature

a, b	Fitting parameters
AMD	Acid mine drainage
E_a	Activation Energy, kJ/mol
FISH	Fluorescent in situ hybridization
t	Time, hours
T	Temperature, ^oC
T_{MIN}	Minimum temperature of operation, ^oC
T_{MAX}	Maximal temperature of operation, ^oC
TOC	Total organic carbon, ppm (mg/L)
X	Microbial concentration, cells/mL
X_o	Initial Microbial concentration, cells/mL

Greek Letters

μ	Specific growth rate, h^{-1}

References

Baumler, D. J., Jeong, K.-C., Fox, B. G., Banfield, J. F., & Kaspar, C. W. (2005). Sulfate requirement for heterotrophic growth of \"*Ferroplasma* acidarmanus\" strain fer1. *Research in Microbiology, 156*(4), 492-498.

Bond, P. L., & Banfield, J. F. (2001). Design and performance of rRNA targeted oligonucleotide probes for in situ detection and phylogenetic identification of microorganisms inhabiting acid mine drainage environments. *Microbial Ecology, 41*(2), 149-161.

Dopson, M., Baker-Austin, C., Hind, A., Bowman, J. P., & Bond, P. L. (2004). Characterization of *Ferroplasma* isolates and *Ferroplasma* acidarmanus sp. nov., extreme acidophiles from acid mine drainage and industrial bioleaching environments. *Applied and Environmental Microbiology, 70*(4), 2079-2088.

Drogui, P., Mercier, G., & Blais, J.-F. (2005). Bioproduction of Ferric Sulfate Used during Heavy Metals Removal from Sewage Sludge. *J. Environ Qual, 34*, 816-824.

Edwards, K. J., Bond, P. L., Gihring, T. M., & Banfield, J. F. (2000). An Archaeal iron-oxidizing extreme acidophile important in acid mine drainage. *Science (Washington, D. C.), 287*(5459), 1796-1799.

Franzmann, P. D., Haddad, C. M., Hawkes, R. B., Robertson, W. J., & Plumb, J. J. (2005). Effects of temperature on the rates of iron and sulfur oxidation by selected bioleaching bacteria and archaea: Application of the Ratkowsky equation. *Minerals Engineering, 18*(13-14), 1304-1314.

Golyshina, O. V., Pivovarova, T. A., Karavaiko, G. I., Kondrat'eva, T. F., Moore, E. R. B., Abraham, W.-R., et al. (2000). *Ferroplasma acidiphilum* gen. nov., sp. nov., an acidophilic, autotrophic, ferrous-iron-oxidizing, cell-wall-lacking, mesophilic member of the Ferroplasmaceae fam. nov., comprising a distinct lineage of the Archaea. *International Journal of Systematic and Evolutionary Microbiology, 50*(3), 997-1006.

Ingledew, W. J. (1982). Thiobacillus *ferrooxidans*. The bioenergetics of an acidophilic chemolithotroph. *Biochimica et biophysica acta, 683*(2), 89-117.

Jensen, A. B., & Webb, C. (1995). Ferrous sulfate oxidation using Thiobacillus *ferrooxidans*: a review. *Process Biochemistry (Oxford), 30*(3), 225-236.

Karamanev, D. G., Nikolov, L. N., & Mamatarkova, V. (2002). Rapid simultaneous quantitative determination of ferric and ferrous ions in drainage waters and similar solutions. *Minerals Engineering, 15*(5), 341-346.

Okibe, N., Gericke, M., Hallberg Kevin, B., & Johnson, D. B. (2003). Enumeration and characterization of acidophilic microorganisms isolated from a pilot plant stirred-tank bioleaching operation. *Applied and environmental microbiology, 69*(4), 1936-1943.

Smith, P. F., Langworthy, T. A., & Smith, M. R. (1975). Polypeptide nature of growth requirement in yeast extract for Thermoplasma acidiphilum. *Journal of Bacteriology, 124*(2), 884-892.

Tabita, R., & Lundgren, D. G. (1971). Utilization of glucose and the effect of organic compounds on the chemolithotroph Thiobacillus *ferrooxidans*. *Journal of Bacteriology, 108*(1), 328-333.

CHAPTER 5

Biokinetic Study of Biofuel Cells

5.1. Introduction

In this fuel cell system, the substrate used in the cathode is ferric ions. These are in turn reduced to ferrous ions that are regenerated by microbes via a bioreactor. Like a conventional PEMFC, the hydrogen is oxidized at the anode, producing hydrogen and ions and electrons. The electrons travel through a circuit from the anode to the cathode, where iron reduction takes place. Furthermore, the hydrogen ions travel through the proton exchange membrane from anode to cathode compartment.

There are many factors that affect the efficiency of this system, specifically the bacteria, bioreactor conditions and the electrode materials in the fuel cell. A schematic representation of this system is shown in figure 5.1.

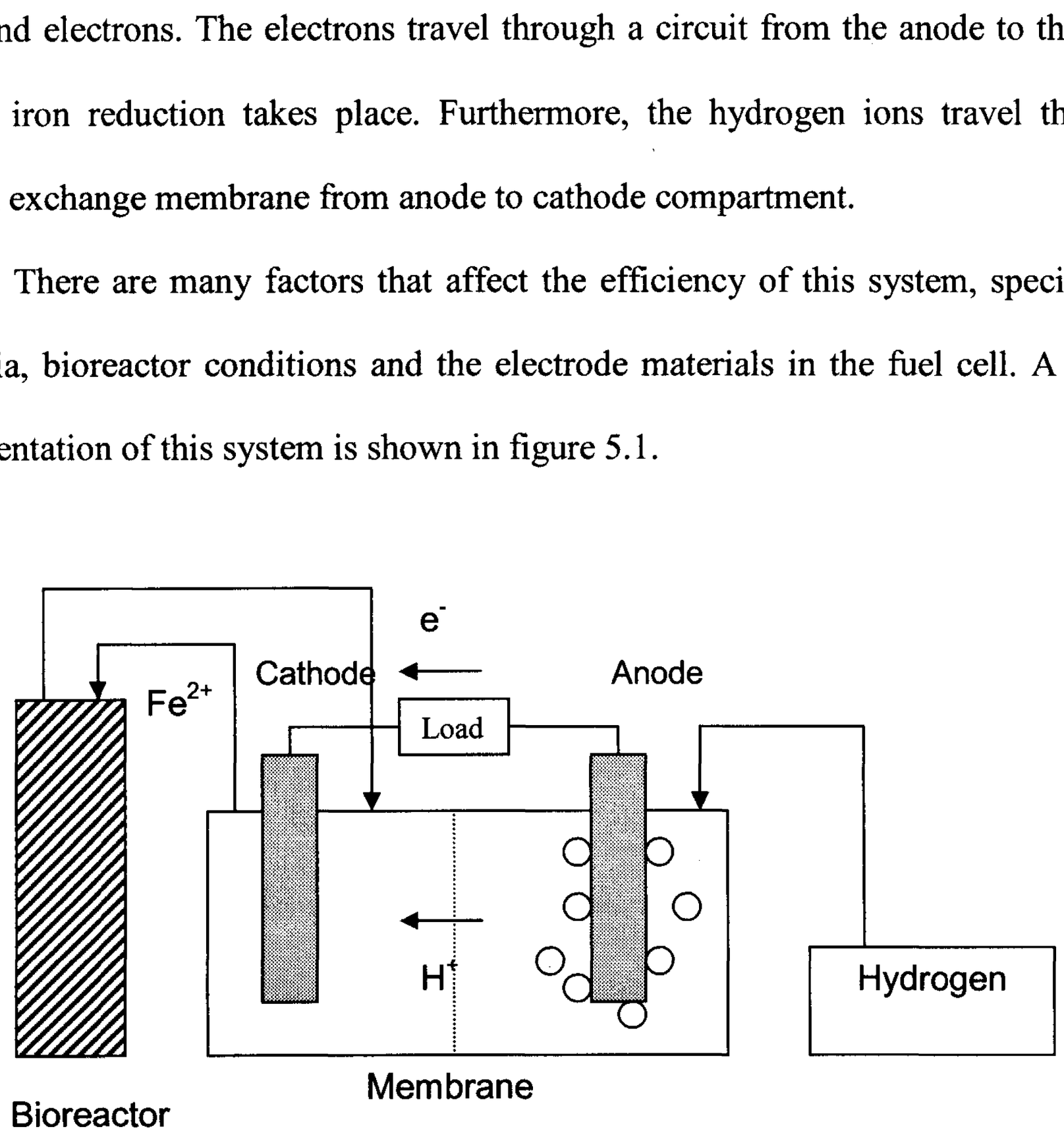

Figure 5.1 - Biofuel cell configuration

5.1.1. Bacteria

The experiments conducted in chapters 3 and 4 have shed some light into the appropriateness of bacterial selection for fuel cell applications. Firstly, the problem of jarosite precipitation was investigated. Jarosite buildup due to ferric iron accumulation has the potential of disrupting iron solution flow inside the fuel cell flow channels by creating mechanical resistance as well as accumulating on the carbon felt electrode, thus limiting electron transfer and increasing resistance. In chapter 3, it was concluded that the classic iron oxidizing microorganism, *A. ferrooxidans*, was capable of minimizing jarosite precipitation to 0.0125-0.0209 g while maintaining high oxidation rates of .181-0.194 g/L·h at pH of 1.6 and temperature of 35 C. However, this value of jarosite precipitation is still high considering the small amount of total iron in solution. Therefore, it is recommended to operate at even lower pHs in order to counteract the precipitation of jarosite. A newly researched chemolithotrophic iron-oxidizing strain, *Leptospirillum* sp., is capable of operating at pHs as low as 1.0 while not compromising iron oxidation, thus further minimizing jarosite precipitation and is thus highly recommended for out application.

The second main limiting factor of the biofuel cell system is the organic metabolite accumulation that occurs as a result of the buildup of dead biomass and release of metabolic intermediates in glycolysis, citric acid cycle and electron transport chain. In the chemolithotrophic iron-oxidizing strains, *A. ferrooxidans* and *Leptospirillum* sp., once organics reach a level of 250 ppm TOC or above, the ribulose diphosphate (RuDP) enzyme is repressed, which is responsible for CO_2 fixation. In chapter 4, we

investigated a mixotrophic iron-oxidizing strain, *Ferroplasma acidiphilum*, which shares the same ecological niche as the chemolithotrophs, with the goal of utilizing the organotrophic characteristics of the bacteria to consume the organic waste products of the chemolithotrophs, thus controlling the level of organics and preventing the lethal TOC concentration to be reached. It was concluded that *F. acidiphilum* was able to grow in a mixed culture with *Leptospirillum* (at an intermediate pH and temperature that allow for growth of both strains) after initial chemolithotroph domination. Once oxidation progressed and organic levels increased, the mixotroph became more active and assumed domination of the culture. These results provide a very promising tool in controlling the organic accumulation in the bioreactor portion of biofuel cell system. However, *F. acidiphilum* shares similar operating conditions to *A. ferrooxidans*, which are not acceptable for use in the fuel cell due to the first problem of jarosite precipitation, and are not capable of effectively growing at the lower pHs of *Leptospirillum*.

Therefore, for our current biofuel cell system, it is recommended to solely use the chemolithotrophic strain *Leptospirillum* at a low pH of 1.0 in order to limit the jarosite precipitation while providing a very high redox potential in comparison to other iron-oxidizing strains (Rawlings et al., 1999).

5.1.2. Bioreactor

As mentioned earlier, iron oxidation by mesoacidophiles belonging to the genera *Acidithiobacillus, Leptospirillum, and Ferroplasma* is the basis of bacterial ferric leaching (Kinnunen & Puhakka, 2004).

Past studies with *Leptospirillum* sp. have reported high observed oxidation rate (Kinnunen & Puhakka, 2004)), which leads to a higher current production in the fuel cell.

Furthermore, *Leptospirillum* possesses a very high redox potential (Rawlings et al., 1999) relative to its iron-oxidizing counterparts, which translates into a higher potential in the fuel cell. Therefore, *Leptospirillum* is the vital iron-oxidizing organism in the bioreactor portion of the biofuel cell system. However, efficiency studies in a bioreactor setting that is continuously regenerated with ferrous ions have not been analyzed. Moreover, it is vital for fuel cell systems to provide a substrate that is free from solid particulates, such as jarosites, and organics, which pose problems for the microbes as well as the reduction efficiency at the cathode. These byproducts are continually accumulated by microbial iron oxidation.

According to literature and reported values in table 2.2, it is recommended to use an agitated reactor with a bubble reactor type configuration due to its design flexibility and high oxidation rates. This will also give a thorough analysis of the jarosite accumulation and further limiting factors of the biofuel cell system.

5.1.3. Fuel Cell

An important aspect of the microbial biofuel cell system is the fuel cell itself. The cathode material has been carefully selected in order to ensure maximum reduction efficiency which in turn gives better fuel cell operation. Given the byproducts of iron oxidation, which hinders the mass transfer characteristics of the electrode, it is vital to work with a material that provides maximal mass transfer.

In order to efficiently produce current, there need to be maximum mass transfer between the species to be reduced and the cathode electrode. Therefore, the study of porous electrodes is a matter of increasing interest (Carta et al., 1991). In this study, carbon felt is used as the cathode electrode, since it has provided promising results (Oren

& Soffer, 1983) owing to their favorable physico-chemical characteristics: high chemical stability, large specific surface area, good fluid permeability and high electric conductivity, together with continuity of the electronic contact throughout the electrode (Carta et al., 1991).

Another important aspect of the fuel cell that must be taken into consideration is the reduction rate that occurs at the cathode of the fuel cell. By varying the amount of current running through the fuel cell (by applying an external resistance load), the amount of reduced ferric iron and therefore the regenerated ferrous iron fed to the bioreactor portion can be controlled. The following is a derivation of the relationship between current and reduction rate of ferric iron in the fuel cell.

1 A = 1 C/s

For 1 hour of operation,

1 A·hour = 3600 C

Iron reduction involves ferric iron and electron in the ratio of 1:1, therefore using Faraday's constant for amount of electric charge in 1 mole of electrons (96500 C/mole e^-):

$$\frac{3600\ C}{96500\ C/mole\ e^-} = 0.0373\ mole \cdot e^- = 0.0373\ mole \cdot Fe^{3+}$$

In terms of mass of iron reduced per hour,

$$0.0373\ mole \cdot Fe^{3+} \times \frac{55.85\ g\ Fe^{3+}}{mole \cdot Fe^{3+}} = 2.0727\ g\ Fe^{3+}$$

Equation 5.1 gives the relationship between the current running through the fuel cell, the reduction rate, $r_{reduction}$, in the cathode and oxidation rate, $r_{oxidation}$, in the bioreactor.

$$I(A) = 0.48 \cdot r_{reduction} = 0.48 \cdot r_{oxidation} \qquad (5.1)$$

5.1.4. Purpose of this study

The main goal of this study is to operate an open biofuel cell system that contains a viable bioreactor, operating continuously with a fuel cell. The operation of this biofuel cell system is based on the results and findings from chapters 3 and 4 which investigate jarosite precipitation and organic accumulation, respectively. The results of this experiment will provide insight into the next steps to take in order to prolong and improve fuel cell operation.

5.2. Materials and Methods

This experiment involves the operation of a biofuel cell system while monitoring various factors such as biomass concentration, redox potential, current, potential, and Fe^{2+} and Fe^{3+} ion concentrations. A schematic representation of the experimental set up is shown in figure 5.2.

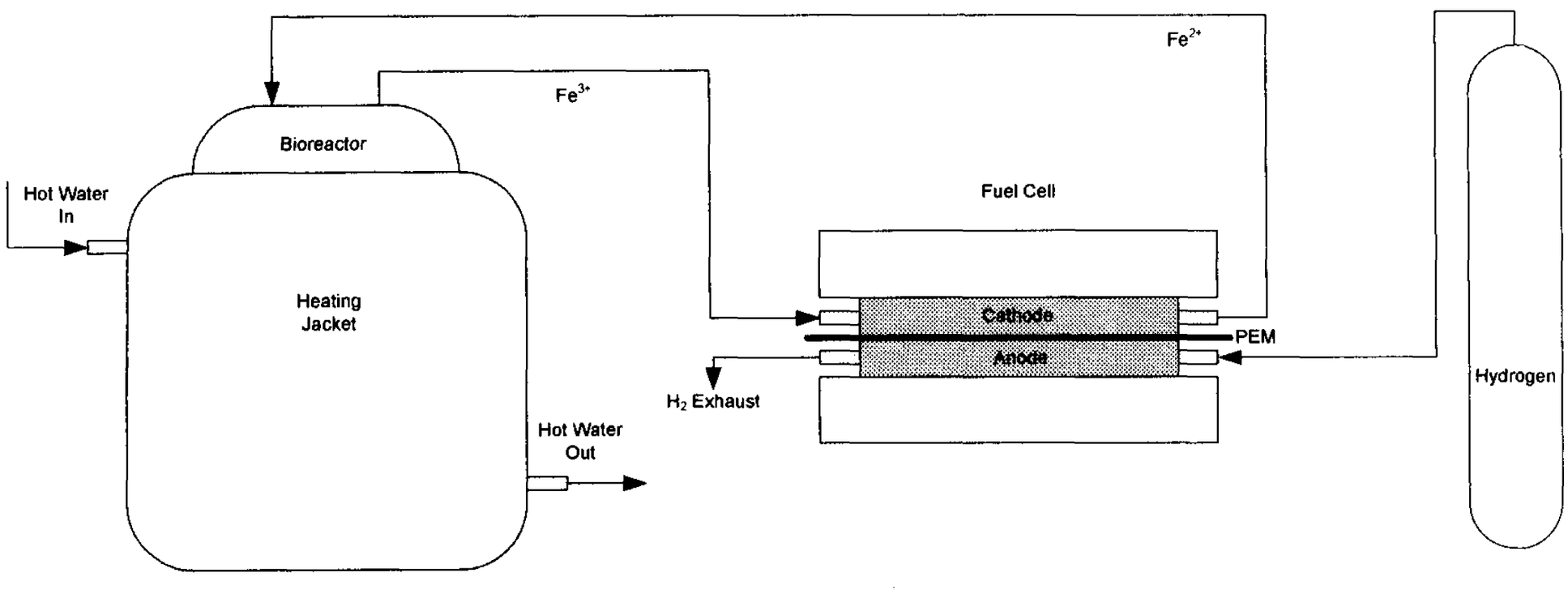

Figure 5.2 - Schematic representation of experimental set-up

5.2.1. Equipment

The pH was adjusted using sulfuric acid and monitored using a pH meter (Orion Model No. 420A; same Orion meter measures for redox potential). For the ferric and total iron analyses, we used a spectrophotometer (Varian Cary 50) with the appropriate procedure (Karamanev et al., 2002). For the TOC measurement, we used a Tekmar Dohrmann Apollo 9000 TOC analyzer, which uses a combustion-based analyzer of organic carbon. Moreover, to measure biomass, we used a Zeiss Axioskop 40 upright microscope, and viewed 5 uL samples under 100x objective lenses, which are calibrated according to the viewing area in relation to the pixel area.

In order to measure the potential and current in the fuel cell, a digital voltmeter and ammeter were used, respectively. Furthermore, to vary the load, a 12 Ω variable resistor was used.

5.2.2. Bioreactor

The bioreactor used in this experiment is an agitated reactor with a bubble reactor type configuration. The reactor had a volume of 5 L and was made of glass, 15 cm in diameter and 30 cm in height. The reactor is placed in a bucket filled with hot water at 40 ^{o}C that is continuously regenerated by a VWR immersion circulator (model 1122S). 2.5 liters of 9K medium containing 40 g/L of ferrous iron were added to the reactor and inoculated with 100 mL of 10^{9} cells/mL of *Leptospirillum* sp. (obtained from Iron Mountain, California). The oxidation in the reactor was allowed to react >90% completion before the fuel cell was connected. Iron oxidation, TOC, pH and redox potential in the reactor were measured daily during biofuel cell operation; this was accomplished by the sulfosalicylic acid method, TOC analyzer, a pH meter, and a redox potential meter, respectively. Once the fuel cell was connected to the bioreactor and the

biofuel cell system was operational, it was vital to monitor and vary the conditions in order to maintain a pH of 1.0 and temperature of 40 °C in the reactor, which according to chapter 3, should be effective in limiting jarosite interference.

5.2.3. Fuel Cell

The fuel cell component of the system was assembled according to classic membrane electrode assembly (MEA). Figure 5.3 presents an exploded view of the fuel cell assembly.

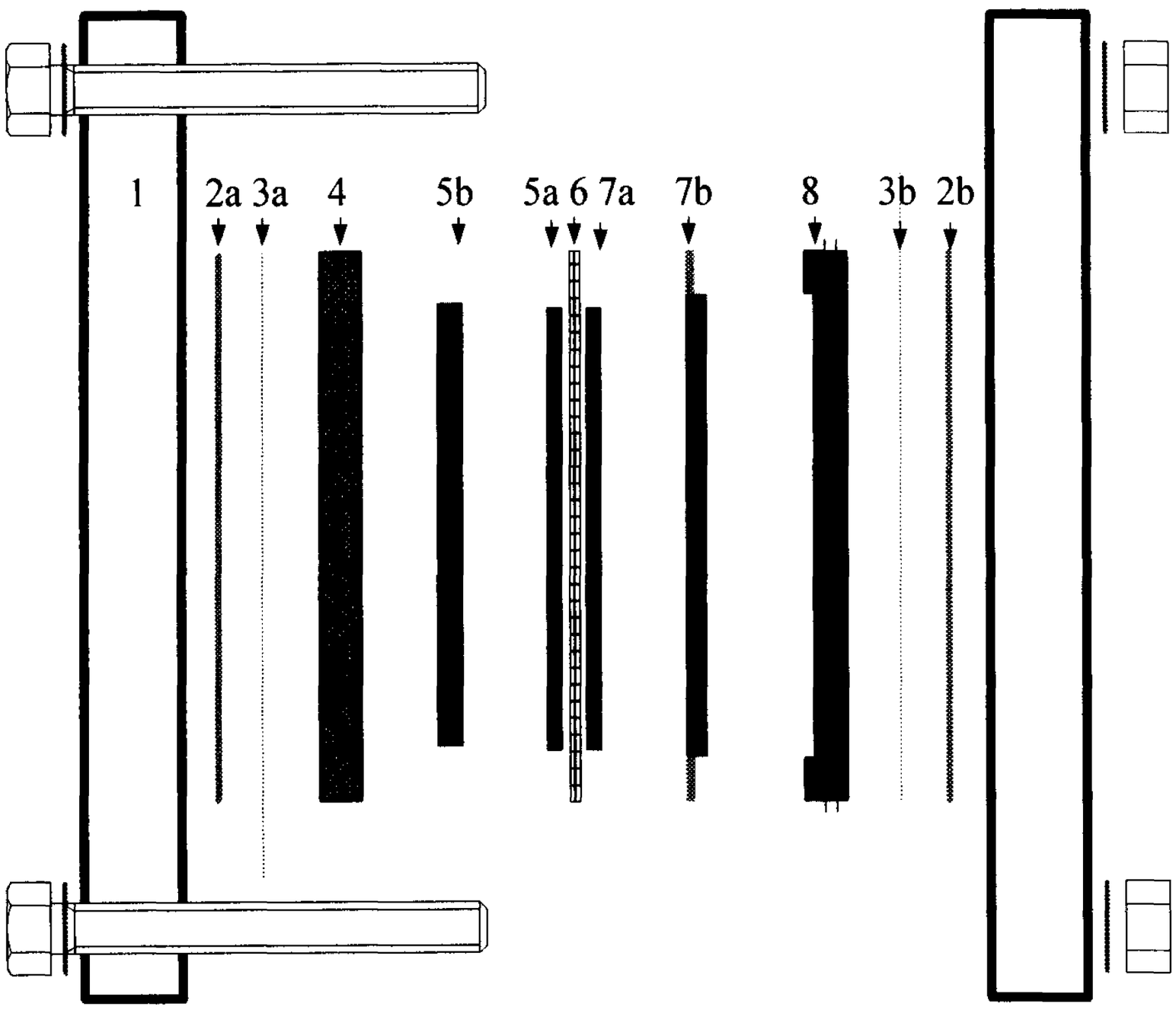

Figure 5.3 - Exploded view of fuel cell assembly

The corresponding hardware description to figure 5.4 is given in table 5.1.

Table 5.1 - Fuel cell hardware

Part	*Dimensions (L*W*H) (cm)*	*Material*
1. Base plate	15*15*1.0	Plexiglass
2a/b. Gasket	12*12*0.079	Rubber
3a/b. Current collector	12*12*0.035	Copper foil
4. Anodic endplate	12*12*0.7	Graphite
5a. Grey silicon gasket (SI-60 ROBCO inc.)	12*12*0.035	Silicon polymer
5b. Anode	10*10*0.045	ETEK Hydrogen electrode
6. Nafion H^+ ion exchange membrane	10*10*0.015	Nafion®
7a. Grey silicon gasket (SI-60 ROBCO inc)	12*12*0.035	Silicon polymer
7b. Cathode	10*10*0.15	Activated carbon felt Kynol™
8. Cathodic endplate	12*12*0.7	Graphite

Hydrogen fuel was passed over the anode at a pressure of 2-3 kPa gauge directly from the hydrogen cylinder. The ferric iron oxidant from the bioreactor was passed over the cathode at 1 L/hour using a Masterflex pump. The positive terminal of the fuel cell assembly was connected to a 12 Ω variable resistor which was connected to a digital ammeter. The digital ammeter completed the circuit through connection to the negative terminal of the fuel cell assembly. Furthermore, a digital voltmeter was then connected in parallel to the terminals of the fuel cell assembly. Figure 5.4 shows a schematic diagram of the fuel cell. Figures 5.5 and 5.6 show the lab biofuel cell view and the serpentine flow channels used in the fuel cell, respectively.

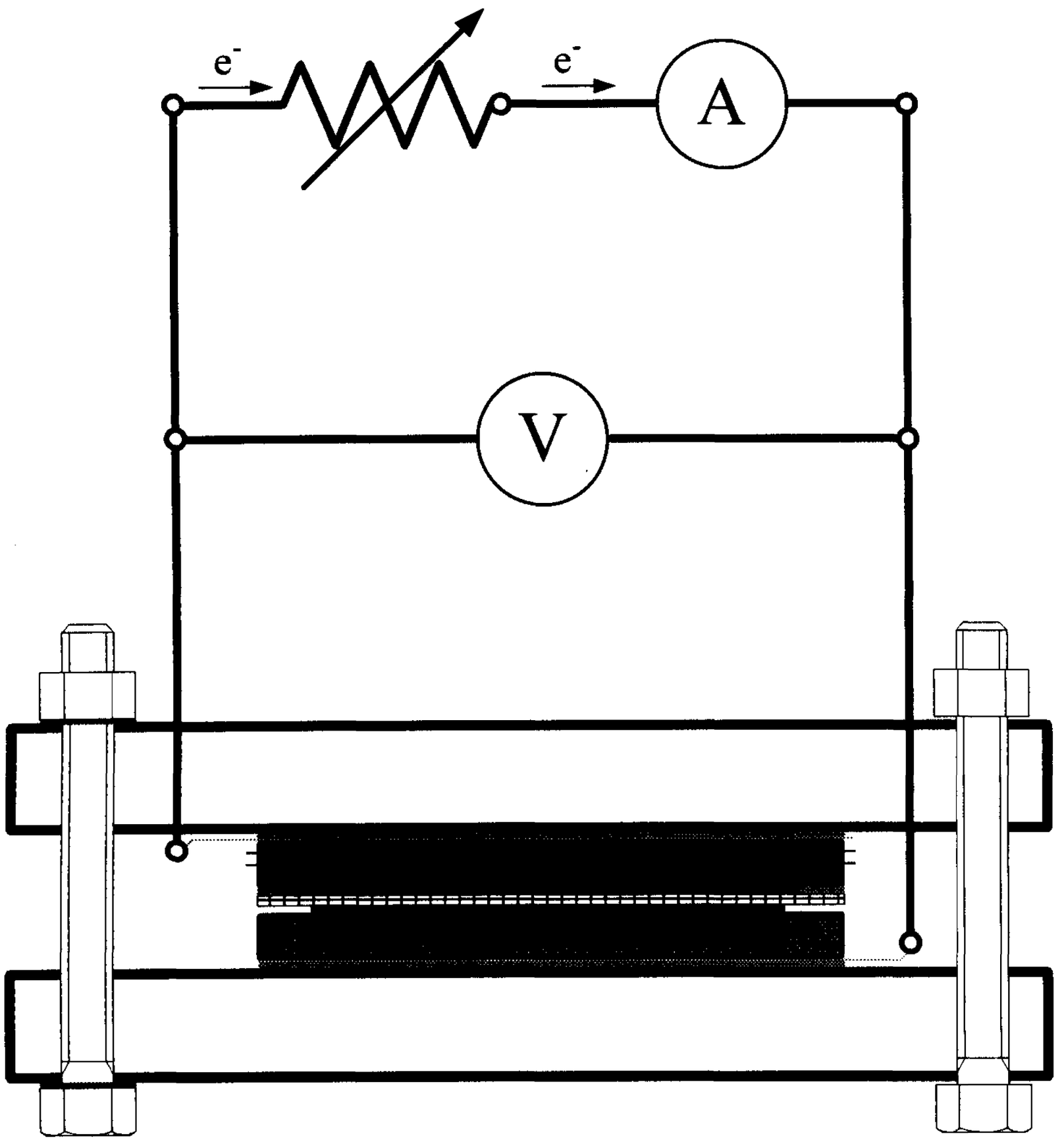

Figure 5.4 - Schematic fuel cell representation

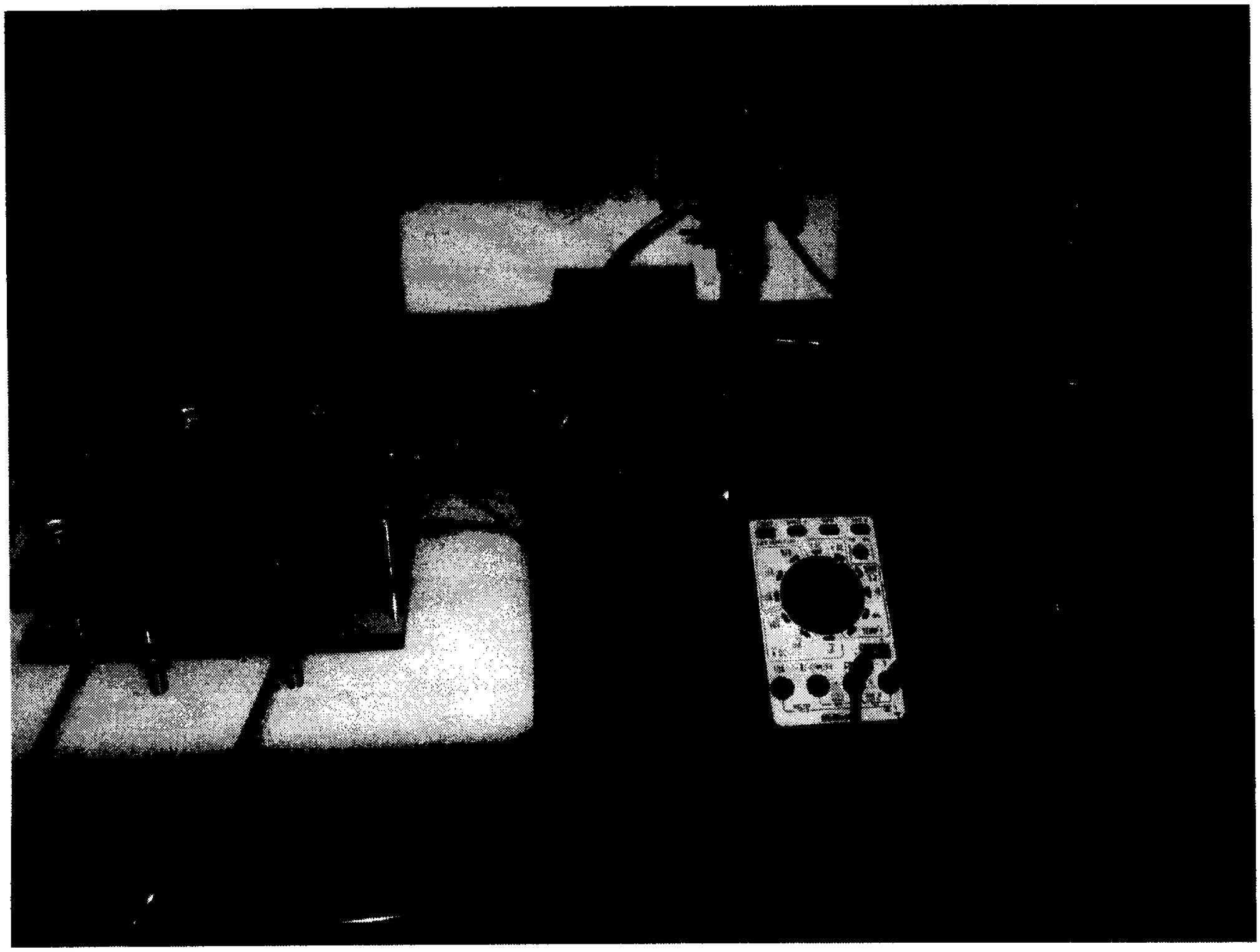

Figure 5.5 - Common view of the lab setup

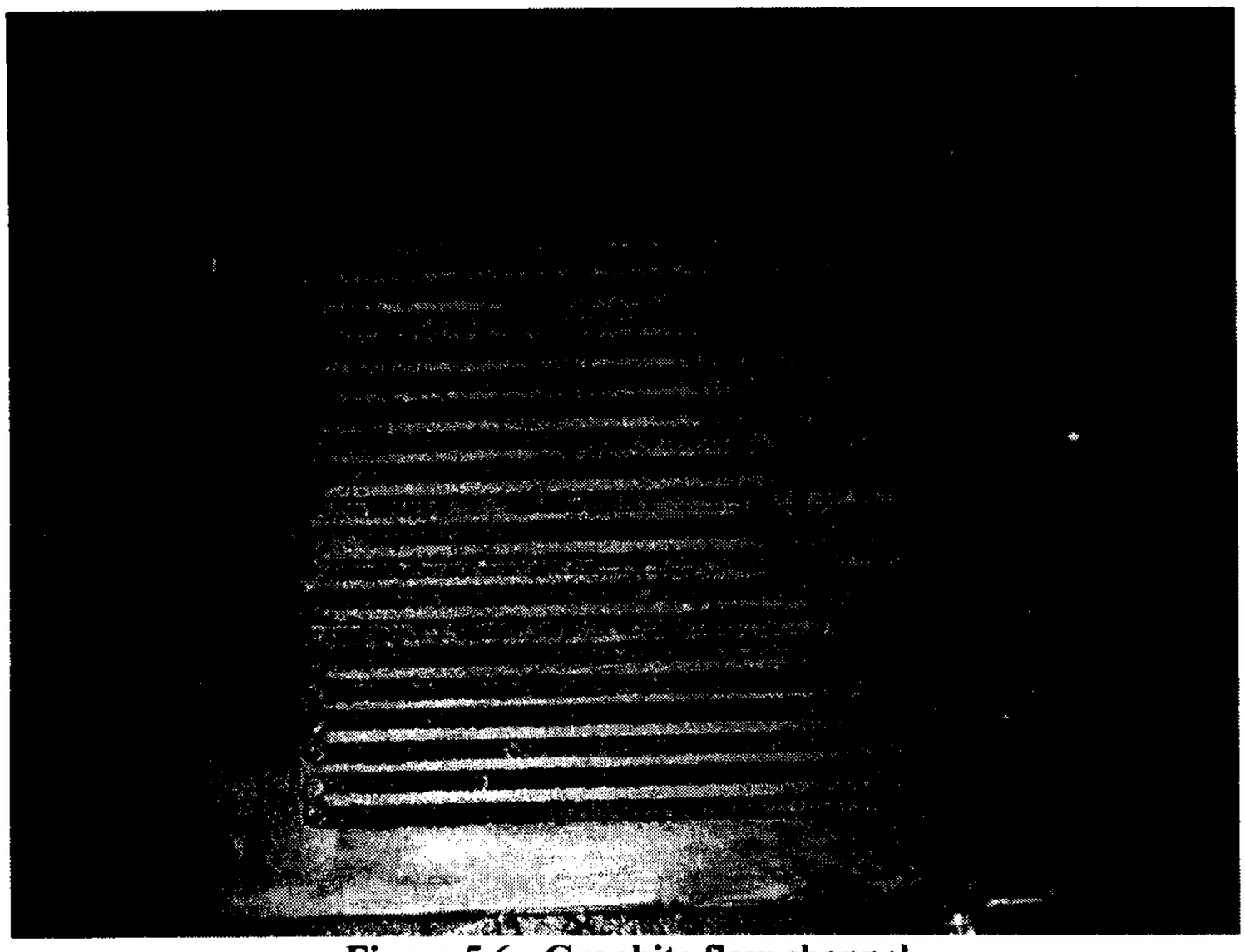

Figure 5.6 - Graphite flow channel

5.3. Results and Discussions

The bioreactor portion of the biofuel cell system was first allowed to reach >90% iron oxidation prior to connecting it to the fuel cell and commencing the biofuel cell system. It was vital to maintain the reactor at pH 1.0 and temperature of 40 °C throughout the course of the experiment; this was accomplished by varying the resistance and current in the fuel cell accordingly. Once connected the parameters mentioned above were monitored on a daily basis. Figure 5.7 is a plot of the current and potential in the fuel cell throughout the course of the experiment. It is very clear that the current fluctuates around 1.3 A and maintains an inverse relationship with respect to the potential which fluctuates around 0.65 V, giving an average power generation of 0.845 W. Using equation 5.1, this relationship gives an oxidation rate of 2.69 g/hour. Since the reactor contains 2.5 L, this translates to 1.08 g/L·h.

It is very important to note that throughout the course of the experiment, the variable resistance had to be daily decreased in order to maintain the current through the fuel cell, which indicates an increasing resistance to electron flow in the fuel cell. This is the reason the operation of the biofuel system had to be halted in order to investigate this occurrence.

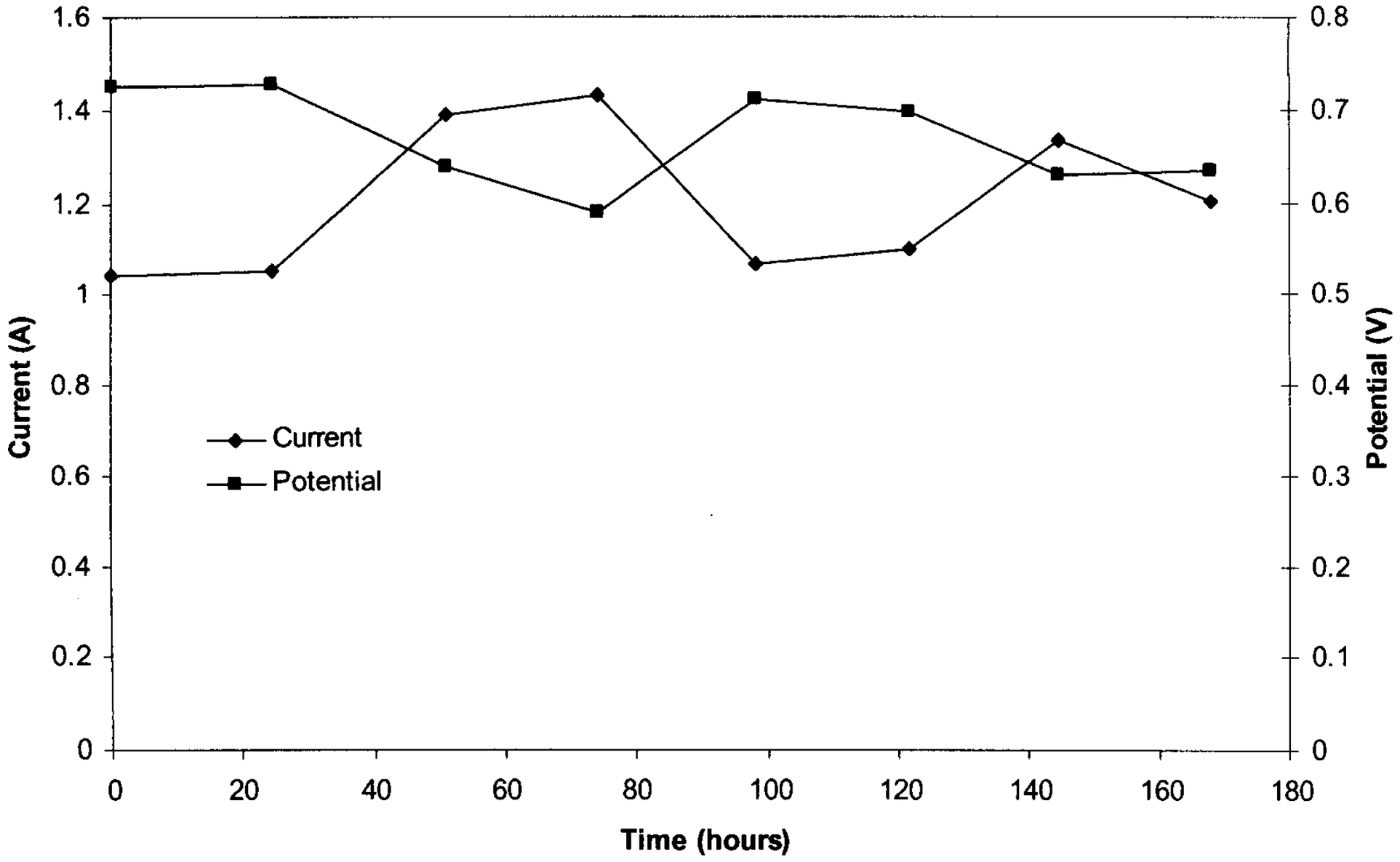

Figure 5.7 - Current and potential vs. time in the fuel cell

Figure 5.8 displays the trend of biomass concentration in the bioreactor throughout the operation of the biofuel cell system. There is a clear initial increase in the cell concentration, however, the cell concentration remains constant at the approximately 3.2×10^9 cells/mL.

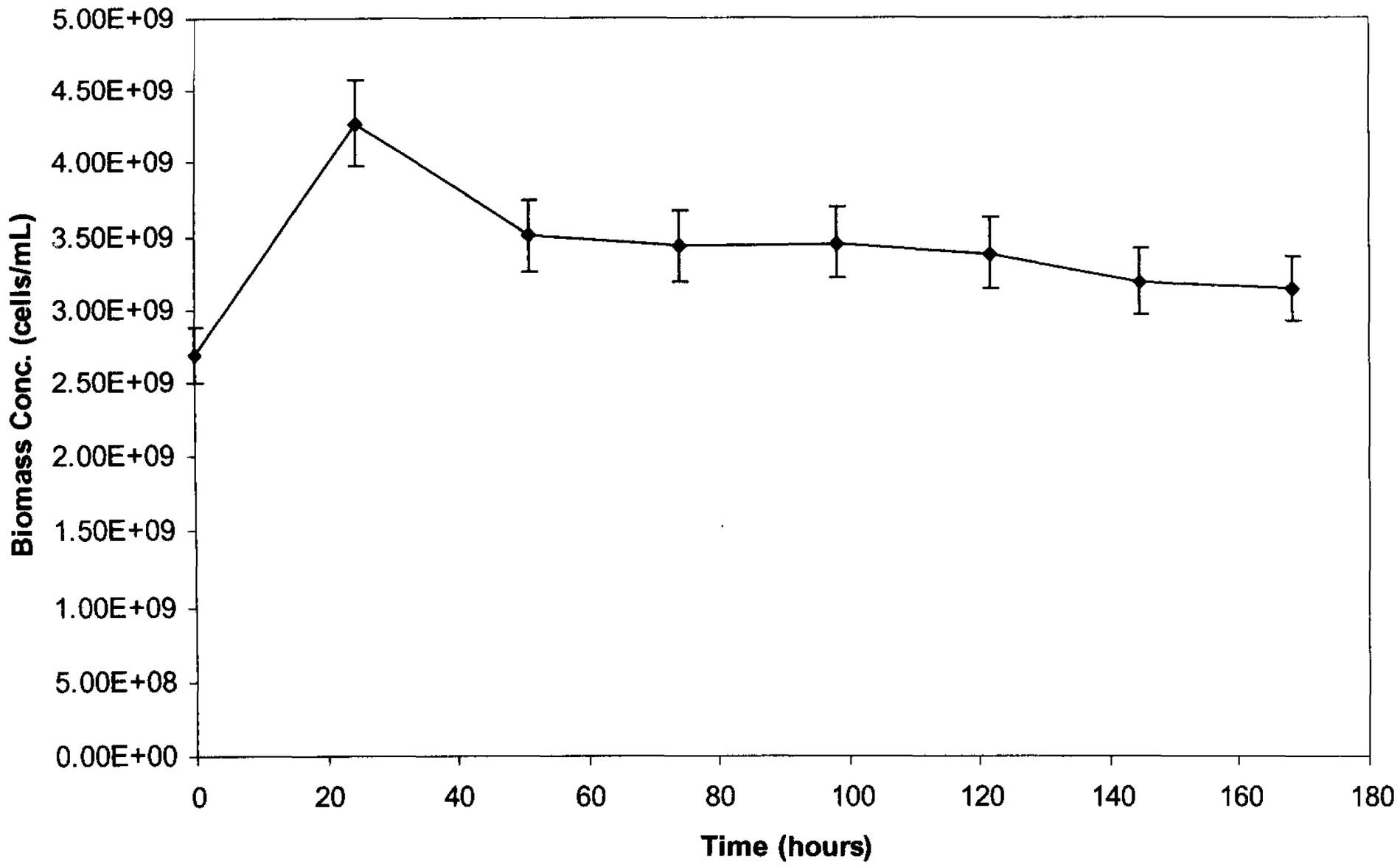

Figure 5.8 - Biomass concentration vs. time for the bioreactor portion in the system

Figure 5.9 shows the trend in TOC in the bioreactor during the operation of the biofuel cell system. It is clear that the TOC of the system gradually increases, approaching the threshold concentration of 250 ppm, discussed earlier in chapter 4.

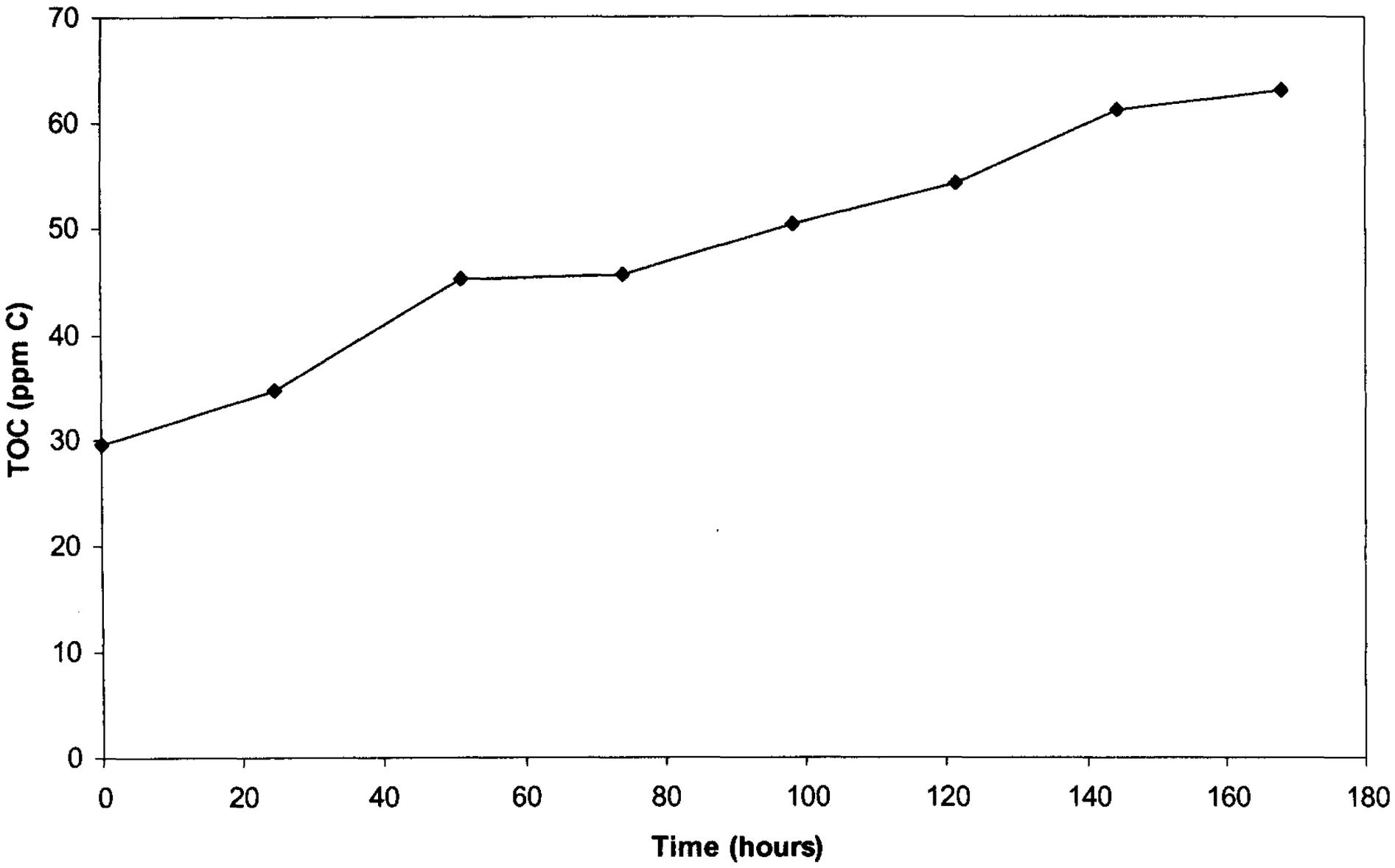

Figure 5.9 - TOC vs. time for the bioreactor portion in the system

After halting the operation of the system due to the increasing resistance in the fuel cell, we examined the fuel cell compartments to determine the source of the increased resistance. It was found that jarosite had accumulated on the cathode compartment of the fuel cell as well as the graphite flow channel for iron, which raises further questions regarding the optimal conditions of running the biofuel cell system. Figure 5.10 shows the cathodic flow channel for iron and the carbon felt electrode after the experiment was stopped. It is clear that the jarosite deposits have accumulated on both components of the fuel cell, thus inducing increased resistance by clogging the flow channels, and limiting mass transfer to the cathode.

Figure 5.10 - Post-experiment flow channel and cathode

5.4. Conclusions

The purpose of this experiment was to operate a functional biofuel cell system and to further investigate any restraints on the system's operation. The biofuel cell system yielded a relatively high current and potential at 1.3 A and 0.65 V, respectively. This translates into a power generation of 0.845 W and a bacterial oxidation rate of 1.08 g/L·h. The TOC of the system was also observed to rise gradually, approaching the critical limit of 250 ppm. More importantly, the resistance of the fuel cell was increasing throughout the biofuel cell operation due to significant jarosite deposits in the fuel cell flow channel for iron and the cathode carbon felt material. This result suggests an alternative method

for addressing the jarosite accumulation problem, which proved to be the ultimate restraint on biofuel cell operation.

References

Carta, R., Palmas, S., Polcaro, A. M., & Tola, G. (1991). Behavior of a carbon felt flow by electrodes. Part I: Mass transfer characteristics. *Journal of Applied Electrochemistry, 21*(9), 793-798.

Karamanev, D. G., Nikolov, L. N., & Mamatarkova, V. (2002). Rapid simultaneous quantitative determination of ferric and ferrous ions in drainage waters and similar solutions. *Minerals Engineering, 15*(5), 341-346.

Kinnunen, P. H. M., & Puhakka, J. A. (2004). High-Rate Ferric Sulfate Generation by a *Leptospirillum sp.*-Dominated Biofilm and the Role of Jarosite in Biomass Retainment in a Fluidized-Bed Reactor. *Biotechnology and Bioengineering, 85*, 697-705.

Oren, Y., & Soffer, A. (1983). Graphite felt as an efficient porous electrode for impurity removal and recovery of metals. *Electrochimica Acta, 28*(11), 1649-1654.

Rawlings, D. E., Tributsch, H., & Hansford, G. S. (1999). Reasons why "*Leptospirillum*"-like species rather than Thiobacillus *ferrooxidans* are the dominant iron-oxidizing bacteria in many commercial processes for the biooxidation of pyrite and related ores. *Microbiology (Reading, United Kingdom), 145*(1), 5-13.

Overall Conclusions

Biofuel cell operation is hindered by various factors including jarosite formation and organic metabolite formation. Jarosite precipitation has the potential of blocking flow channels and depositing on the cathode material in a fuel cell causing mechanical and electrical resistance. Furthermore, organic accumulation in the bioreactor portion of the biofuel cell system has the potential of inhibiting the metabolic pathway of the main chemolithotrophic iron oxidizing bacteria, thus diminishing iron oxidation and in turn current flow.

The first experiment in this study involved the study of jarosite formation using the classic chemolithotrophic iron-oxidizing bacteria, *A. ferrooxidans*, which yielded favorable results of providing conditions of low pHs of 1.6-1.7 that minimize jarosite precipitation to 0.0125-0.0209 g while maintaining high iron oxidation of 0.181-0.194 g/L·h. However, this jarosite precipitation, given the small amount of iron in the experiment, is still relatively high and remains a problem to biofuel cell operation. It is therefore more favorable to operate at even lower pHs, which is possible with the newly researched chemolithotroph *Leptospirillum* sp., which is capable of high iron oxidation rates at pH 1.0.

The second experiment addressed the issue of organic accumulation in the bioreactor portion of the biofuel cell system. The main aim was to use a mixotrophic iron oxidizing strain, *Ferroplasma acidiphilum*, with the hope of consuming the organic by-products of the chemolithotrophic cell growth. The biokinetic characterization of F. acidiphilum provided valuable insight into the iron oxidizing capabilities of the strain as well as its organic dependence and growth rate. *F. acidiphilum* was able to be cultured

with the chemolithotroph *Leptospirillum* and successfully controlled the organic levels as oxidation progressed. The total organic carbon was efficiently maintained at 20 ppm, well below the lethal threshold level of 250 ppm. Although F. acidiphilum provided promising results with respect to controlling organic levels, its pH optimum was similar to that of A. ferrooxidans, thus allowing an unacceptable amount of jarosite precipitation.

The final experiment involved the application of previous findings in order to operate a functional biofuel cell system at pH of 1.0 and temperature of 40 ^{o}C. Since jarosite precipitation poses the biggest threat to fuel cell operation, *Leptospirillum* sp. was the only bacteria selected to be used in the bioreactor of the biofuel cell system. Results yielded a prolonged operation period where the current produced was maintained at 1.3 A and 0.65 V (power of 0.845 W), indicating a relatively high oxidation rate of 1.08 g/L·h, and a high biomass concentration of 3.3 x 10^{9} cells/mL. The TOC of the system was also approaching the critical level. However, the resistance inside the fuel cell increased throughout the course of the operation. This was due to the high jarosite deposits on the cathode and flow channels for iron, despite the low pH of operation, thus suggesting alternative operation conditions.

Recommendations

For the studies performed in this research, it is clear that the main factor restraining biofuel cell operation is the jarosite deposition. This was very clear from the results in chapter 5. Also, at the low pHs required for fuel cell operation, we are unable to use the mixotroph in order to control the organic levels, which again poses another problem.

A plausible solution to this dilemma is to acquire a new heterotrophic iron-oxidizing microorganism, *Ferroplasma acidarmanus*, which shares similar phenotypic characteristics as the *Ferroplasma acidiphilum* strain, except it can operate effectively at pHs as low as zero. This would permit us to lower the pH of the biofuel cell system to below 1 in order to further counter the jarosite formation and also address the organic accumulation.

APPENDIX A – EQUIPMENT

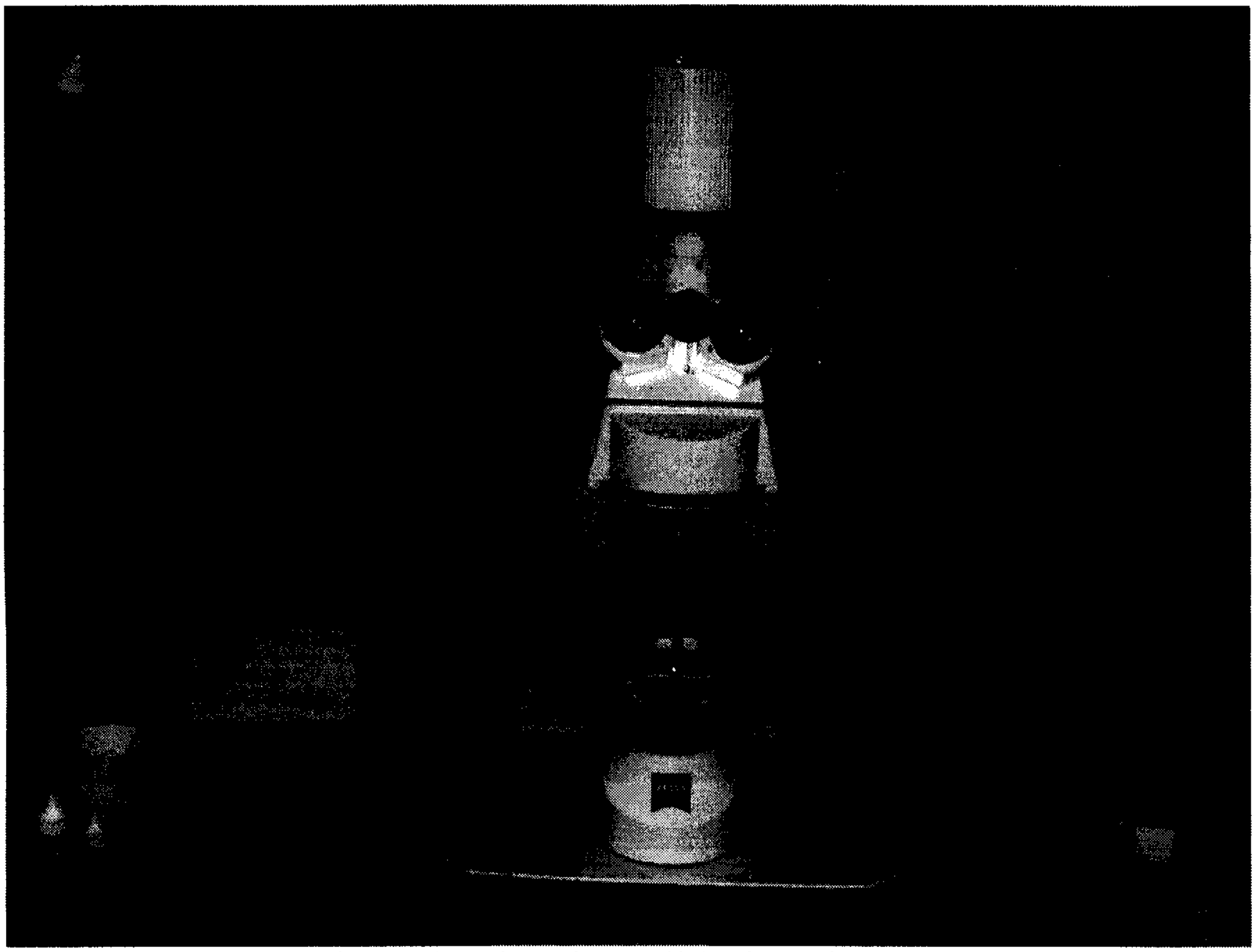

Figure A1 - Zeiss Axioskop 40 Upright Microscope

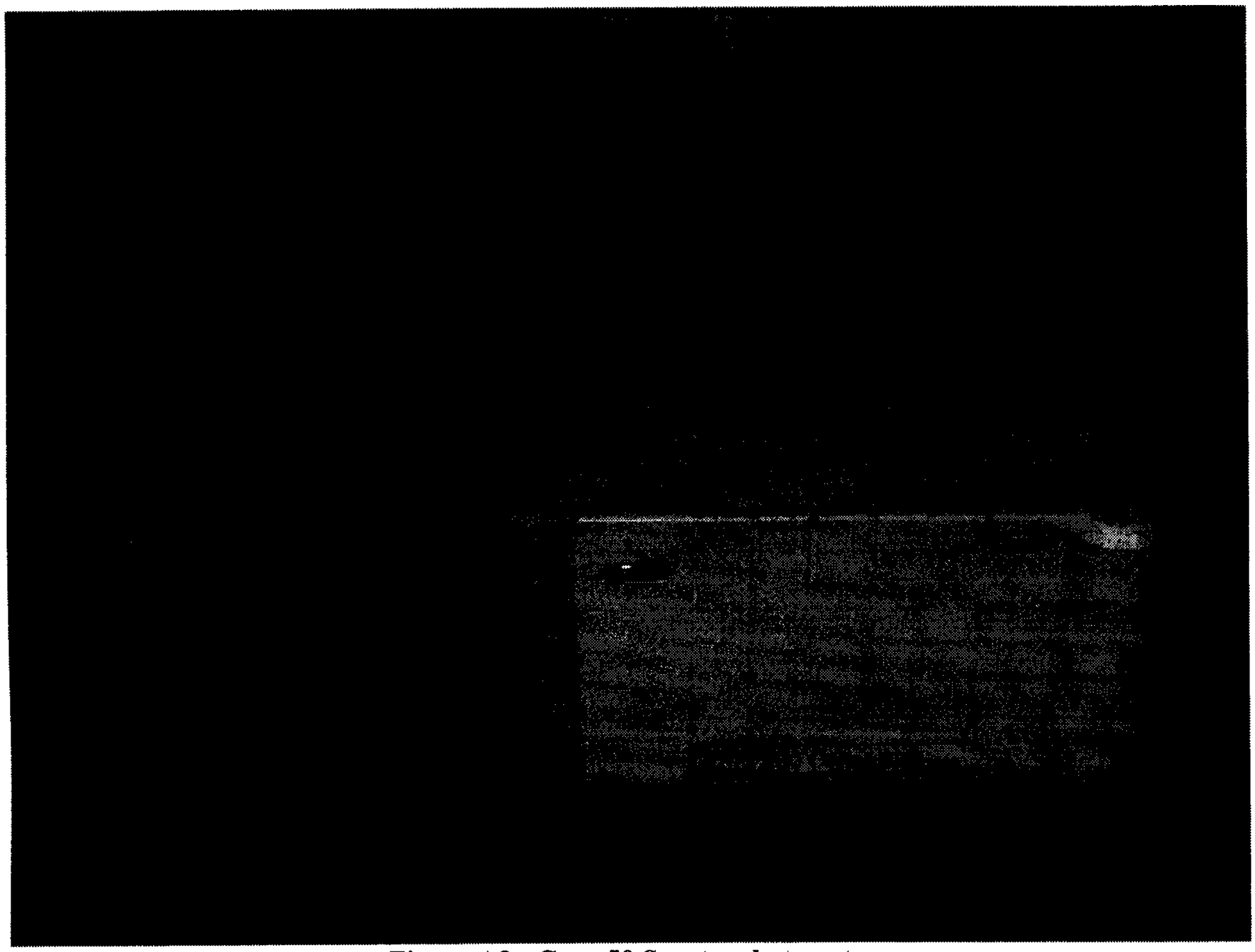

Figure A2 - Cary 50 Spectrophotometer

APPENDIX B – CALIBRATION

For spectrophotometer:

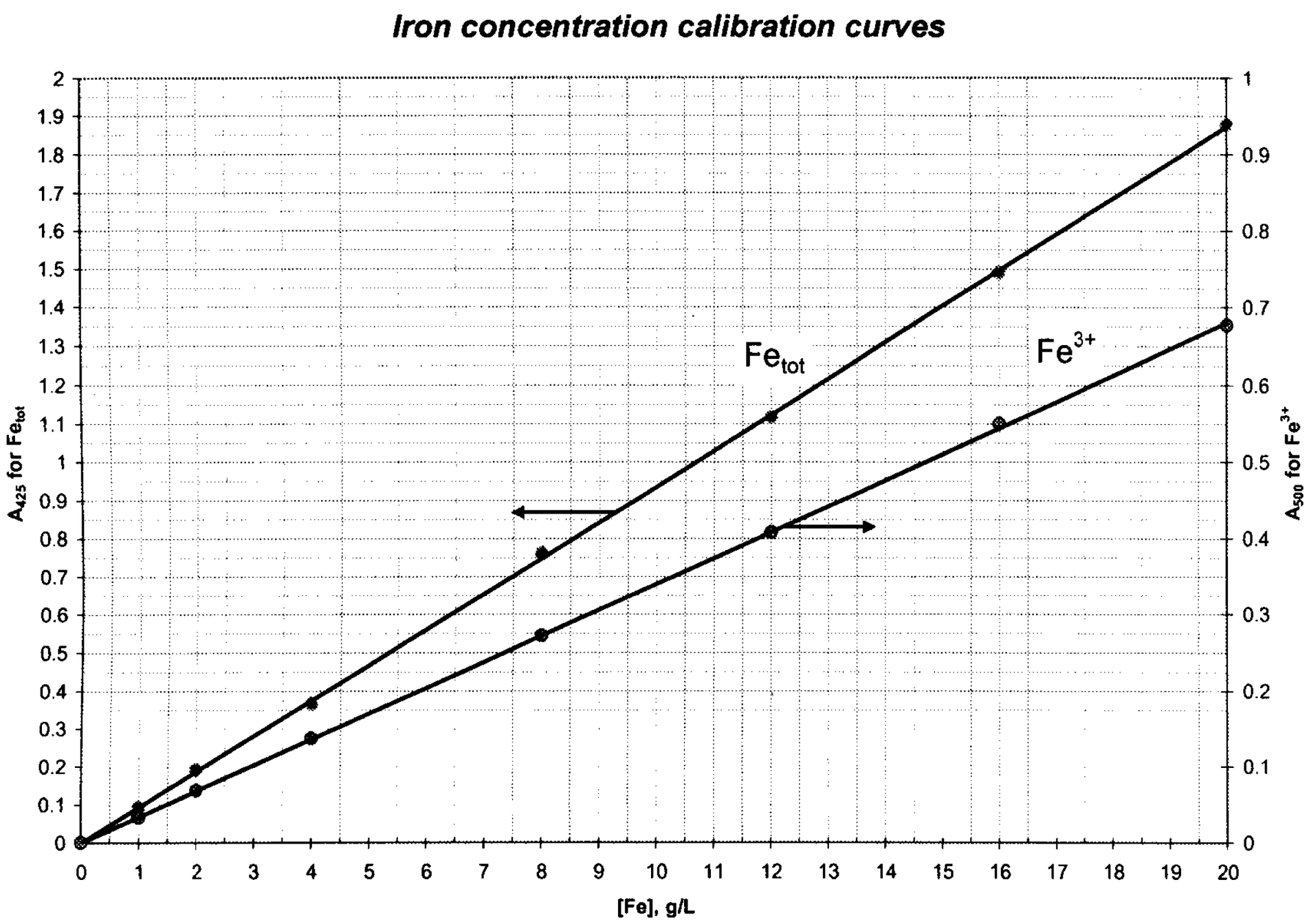

Figure B1 - Spectrophotometer calibration

$Fe^{3+} = Absorbance_{500nm} / 0.03402$

$Fe_{TOTAL} = Absorbance_{425nm} / 0.09359$

Error < 0.5%

For Microscope:

Under 100x magnification viewing field:

5 pixels = 1 um
1 $pixel^2$ = (1/25) um^2

Viewing Field Pixel Area = 351204 $pixel^2$ * (1/25) $um^2/pixel^2$ = 1.405 x 10^4 um^2

Coverslip Area = 254 mm^2 * 1x10^6 um^2/mm^2 = 2.545 x 10^8 um^2

Ratio of Coverslip area : Viewing field area = 1.811 x 10^4
Therefore bacterial count under viewing area (assuming 5 uL forms a monolayer under coverslip):

1.811 x 10^4 / 5 uL = 3.622 x 10^3 bacterial count / uL = 3.622 x 10^6 bacterial count / mL

* All other equipment used were internally calibrated before use

APPENDIX C – DATA

All experimental data is provided in the attached CD.